

BEHAVIOR OF EXTRACTION PARACHUTES IN THE WAKE OF A POWERED AIRPLANE MODEL

*H. G. HEINRICH
G. D. HULCHER*

University of Minnesota

*** Export controls have been removed ***

This document is subject to special export controls and each transmittal to foreign governments or foreign nationals may be made only with prior approval of the Vehicle Equipment Division (FDF), Air Force Flight Dynamics Laboratory, Wright-Patterson AFB, Ohio.

FOREWORD

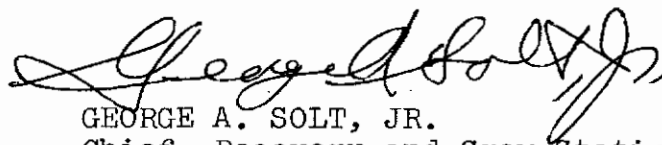
This report was prepared by the Department of Aeronautics and Engineering Mechanics of the University of Minnesota in compliance with U. S. Air Force Contract No. F33615-67-C-1010, "Theoretical Deployable Aerodynamic Decelerator Investigations," Task 606503, "Parachute Aerodynamics and Structures," Project 6065, "Performance and Design of Deployable Aerodynamic Decelerators." The work on this report was performed between August 1, 1966, and July 31, 1967.

The work accomplished under this contract was sponsored jointly by U. S. Army Natick Laboratories, Department of the Army; Bureau of Aeronautics and Bureau of Ordnance, Department of the Navy; and Air Force Systems Command, Department of the Air Force, and was directed by a Tri-Service Steering Committee concerned with Aerodynamic Retardation. The work was administered under the direction of the Recovery and Crew Station Branch, Air Force Flight Dynamics Laboratory, Research and Technology Division. Mr. James H. DeWeese was the project engineer.

The study was conducted in cooperation with Messrs. E. L. Haak and R. A. Noreen. Several students of Aerospace Engineering of the University of Minnesota participated in the performance of the tests and data reduction. The authors wish to express their gratitude to all who rendered their services to the accomplishment of this work.

This report was submitted by the authors in December 1967.

This technical report has been reviewed and is approved.



GEORGE A. SOLT, JR.
Chief, Recovery and Crew Station Branch
Air Force Flight Dynamics Laboratory

ABSTRACT

The drag and stability characteristics of single and clustered solid flat and ringslot parachutes as cargo extraction systems in the wake of a model of the Caribou airplane with windmilling and powered propellers are reported. The investigation also includes the effect of actuated wing trailing flaps, and the variation of the parachute performance parameters in midair and near the ground. It was found that in all cases the drag coefficient of the cluster decreases with the increased number of canopies in the cluster, and a single ringslot parachute is more stable than the most stable cluster of solid flat canopies. The effects of the powered propeller slipstream and flap actuation are noticeable but not dominating. Also, wake surveys of the airplane showed characteristic dynamic pressure defects or increases for power off or on flight conditions. The location of these pressure fields was noticeably influenced by flap actuation and ground effects.

This abstract has been approved for public release and sale; its distribution is unlimited.

TABLE OF CONTENTS

	PAGE
I. Introduction	1
II. Models	2
A. Parachute Models	2
1. Ringslot Parachutes	2
2. Solid Flat Parachutes	2
3. Extraction Line and Risers	2
B. Aircraft Models	3
III. Experimental Apparatus	5
IV. Experimental Procedure	6
V. Results	8
A. Steady State Drag Coefficients	8
B. Parachute Cluster Attitude and Stability	9
VI. Wake Surveys	11
A. Introduction	11
B. Models	11
C. Experiments	12
D. Results	13
VII. Conclusions	14
References	15

ILLUSTRATIONS

FIGURE		PAGE
1.	Gore Patterns for Ringslot and Solid Flat Parachute Models	16
2.	Model Arrangement	17
3.	Three Views of Model Aircraft Used for Extraction Parachute Studies	18
4.	Location of Root and Inboard Flaps on the CV-2 Caribou Aircraft	19
5.	Cross Section View of Double Slotted Fowler Flap in Normal and Deflected Position	20
6.	Root and Inboard Flap Deflections (15°) on 1/16 Scale Caribou Model	21
7.	Propeller Motor for Caribou Airplane Model, Scale 1/16	22
8.	University of Minnesota Horizontal Return Wind Tunnel	23
9.	Aircraft Model Installation as seen from Downstream and Normal Cameras	24
10.	Aircraft Ground Plane Installation	25
11.	Definitions of Stability Characteristics	26
12.	Drag Coefficient Ratios of Single and Clustered Solid Flat and Ringslot Parachutes under Powered and Unpowered Flight Conditions	27
13.	Drag Coefficient Ratios of Single and Clustered Solid Flat and Ringslot Parachutes with and without Flap Deflection	28
14.	Drag Coefficient Ratios of Single and Clustered Solid Flat and Ringslot Parachutes in Freestream and with Ground Effects	29
15.	Steady State Drag on Cluster of 3 Ringslot Parachutes versus Time	30

ILLUSTRATIONS (CONT.)

FIGURE		PAGE
16.	Schematic Illustration of Extreme Extraction Line Positions for Solid Flat Configurations with Power, No Flap Deflection	31
17.	Extraction Line Range of Movement for Single Ringslot Parachute Configurations	32
18.	Envelopes of the Areas Swept by the Confluence Points of the Solid Flat Parachute Configurations, Power-Off, 0° Flap Setting and Freestream Condition	33
19.	Envelopes of the Areas Swept by the Confluence Points of the Solid Flat Parachute Configurations, Power-Off, 0° Flap Setting and near the Ground Condition ($h/D_0 = 2.34$)	34
20.	Envelopes of the Areas Swept by the Confluence Points of the Solid Flat Parachute Configurations, Power-Off, 0° Flap Setting and near the Ground Condition ($h/D_0 = 1.17$)	35
21.	Envelopes of the Areas Swept by the Confluence Points of the Solid Flat Parachute Configurations, Power-On, 0° Flap Setting and Freestream Condition	36
22.	Envelopes of the Areas Swept by the Confluence Points of the Solid Flat Parachute Configurations, Power-On, 0° Flap Setting and near the Ground Condition ($h/D_0 = 2.34$)	37
23.	Envelopes of the Areas Swept by the Confluence Points of the Solid Flat Parachute Configurations, Power-On, 0° Flap Setting and near the Ground Condition ($h/D_0 = 1.17$)	38
24.	Envelopes of the Areas Swept by the Confluence Points of the Solid Flat Parachute Configurations, Power-Off, 15° Flap Setting and Freestream Condition	39

ILLUSTRATIONS (CONT.)

FIGURE		PAGE
25.	Envelopes of the Areas Swept by the Confluence Points of the Solid Flat Parachute Configurations, Power-Off, 15° Flap Setting and near the Ground Condition ($h/D_0 = 2.34$)	40
26.	Envelopes of the Areas Swept by the Confluence Points of the Solid Flat Parachute Configurations, Power-Off, 15° Flap Setting and near the Ground Condition ($h/D_0 = 1.17$)	41
27.	Envelopes of the Areas Swept by the Confluence Points of the Solid Flat Parachute Configurations, Power-On, 15° Flap Setting and in Freestream Condition	42
28.	Envelopes of the Areas Swept by the Confluence Points of the Solid Flat Parachute Configurations, Power-On, 15° Flap Setting and near the Ground Condition ($h/D_0 = 2.34$)	43
29.	Envelopes of the Areas Swept by the Confluence Points of the Solid Flat Parachute Configurations, Power-On, 15° Flap Setting and near the Ground Condition ($h/D_0 = 1.17$)	44
30.	Envelopes of the Areas Swept by the Confluence Points of the Ringslot Parachute Configurations, Power-Off, 0° Flap Setting and in Freestream Condition	45
31.	Envelopes of the Areas Swept by the Confluence Points of the Ringslot Parachute Configurations, Power-Off, 0° Flap Setting and near the Ground Condition ($h/D_0 = 2$)	46
32.	Envelopes of the Areas Swept by the Confluence Points of the Ringslot Parachute Configurations, Power-Off, 0° Flap Setting and near the Ground Condition ($h/D_0 = 1$)	47

ILLUSTRATIONS (CONT.)

FIGURE		PAGE
33.	Envelopes of the Areas Swept by the Confluence Points of the Ringslot Parachute Configurations, Power-On, 0° Flap Setting and in Freestream Condition	48
34.	Envelopes of Areas Swept by the Confluence Points of the Ringslot Parachute Configurations, Power-On, 0° Flap Setting and near the Ground Condition ($h/D_0 = 2$)	49
35.	Envelopes of Areas Swept by the Confluence Points of the Ringslot Parachute Configurations, Power-On, 0° Flap Setting and near the Ground Condition ($h/D_0 = 1$)	50
36.	Envelopes of Areas Swept by the Confluence Points of the Ringslot Parachute Configurations, Power-Off, 15° Flap Setting and in Freestream Condition	51
37.	Envelopes of Areas Swept by the Confluence Points of the Ringslot Parachute Configurations, Power-Off, 15° Flap Setting and near the Ground Condition ($h/D_0 = 2$)	52
38.	Envelopes of Areas Swept by the Confluence Points of the Ringslot Parachute Configurations, Power-Off, 15° Flap Setting and near the Ground Condition ($h/D_0 = 1$)	53
39.	Envelopes of Areas Swept by the Confluence Points of the Ringslot Parachute Configurations, Power-On, 15° Flap Setting and in Freestream Condition	54
40.	Envelopes of Areas Swept by the Confluence Points of the Ringslot Parachute Configurations, Power-On, 15° Flap Setting and near the Ground Condition ($h/D_0 = 2$)	55

ILLUSTRATIONS (CONT.)

FIGURE		PAGE
41.	Envelopes of Areas Swept by the Confluence Points of the Ringslot Parachute Configurations, Power-On, 15° Flap Setting and near the Ground Condition ($h/D_0 = 1$)	56
42.	Three View of the 1/48 Scale Caribou Model Aircraft Used for Wake Surveys . . .	57
43.	Caribou Airplane Model, 1/48 Scale, with Inboard Flaps	58
44.	Airplane Models Suspended in Wind Tunnel Test Sections	59
45.	Pressure Survey Rake	60
46.	Rake Positions for Wake Survey of Caribou Aircraft	61
47.	Pressure Field Indications and Constructed Isobars	62
48.	Dynamic Pressure Distribution of Caribou Airplane Model at Station 1 in Free-stream, Unpowered and Flaps Normal Conditions	63
49.	Dynamic Pressure Distribution of Caribou Airplane Model at Station 1 in Free-stream, Powered and Flaps Normal Conditions	64
50.	Dynamic Pressure Distribution of Caribou Airplane Model at Station 1 in Free-stream, Unpowered and Flaps Down Conditions	65
51.	Dynamic Pressure Distribution of Caribou Airplane Model at Station 1 in Near Ground, Unpowered and Flaps Down Conditions	66
52.	Dynamic Pressure Distribution of Caribou Airplane Model at Station 2 in Free-stream, Unpowered and Flaps Normal Conditions	67

ILLUSTRATIONS (CONT.)

FIGURE		PAGE
53.	Dynamic Pressure Distribution of Caribou Airplane Model at Station 2 in Free-stream, Unpowered and Flaps Down Conditions	68
54.	Dynamic Pressure Distribution of Caribou Airplane Model at Station 2 in Near Ground, Unpowered, Flaps Down Conditions	69
55.	Dynamic Pressure Distribution of Caribou Airplane Model at Station 3 in Free-stream, Unpowered and Flaps Normal Conditions	70
56.	Dynamic Pressure Distribution of Caribou Airplane Model at Station 3 in Free-stream, Powered and Flaps Normal Conditions	71
57.	Dynamic Pressure Distribution of Caribou Airplane Model at Station 3 in Free-stream, Unpowered and Flaps Down Conditions	72
58.	Dynamic Pressure Distribution of Caribou Airplane Model at Station 3 in Near Ground, Unpowered and Flaps Normal Conditions	73
59.	Dynamic Pressure Distribution of Caribou Airplane Model at Station 3 in Near Ground, Unpowered and Flaps Down Conditions	74
60.	Airplane Axes X and X'	75
61.	Dynamic Pressure Distribution of Caribou Airplane Model in Vertical Plane Containing Airplane Axis X in Free-stream, Unpowered and Powered, Flaps Normal and Deflected Conditions	76
62.	Dynamic Pressure Distribution of Caribou Airplane Model in Vertical Plane Containing Airplane Axis X' in Free-stream, Unpowered and Powered, and Flaps Normal Conditions.	77

ILLUSTRATIONS (CONT.)

FIGURE		PAGE
63.	Dynamic Pressure Distribution of Caribou Airplane Model in Vertical Plane Containing Airplane Axis X' in Free- stream, Unpowered and Flaps Deflected Conditions	78
64.	Dynamic Pressure Distribution of Caribou Airplane Model in Vertical Plane Containing Airplane Axis X' in Near Ground, Unpowered and Flaps Deflected Conditions . .	79

TABLES

	PAGE
I. Test Program for Study of Drag and Stability Characteristics of Extraction Parachute Systems (Wind Tunnel Velocity $V_{\infty} = 91$ fps) .	80
II. Drag and Stability Characteristics of the Solid Flat Parachute Configurations	81
III. Drag and Stability Characteristics of the Ringslot Parachute Configurations	83
IV. Wake Survey Test Configurations	85

SYMBOLS*

C_{D_0}	drag coefficient based on nominal diameter
D	steady state drag
D_0	nominal diameter
D_p	projected diameter
d	propeller diameter
h	distance between ground plane and aircraft center of gravity
N	propeller RPM
n	number of parachutes
q	local dynamic pressure
S_0	nominal area
T	propeller thrust (per propeller)
V	air velocity
α	parachute cluster angle of attack
$\beta_{3/4}$	propeller pitch at 0.75 radius
θ	root and inboard flap deflection
ϕ	deflection angle of extraction line

Subscripts:

f	full-scale conditions
m	scaled model conditions
s	slipstream conditions
∞	freestream conditions

*Additional symbols, when used, are defined in the text.

Contrails

I. INTRODUCTION

In conventional air cargo delivery systems, either a single or a cluster of parachutes exert their force upon an extraction line which, in turn, moves the cargo platform out of the airplane and then deploys the main parachutes. The general behavior of this parachute extraction system in the wake of an unpowered airplane model has been investigated previously (Ref 1). In the following study certain parachute performance characteristics of the extraction system have been investigated in the wake of the same airplane model but with windmilling or powered propellers, with wing trailing flaps in normal and deflected positions, and with or without ground effects. As substantiation of the expected findings, the pressure distribution in the wake of the powered and unpowered airplane models was measured.

In particular, the following experiments have been performed:

- 1) Measurement of the steady state drag coefficients for single and clustered parachutes of up to four canopies in the wake of the aircraft.
- 2) Study of stability characteristics of single and clustered parachutes in the airplane wake.
- 3) Measurement of the pressure distribution of the powered and unpowered airplane models in three different planes in the wake.

All experiments involving parachutes were carried out with models of circular solid flat and circular flat ringslot parachutes.

II. MODELS

Except for some modifications, the models and the equipment used in these studies were the same as those used in Ref 1. However, for orientation purposes the main model characteristics shall be repeated.

The model parachutes were made as flexible as standard parachute material and conventional fabrication methods permit. Furthermore, the models were as large as possible in view of acceptable wind tunnel blockage effects. Under consideration of the various circumstances, parachute models with a nominal diameter of about 16 in. and a model aircraft with a 6 ft wingspan were then selected. These dimensions correspond to a scale factor of 1/16.

A. Parachute Models

Figure 1 shows gore patterns for both circular flat ringslot parachutes and circular solid flat parachutes.

1. Ringslot Parachutes

The flat ringslot parachute models simulated the standard 22 ft diameter, 28 gore ringslot extraction parachutes. The models were fabricated with the constructed diameter shown in Fig 1a, yielding a nominal diameter, D_0 , of 16.0 in. and a calculated total porosity of approximately 12.7%.

2. Solid Flat Parachutes

The circular solid flat models were scaled from an assumed solid flat parachute which has the same drag area as the standard 22 ft diameter ringslot parachute. The nominal diameter of this prototype parachute amounted to 18.2 ft. Thus, the models were fabricated as shown (Fig 1b) having a nominal diameter of 13.65 in. The drag coefficients used in the computation amounted to $C_{D0} = 0.55$ and $C_{D0} = 0.75$ for the ringslot and solid flat parachutes, respectively. The 28 gore solid flat models were constructed of 1.1 oz standard parachute nylon cloth with an air permeability of 90-120 ft³/ft²-min.

3. Extraction Line and Risers

The single extraction parachute and the clusters are, in full size, equipped with a 60 ft extraction line to which each parachute is connected by means of a 5 ft riser. Scaling these lengths gave model lines of 45 in. and 3.75 in., respectively (Fig 2).

B. Aircraft Models

For the studies in Ref 1, the de Havilland DHC-4 Caribou was chosen as a typical aircraft, and the de Havilland Aircraft Company of Canada, Ltd., provided the dimensions according to which the 1/16 model had been constructed. Figure 3 shows a schematic drawing of the Caribou with model dimensions.

For the purpose of this newer study, the existing Caribou model with 0° flap deflection was modified to simulate 15° deflection of the root and inboard flaps. The location of the root and inboard sets of the double-slotted Fowler flaps is shown in Fig 4, while Fig 5 shows schematically the cross section of the flaps, including hinge point locations, at deflections of 0° and 15° . The flaps of the finished model are pictured in Fig 6. These deflected flaps were installed such that they can be removed and 0° flaps reinstalled.

To simulate the wake of a powered aircraft, appropriate power plants had to be installed so that the propellers could produce the proper amount of thrust.

The flight conditions of the parachute actuation are:

- 1) Full pitch propellers ($\beta_{3/4} = 20^\circ$)
- 2) Airspeed = 130 knots
- 3) Propeller rpm = 1150-1250.

Corresponding to these conditions, the Hamilton Standard Company, Windsor Locks, Connecticut, provided a value for thrust generated by each propeller, amounting to $T = 1910$ lb.

As criteria for the scaling of the powered propeller, it was postulated that the ratios of the dynamic pressure in the propeller slipstream to the freestream dynamic pressure for the model and the prototype are identical, $(q_s/q_\infty)_m = (q_s/q_\infty)_f$ (Ref 2).

Explicitly this may be written as

$$\left(\frac{T / \frac{d^2 \pi}{4}}{q_\infty} \right)_m = \left(\frac{T / \frac{d^2 \pi}{4}}{q_\infty} \right)_f$$

which represents an equation of thrust coefficients, T_c . Based on information from the propeller manufacturer, the coefficient amounted to $T_c = 1.245$ for 1200 rpm. With the chosen model scale and the wind tunnel velocity, the necessary thrust for the model was found to be $T_m = 1.32$ lb which satisfies the equation and air speed specified above.

From wind tunnel experiments, a motor was selected which provided this thrust yet was small enough to fit the airplane model geometry. Such a motor was obtained from Kearfott Division of General Precision, Inc., with 400 cycles, 3 phase electric input, up to 11,000 rpm, and 3/4 HP. This motor is shown in Fig 7.

III. EXPERIMENTAL APPARATUS

All of the extraction parachute tests were performed with the airplane model, along with the plane which simulates the ground, installed in the open test section of the subsonic horizontal return wind tunnel of the University of Minnesota (Fig 8).

Two movie cameras were used to record the behavior of the parachutes. One camera was placed alongside the open section of the tunnel to obtain a view normal to the free-stream, while the second camera, placed inside the tunnel, took pictures from downstream toward the test section. The camera locations are shown in Fig 8.

A force balance, to which the extraction line was fastened, consisted of a standard strain gage bridge affixed to a cantilever beam. The bridge output was amplified and recorded by means of an oscillograph. The force balance was located at the mean center of gravity of the airplane.

The rate of revolution of the propeller motors could be regulated by means of a varying voltage input which was drawn from a 400 cycle, 3 phase generator with a total capacity of 2.5 kilowatts. Propellers, motors and generator worked satisfactorily throughout the testing period.

IV. EXPERIMENTAL PROCEDURE

The airplane model was suspended in the wind tunnel in two different ways, once for the adjustment of the proper propeller thrust and also for the measurement of the parachute force.

The proper propeller thrust was defined as the one which equaled the drag of the airplane at the particular wind tunnel speed. This could be achieved by regulating the electric input to the motors. For the determination of these power conditions, the airplane model was suspended by means of a vertical strut to the ceiling of the wind tunnel test section. Between ceiling and strut a strain gage was arranged which measured the resultant force between model and wind tunnel, and for the proper power or thrust setting this balance had to show a zero-resultant force. Since the thrust was adjusted to balance the drag, the measurement of the absolute thrust output was not necessary. From measurements of the thrust produced by the motor and model propeller as a unit, the thrust per propeller amounted to approximately 1.3 lbs.

After completion of these measurements, the airplane was securely fastened to the wind tunnel structure by means of the vertical strut, now with inactive strain gage, and by fastening the wing tips to the side walls of the wind tunnel test section. Under these conditions the parachute force was then applied to the centrally located internal strain gage. The results of these measurements then represent the parachute forces under the given conditions of power and flap setting. The suspension of the airplane model in the wind tunnel is illustrated in Fig 9.

To simulate the ground effect, a plywood sheet was installed in the test section of the tunnel at various distances, h , from the airplane centerline. The open section arrangement is shown schematically in Fig 10. The plywood was removed for simulation of freeflight conditions, $h/D_0 = \infty$.

When installed, the ground plane extended one mean aerodynamic chord ahead of the leading edge of the wing, and 1.5 nominal parachute diameters downstream from the vent position of a fully inflated parachute.

The actual test conditions are shown in Table I which also gives the various parachute configurations. In order to record the stability characteristics of the parachute configurations under the different flight conditions, film recordings were made in the two main directions for the duration of 7 to 10 sec during each run. The indicated results

Contrails

are average values obtained from oscillograph recordings covering the same period. Since the single and the clustered parachutes moved very rapidly at random, this time was sufficient to establish average values with satisfactory accuracy.

To obtain the degree of stability and the attitudes of the parachutes from the movies, the angle in the vertical plane swept out by the extraction line during a 7 to 10 sec period was measured with respect to the freestream direction. From downstream the movies give the area, perpendicular to the freestream, swept out by the cluster confluence point. Also, for the ringslot configurations, the angle with freestream (attitude), at which the extraction line would most probably be found at any time, could be determined; hence, an angle of attack was defined. Measurement of the steady state drag (D) was taken during the same 7-10 sec period.

V. RESULTS

The results of the measurements are presented as average drag coefficients and the stability characteristics of the various configurations under the different flight conditions.

The drag coefficients are derived according to the relationship

$$C_{D_0} = \frac{D}{q_{\infty} n S_0}$$

The stability characteristics are presented in terms of deflection angles, θ_1 and θ_2 , of the extraction line from the horizontal direction, an average angle of attack, α , of this line when the extraction system was fairly steady, and in boundary lines of the planes which encompass all observed positions of the confluence point of the short parachute risers. Schematically, these characteristics are illustrated in Figs 2, 11, 16 and 17 through 41.

In detail, the findings can be summarized as follows.

A. Steady State Drag Coefficients

The steady state drag coefficients, C_{D_0} , for various configurations are presented in Tables II and III. From these values, ratios were formed (Figs 12 through 14) whose significant characteristics indicated the following:

- 1) Solid flat parachute drag coefficients behind the powered aircraft model are smaller near the ground than in freestream. Behind the unpowered model, the drag coefficients are larger near the ground than in freestream.
- 2) In general, none of the three variables, i.e., flap setting, ground effects, or powered propellers, appeared to influence the drag coefficient of the ringslot configurations.
- 3) Furthermore, as power is applied, the drag magnitude of ringslot clusters fluctuates considerably more than without power. The drag-time behavior of a cluster with three ringslot parachutes is illustrated in Fig 15. Solid cloth parachutes are less affected.

B. Parachute Cluster Attitude and Stability

As would be expected, the solid flat and ringslot parachutes have markedly different stability characteristics. The solid flat configurations were quite unstable, and the extraction line was in a constant coning motion (Fig 2) with relatively large amplitudes. The extraction line of ringslot clusters performs a slight circular or coning motion about an average attitude or position.

Table II gives the maximum angle of the extraction line of the single and clustered solid flat parachutes above and below the freestream direction, which were observed during the 7 to 10 sec test period.

The same boundary line positions are given in Table III for the ringslot configurations. Since these parachutes are much more stable, their extraction line tends to oscillate through a relatively small range of angle of attack, and the line deviates only occasionally to the limits given by ϕ_1 and ϕ_2 . The angle of deviation from the so-called angle of attack α is given as $\pm \Delta\alpha$ in Table III.

A graphical presentation of the extraction line deflection is given in Figs 16 and 17 for the solid flat and ringslot configurations, respectively. Comparing both figures, one notices that the single solid flat parachute is the most unstable configuration, and that a single ringslot parachute is more stable than the most stable cluster of four solid flat canopies.

The extraction line of all solid flat configurations rubbed on the cargo ramp and frame of the cargo door. This contact occurred under all test conditions, hence the extraction line practically never formed a straight line.

Figure 17 illustrates also the definition of angle of attack of the extraction line, α , the average deflection angle $\pm \Delta\alpha$ and the maximum observed deflection.

The camera located downstream of the airplane model also provided interesting views of the parachute movements. These recordings have been evaluated and are schematically presented in Figs 18 through 41. As stated before, the curves are boundaries of planes in which the confluence points of the single or clustered canopies may be located.

Reviewing these figures one notices again the frequently stated differences in stability behavior of the various configurations. New in appearance and very pronounced in these figures is the ground influence, particularly upon the less stable solid flat parachute configurations.

In addition to the results shown in the graphical presentations, the following observations appear to be important enough to be mentioned.

Contrails

The single and the clustered solid flat parachute configurations move over the indicated swept area relatively fast and erratically. This behavior does not appear to be influenced by the conditions of power-on or -off, or flap deflection. If such an influence existed, the motion of the parachute configurations was too erratic to recognize these trends.

It is also interesting to note that the upper extreme positions of the extraction line do not change due to ground influence.

In the experiments with the ringslot configurations, one of the most interesting observations was that under power-on conditions the configurations display more motion than without powered propellers. This is particularly pronounced in the behavior of a single ringslot parachute. Also, the position of the individual canopies with respect to each other is more unsteady under power-on conditions.

Finally, one canopy in a cluster of three or four ringslot parachutes behind the powered model occasionally rotated about its centerline and the suspension lines of this parachute wrapped around each other beginning at the canopy confluence point. It was noted that if this happened, the drag area of that cluster was markedly reduced. This rotation was not observed with the unpowered model. In this report no data are presented which include a drag area reduction because of twisted suspension lines.

VI. WAKE SURVEYS

A. Introduction

The flow conditions of the region in which parachutes deploy and inflate influence significantly the parachute performance characteristics such as snatch force, opening shock, drag, and stability behavior. Numerical information concerning these facts is given in Ref 1, and the ratio of the drag coefficients of parachutes deployed in the wake of a powered or unpowered airplane model given in the preceding chapters, reflects again the difference in flow conditions at the region of parachute functioning. As indicated, the drag area of single and clustered parachutes may vary as much as 20% depending on the flight condition of the airplane. Knowing this difference of the developed drag, it is of interest to investigate the variation of the velocity or pressure distribution in the wake of the aircraft under consideration of powered or unpowered flight as well as the position of the inboard wing flaps and freestream or near ground flight conditions. Motivated by these circumstances, pressure surveys were made in vertical planes perpendicular to the longitudinal axis of the aircraft at three stations downstream from its aft end. The experiments included powered and unpowered flight conditions, deflected and non-deflected flaps as well as freestream and ground effects. The configurations which were studied are shown in Table IV. The study of all possible configurations under power-off and power-on conditions represent an effort which exceeds the possibilities of this project. Therefore, the investigation in powered flight was primarily concerned with the flow condition of the plane immediately adjacent to the aircraft and in the plane which encompasses the inlet area of the inflated parachute with fully extended extraction line.

B. Models

From earlier investigations (Ref 1) which were concerned with the flow condition behind the airplane with windmilling propellers, a model of the de Havilland Caribou airplane, scale 1/48, (Fig 42) was available and has been used in these newer studies. Also, some of the information in Ref 1 has been utilized in the composition of the following presentation.

A new aspect introduced in this study is the effect of the inboard wing flaps in normal and deflected positions (Fig 43). For all power-off conditions, this 1/48 scale model with flaps has been used. In the flap actuated configurations, the flaps were deflected 15° with respect to the root chord line (Fig 5).

A further objective was a study of the power effect. For this purpose, the Caribou model described in Figs 3 through 6 with electric motors, propellers and adjustable flaps was used. As in the previous case, the thrust of the propellers balanced the drag of the airplane, and was the basic condition of the simulated powered flight. The configurations in which this 1/16 scale model with power was used are shown in Table IV.

The smaller 1/48 scale model was suspended in the closed, high speed section of the wind tunnel whereas the larger powered model was arranged in the lower speed open section of the same wind tunnel (Fig 44a, b). In order to assure the validity of comparison of the measurements performed in the two wind tunnel sections, spot checks of the pressure distribution obtained in both sections were made, and they showed satisfactory agreement.

For the pressure measurements in the closed section, a total and static pressure rake with 49 sensing elements was used. The rake is shown in Fig 45. It will be noted that the pressure tubes are arranged in one plane. The rake was positioned as shown in Fig 46 at Stations 1, 2, and 3. The plane of the rake was arranged horizontally at five different vertical distances centered about the longitudinal axis of the airplane. The plane at Station 3 coincides with the plane of the parachute inlet. The distance of the most outwardly located horizontal survey plane is equal or greater than the projected diameter of the inflated parachute. The model parachute inlet area location corresponds to the inlet area of a full size single parachute with a 60 ft extraction line.

On the powered model, Stations 1 and 3 were surveyed with a similar pressure rake system. However, the pressure pick-up tubes were spaced farther apart corresponding to the larger airplane model.

C. Experiments

The smaller model, in the closed section of the wind tunnel, was exposed to a wind velocity of 140 fps. This corresponds to a Reynolds number of $Re = 2.06 \times 10^5$ based on the chord length at the root of the wing. In the open section, the wind velocity was 90 fps yielding, with the larger model, a Reynolds number of 4.18×10^5 , also based on the root chord length of the wing. Figure 44b shows the suspension of this airplane in the open test section.

The pressure measurements provided a network of points showing the dynamic pressure at the plane under investigation. Into these pressure fields lines connecting the points of equal pressure, isobars, were drawn which in their entity show the distribution of the dynamic pressure in the plane. This technique is illustrated in Fig 47.

D. Results

The results of these experiments, using the evaluation technique described above, are shown in Figs 48 to 59. These indicate the dynamic pressure distribution in the wake of the airplane in vertical planes at Stations 1, 2, and 3. Inspecting these figures, one notices the effects of powered propellers, deflected flaps and the influence of the ground. Details of the most interesting findings are discussed later.

In view of the functioning of the parachutes, the flow conditions behind the airplane longitudinal axis, X, and behind the axis of rotation, X', of the windmilling or powered propellers are of particular interest (Fig 60). Therefore, Figs 48 through 59 were re-evaluated in order to show the dynamic pressure in the vertical planes along the airplane axes X and X'. Figures 61 through 64 illustrate this evaluation. One recognizes from the position, course, and slope of the isobars, the effect of the various flight conditions.

In particular, Fig 61 indicates that the propeller slipstream extends into the central region of the aircraft raising the dynamic pressure by approximately 10% when the flight condition changes from windmilling to powered propeller. The slipstream effect is even more pronounced directly behind the propeller. In this case, the dynamic pressure increases in the plane at Station 3 by almost 50% when the propeller is changed from windmilling to powered conditions. Details of the flow in the plane of X' are shown in Fig 62.

An evaluation of Figs 48 through 59 shows that flap deflection and near ground nonpowered flight do not alter significantly the dynamic pressure distribution in the vertical plane along the longitudinal airplane axis X.

Directly behind the propeller, in the plane containing axis X', a flap deflection displaces, in free-stream, the isobars significantly as a comparison of Figs 62 and 63 indicates. This downward stream deflection is reduced when the airplane flies near the ground (Fig 64).

VII. CONCLUSIONS

Reviewing the behavior of the single and clustered parachutes as summarized in Section V.A in light of the wake survey results, one may identify the following trends.

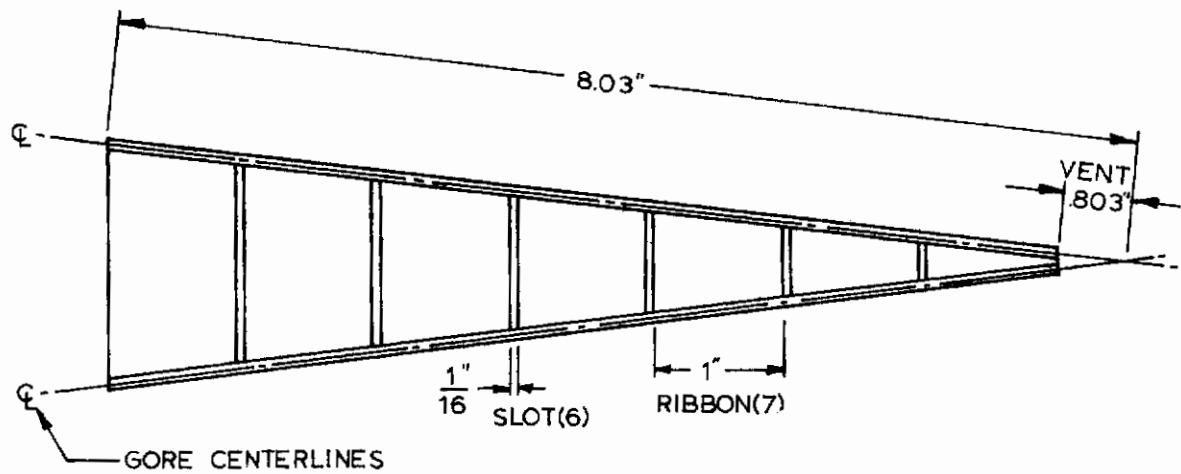
Solid flat parachutes oscillated behind the powered and unpowered aircraft model in a random manner with large amplitudes and varying frequencies, and only general tendencies concerning the drag coefficients of these parachute combinations have been indicated. The wake surveys were not extensive enough to yield explanation of the observed general characteristics.

With the unpowered airplane model, the single and clustered ringslot parachutes remained in a relatively small area surrounding the longitudinal airplane axis, X, regardless of flap setting and distance from the ground. The wake survey indicated that the pressure distribution in this area was affected very little by the airplane configuration and ground proximity. This finding explains the consistent behavior of the ringslot parachutes behind the unpowered aircraft.

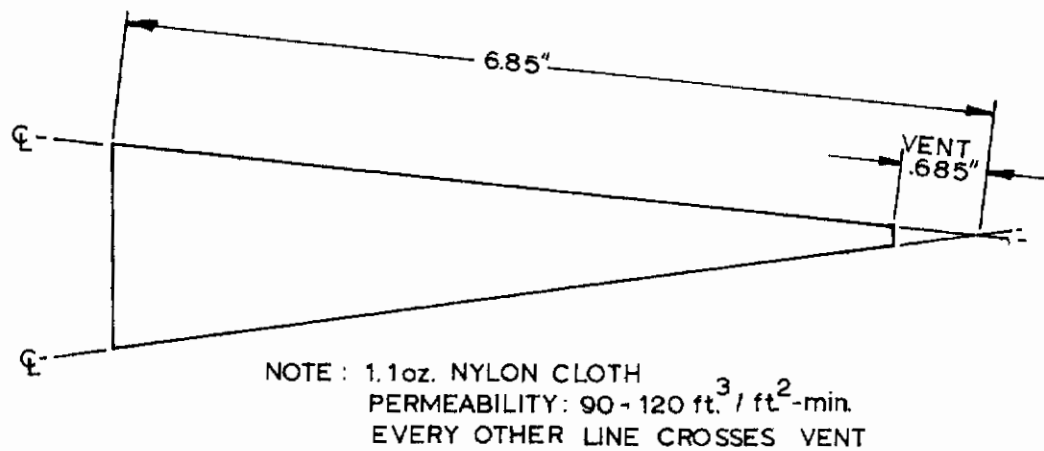
With the powered airplane, the ringslot parachutes showed comparatively stronger fluctuation of the parachute force, and in some cases, larger oscillation amplitudes and higher frequency under the various powered flight conditions. The wake survey indicated that the pressure distribution close to the central axis, X, was changed very slightly by the power effect, but that the area into which the parachute rims extend, showed fields of increased velocity. This probably causes the change of the parachute behavior.

REFERENCES

1. H.G. Heinrich and R. A. Noreen: Drag and Dynamics of Single and Clustered Parachutes in Freestream, and with Wake and Ground Effects, AFFDL-TR-66-104, Wright-Patterson Air Force Base, Ohio, July 1966.
2. Alan Pope: Wind-Tunnel Testing, John Wiley & Sons, Inc., New York, 1954.



a. Gore Pattern for 28-Gore Ringslot Parachute,
 $\lambda_t = 12.67\%$



b. Gore Pattern for 28-Circular Solid Flat Parachute

Fig 1. Gore Patterns for Ringslot and Solid Flat Parachute Models

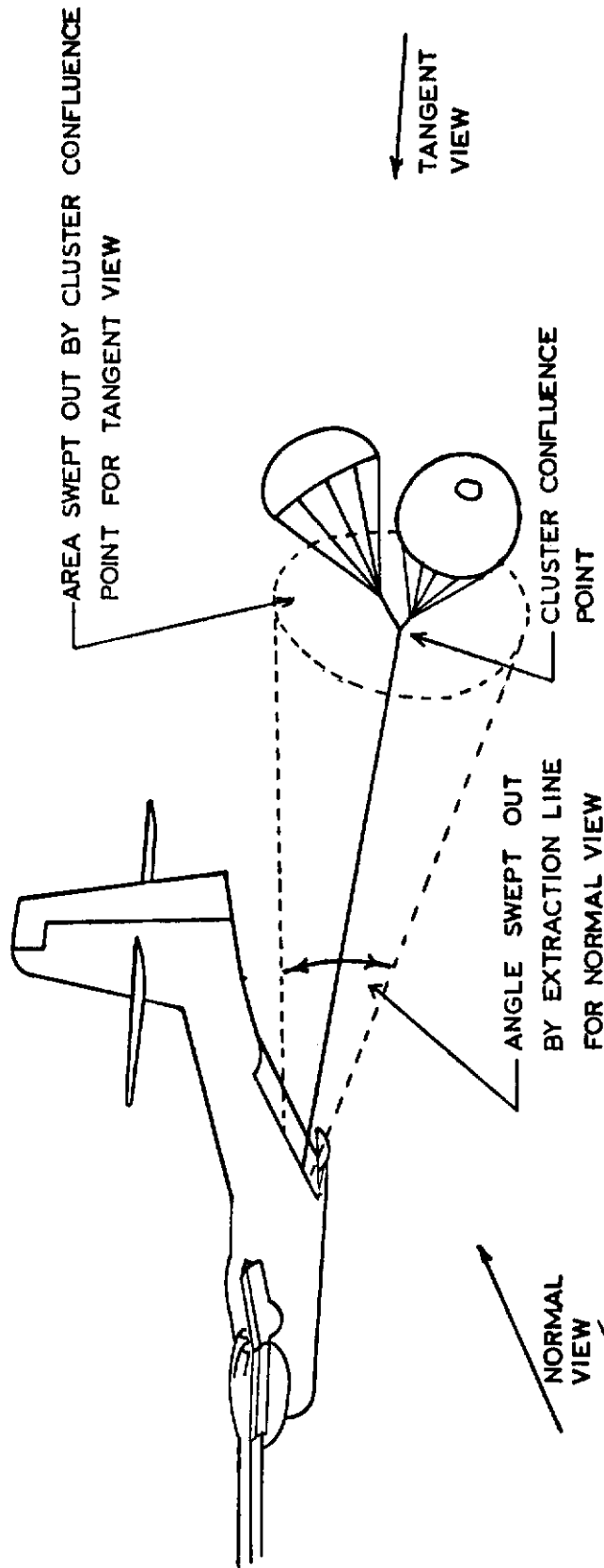
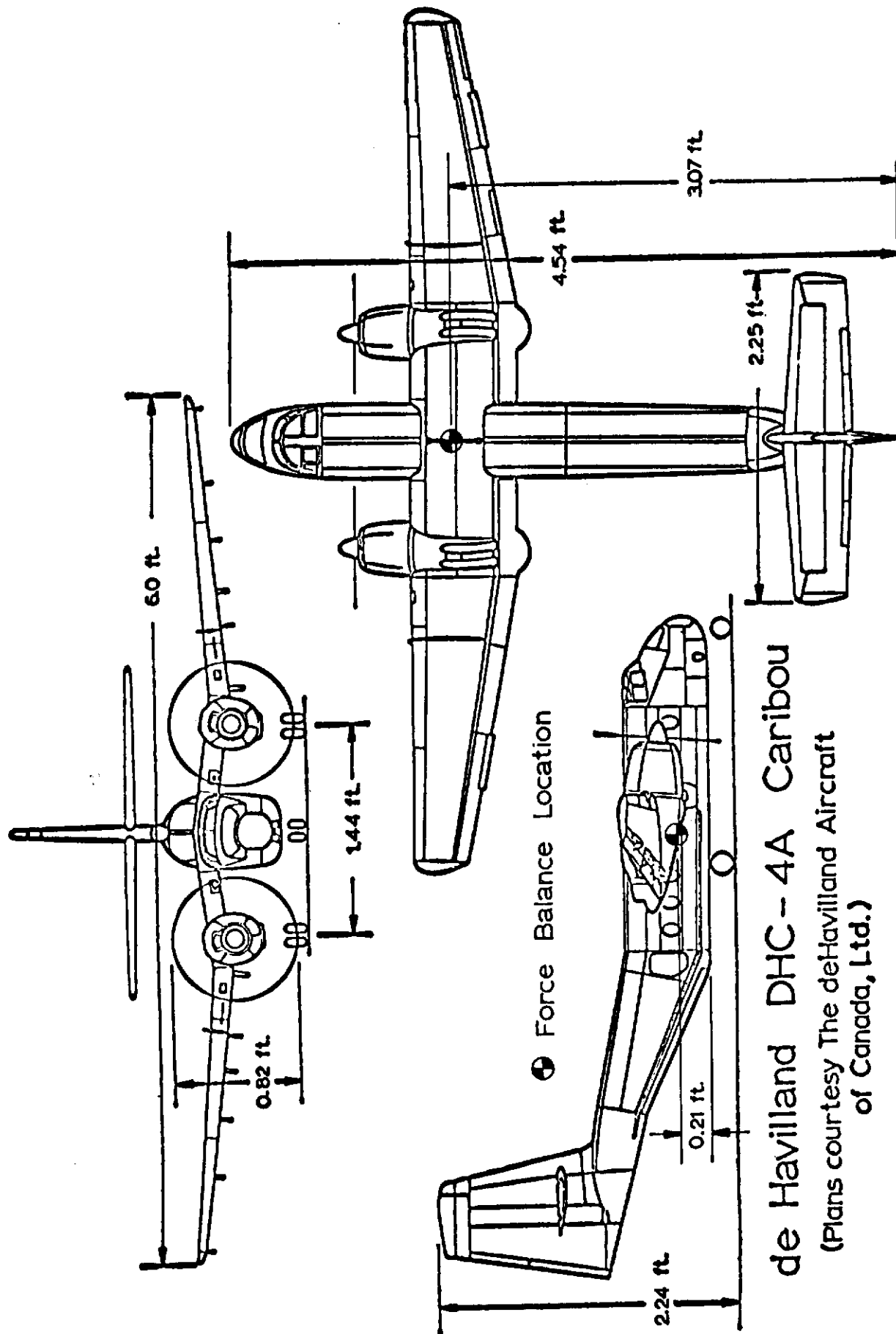


Fig 2. Model Arrangement



de Havilland DHC-4A Caribou
(Plans courtesy The deHavilland Aircraft
of Canada, Ltd.)

Fig 3. Three Views of Model Aircraft Used for Extraction Parachute Studies
(Scale: 1/16)

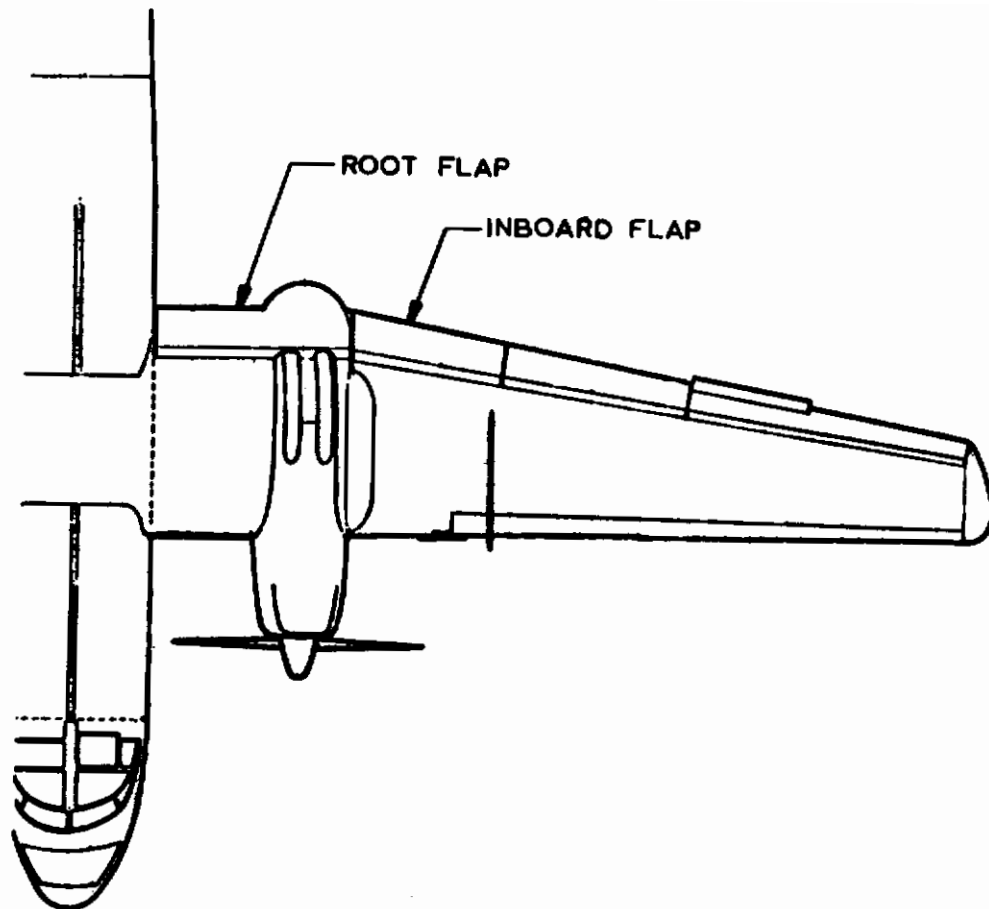


Fig 4. Location of Root and Inboard Flaps on the CV-2 Caribou Aircraft

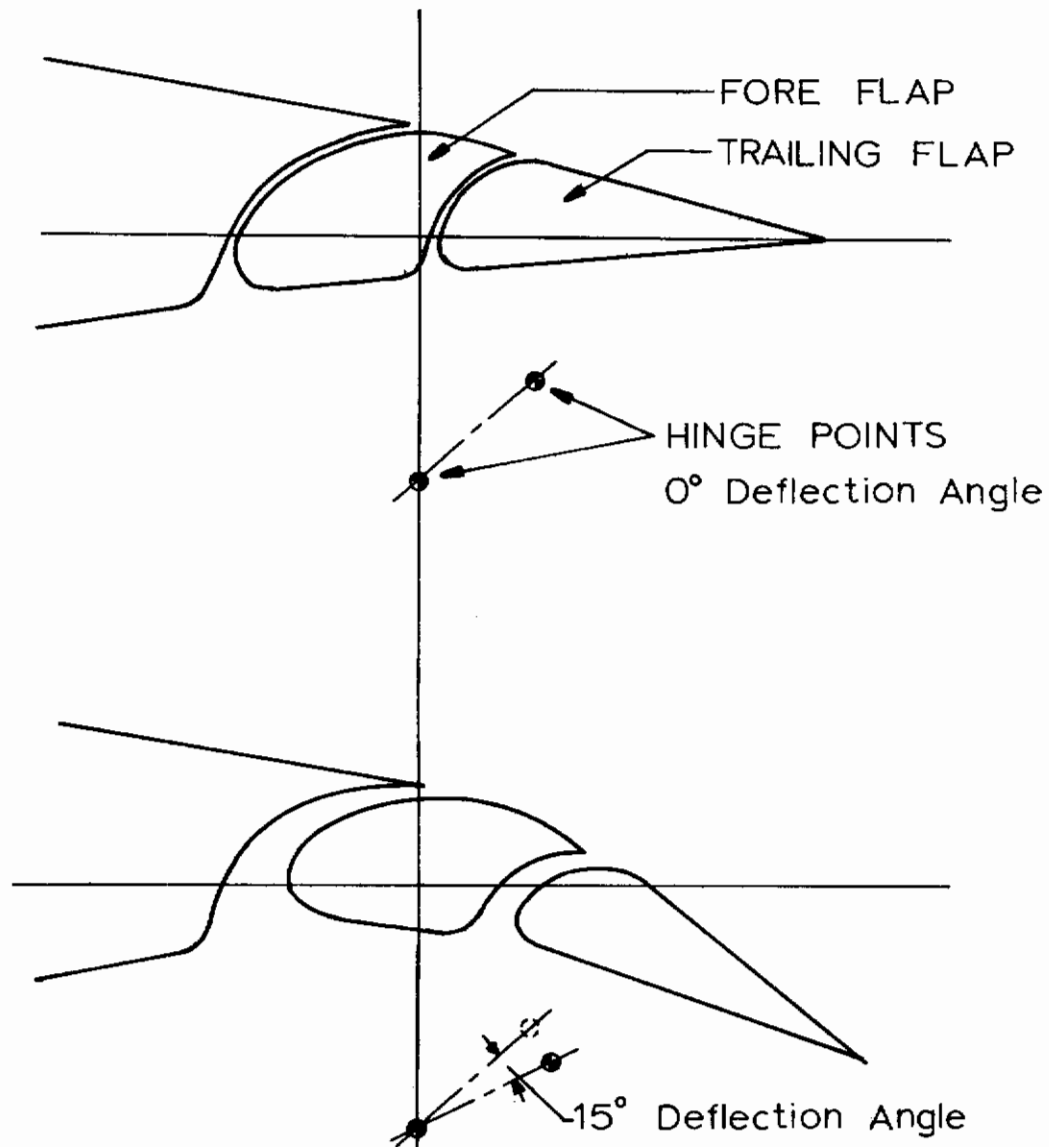


Fig 5.. Cross Section View of Double Slotted Fowler Flap in Normal and Deflected Position

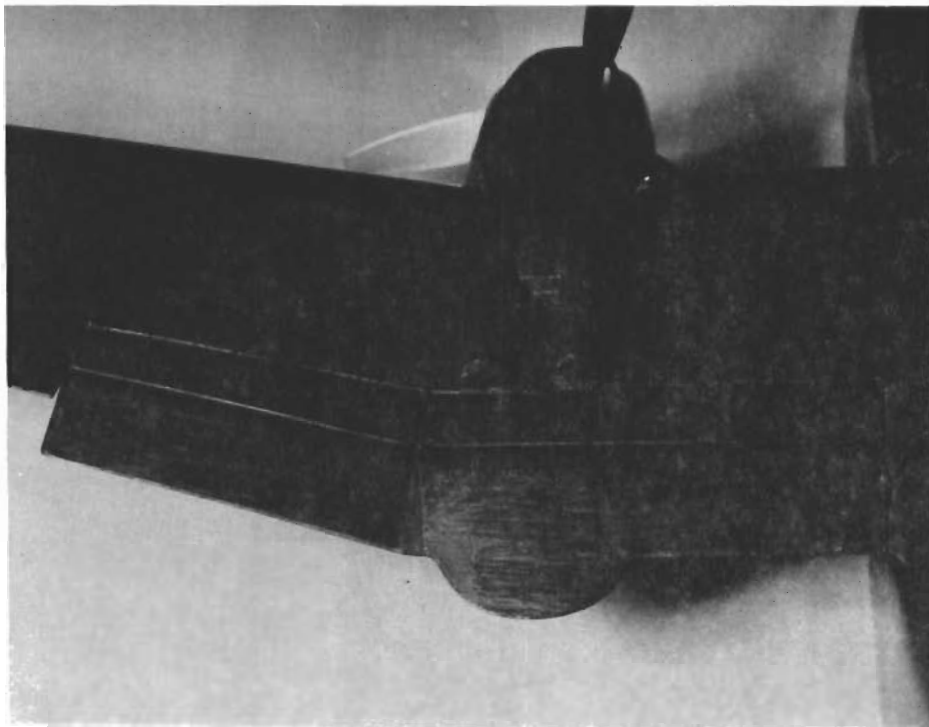
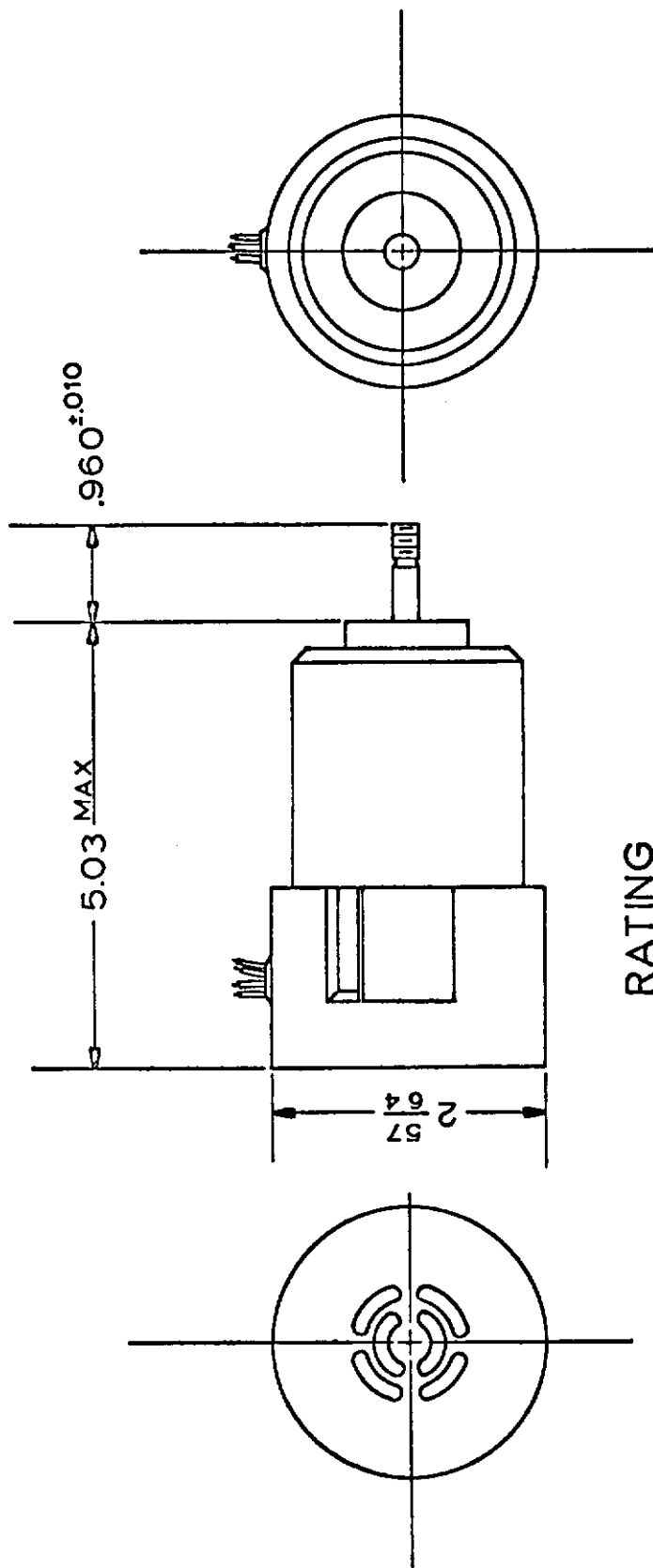


Fig 6. Root and Inboard Flap Deflections (15°) on 1/16 Scale Caribou Model

ALL DIMENSIONS IN INCHES



RATING

0.75 HORSEPOWER, 208 VOLTS
400 CYCLE, 3 PHASE, 11,000 RPM.

Fig 7. Propeller Motor for Caribou Airplane Model, Scale 1/16

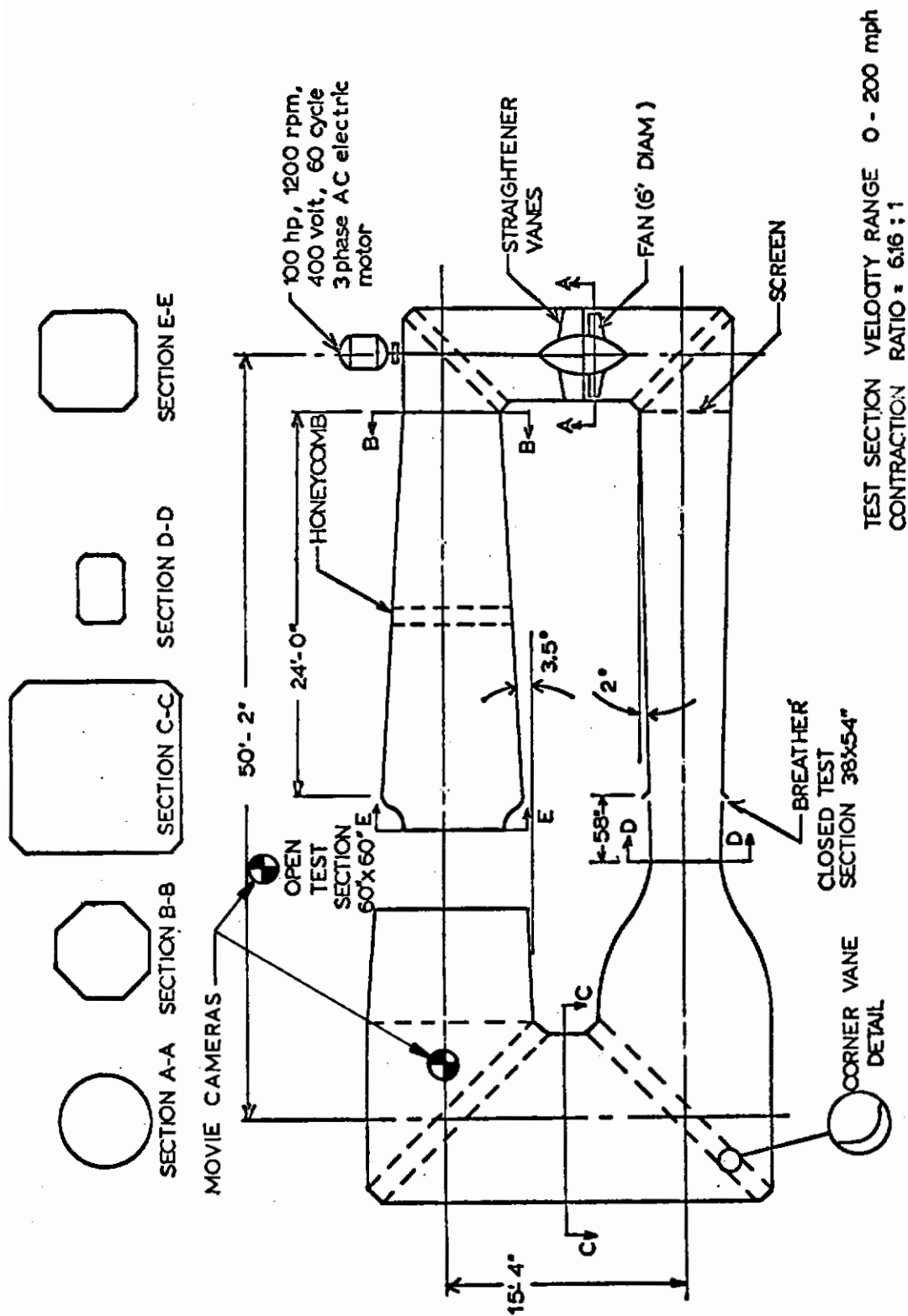
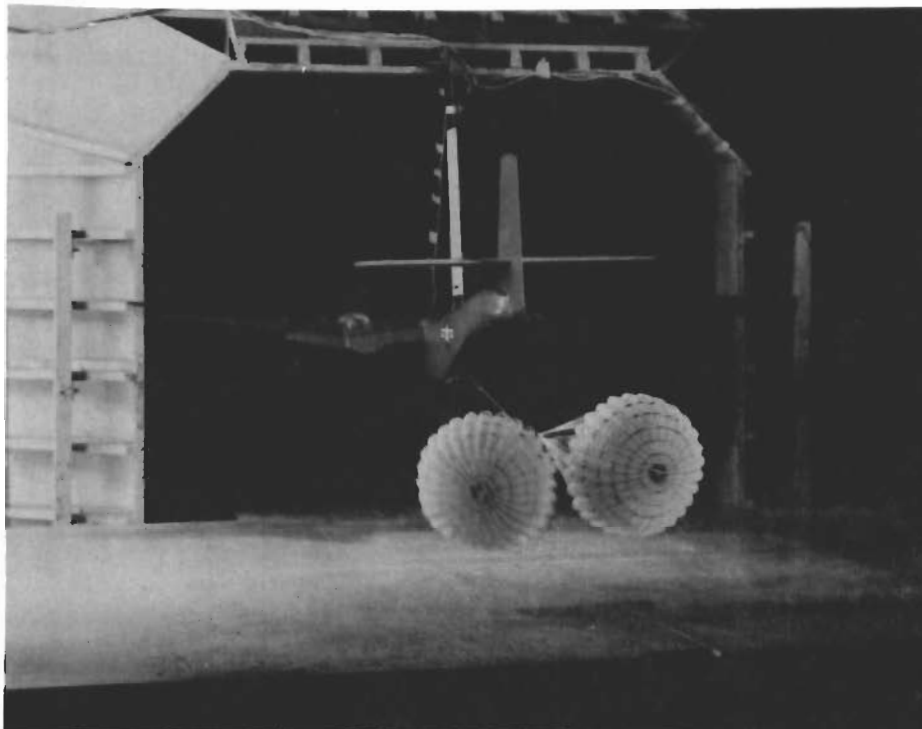
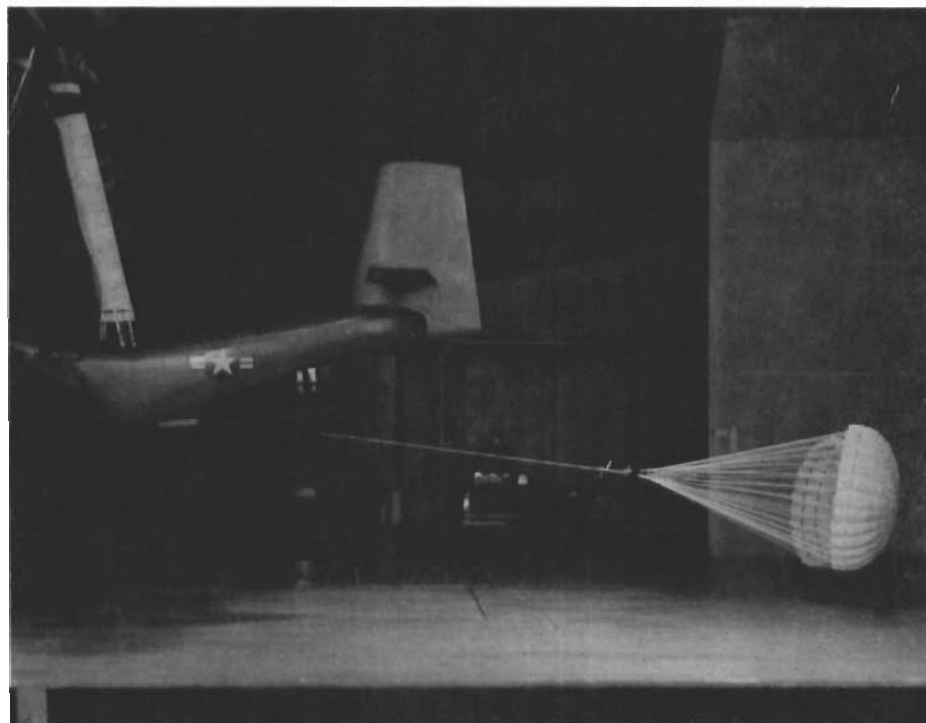


Fig 8. University of Minnesota Horizontal Return Wind Tunnel



a) View of Downstream Camera



b) View from Normal Camera

Fig 9. Aircraft Model Installation as seen from Downstream and Normal Cameras

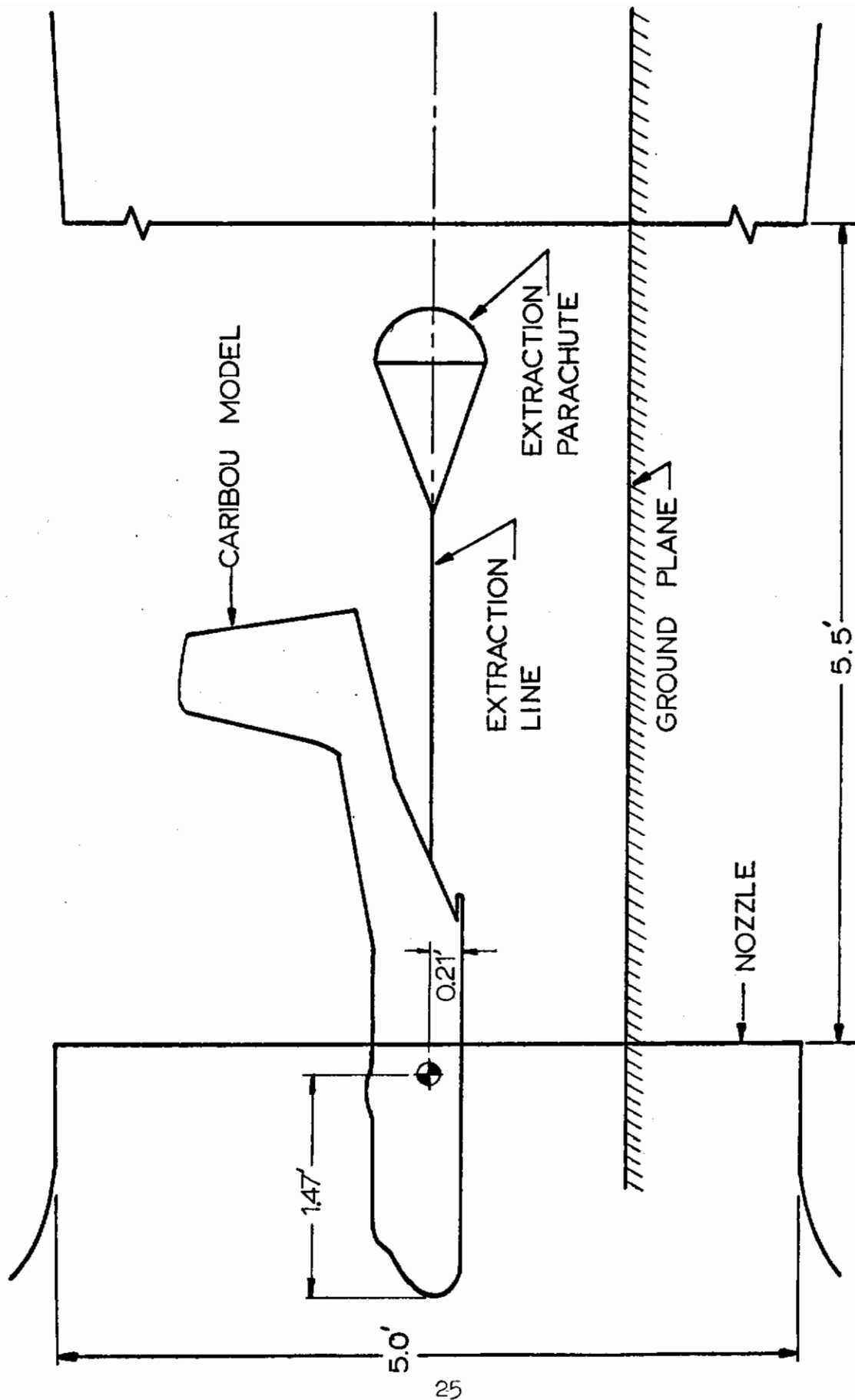


Fig 10. Aircraft Ground Plane Installation

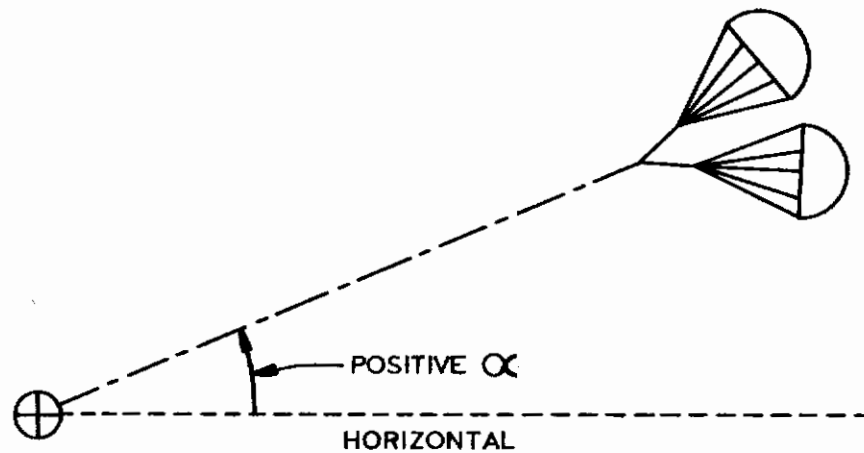
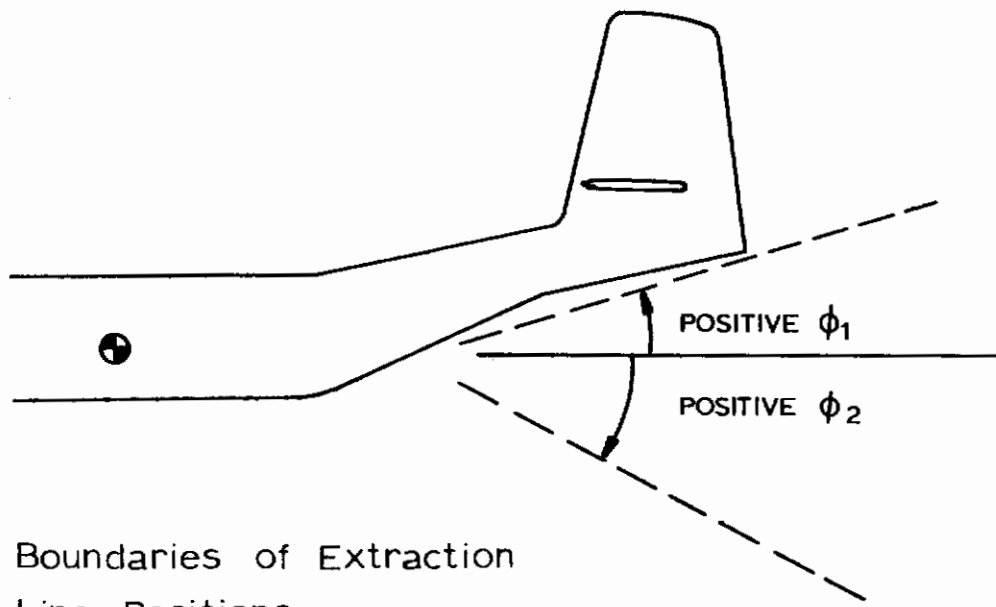
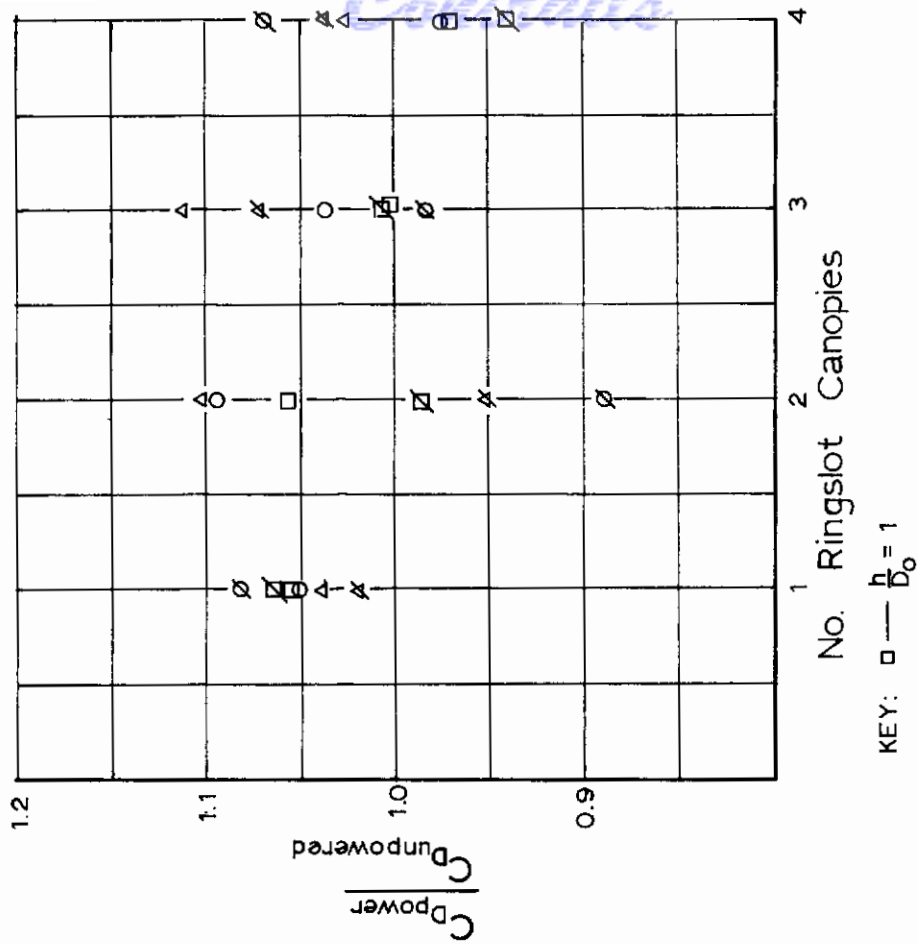
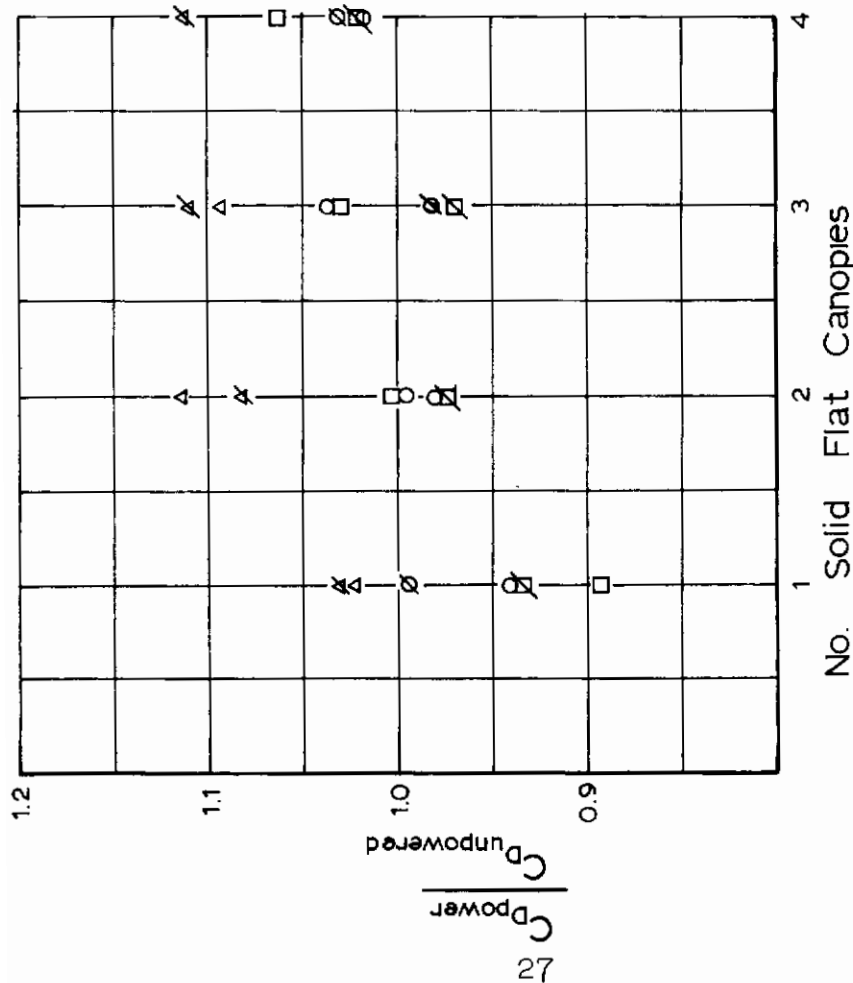
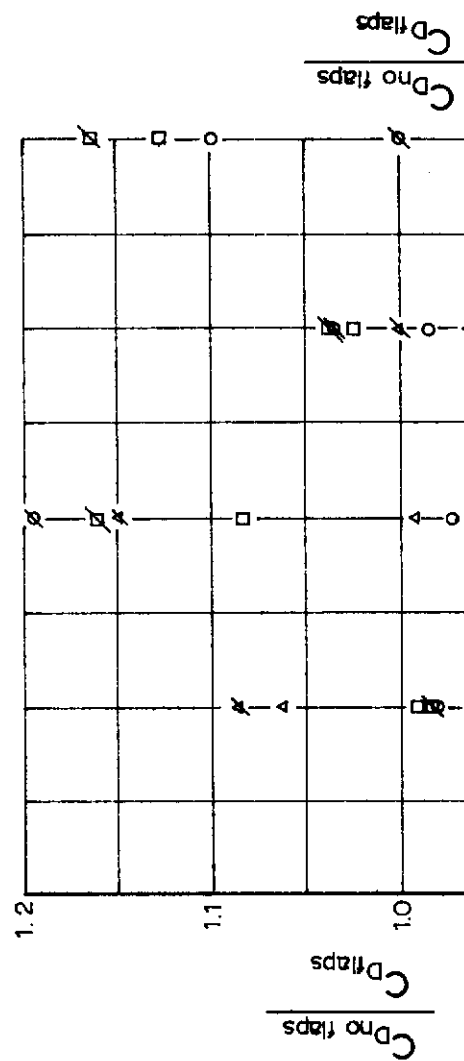


Fig 11. Definitions of Stability Characteristics



SLASHED SYMBOLS INDICATE FLAP DEFLECTION, $\theta = 15^\circ$.

Fig 12. Drag Coefficient Ratios of Single and Clustered Solid Flat and Ringslot Parachutes under Powered and Unpowered Flight Conditions

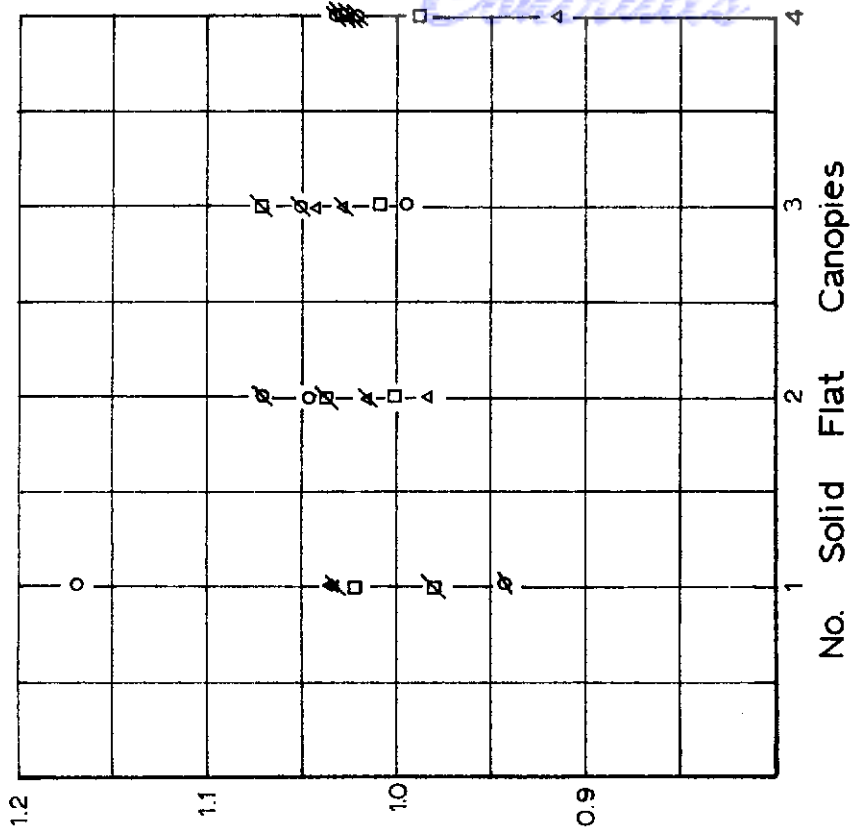


No. Ringslot Canopies

KEY: $\square - \frac{h}{D_0} = 1$

$\circ - \frac{h}{D_0} = 2$

$\Delta - \frac{h}{D_0} = \infty$



No. Solid Flat Canopies

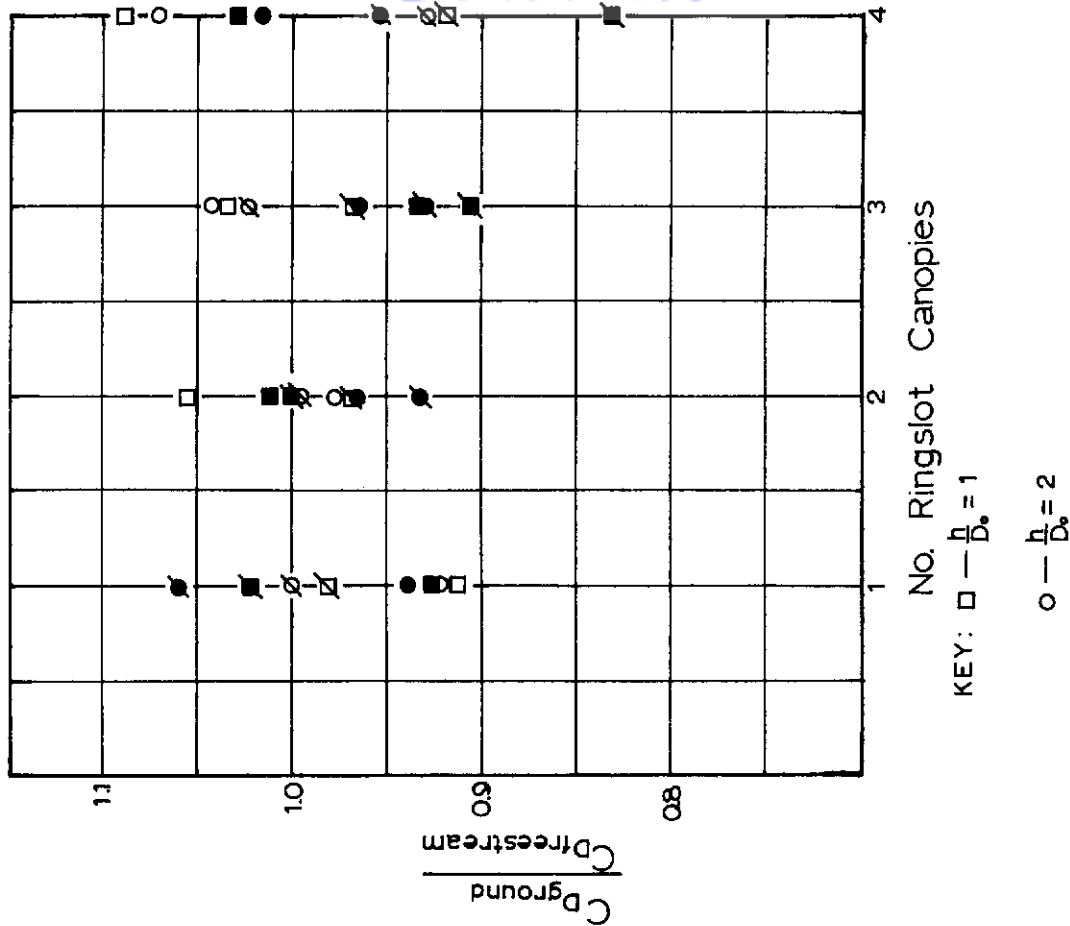
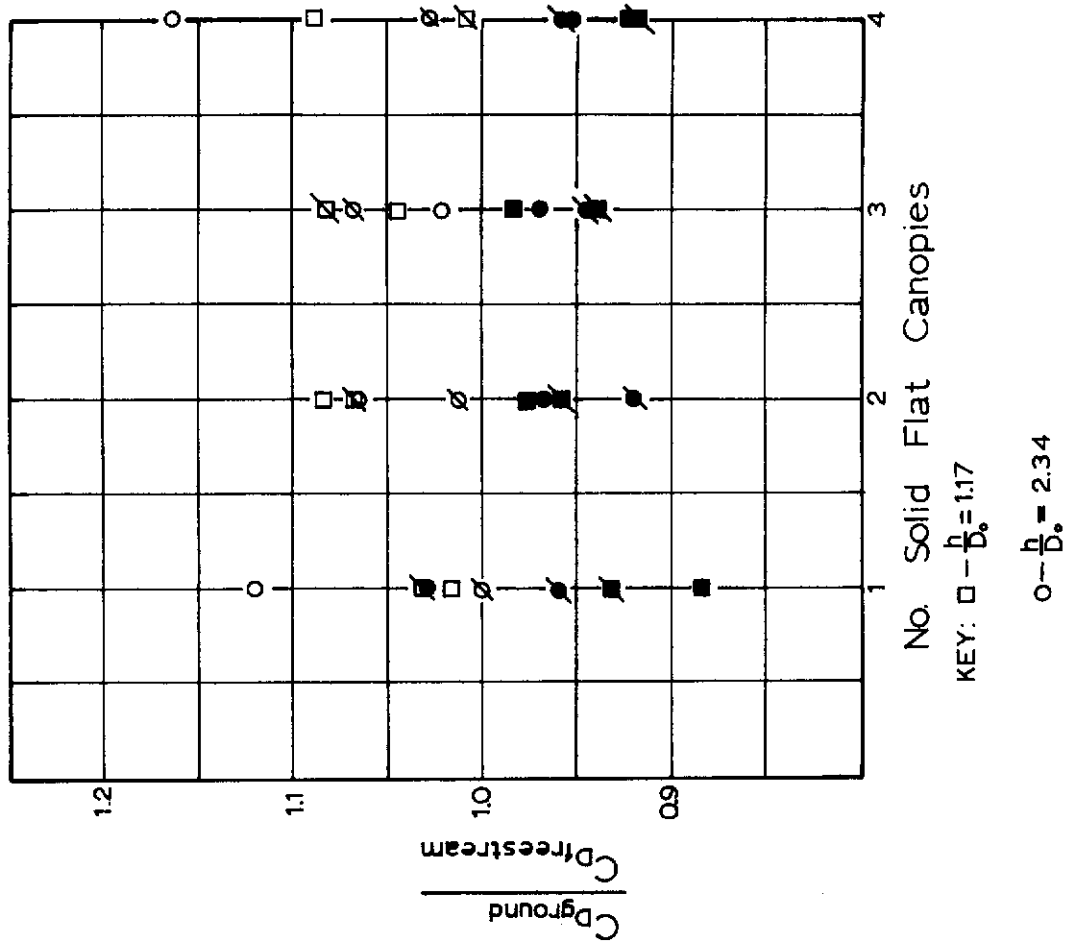
KEY: $\square - \frac{h}{D_0} = 1.17$

$\circ - \frac{h}{D_0} = 2.34$

$\Delta - \frac{h}{D_0} = \infty$

SLASHED SYMBOLS INDICATE POWER ON.

Fig 13. Drag Coefficient Ratios of Single and Clustered Solid Flat and Ringslot Parachutes with and without Flap Deflection



DARKENED SYMBOLS INDICATE POWER ON
SLASHED SYMBOLS INDICATE FLAP DEFLECTION, $\theta = 15^\circ$

Fig 14. Drag Coefficient Ratios of Single and Clustered Solid Flat and Ringslot Parachutes in Freestream and with Ground Effects

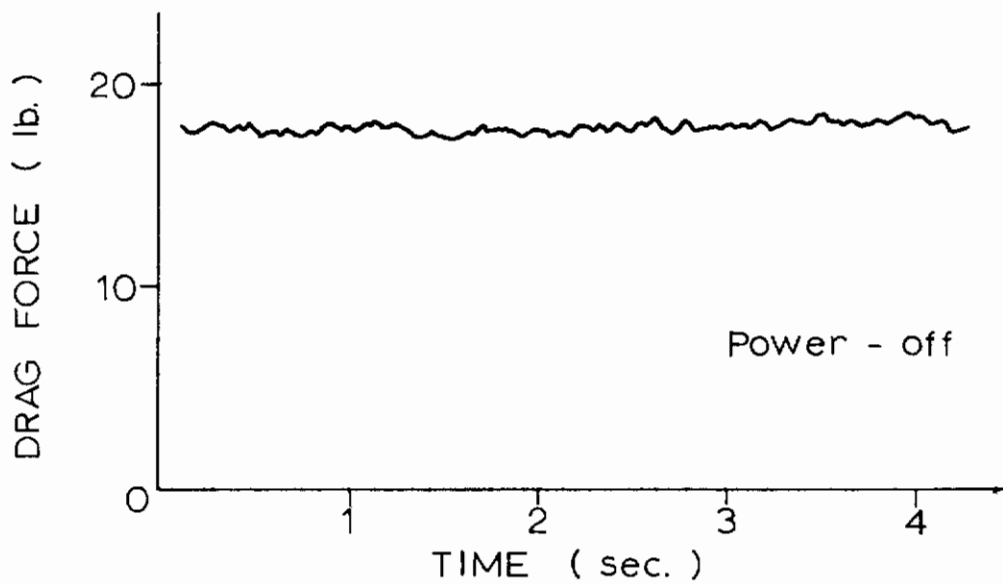
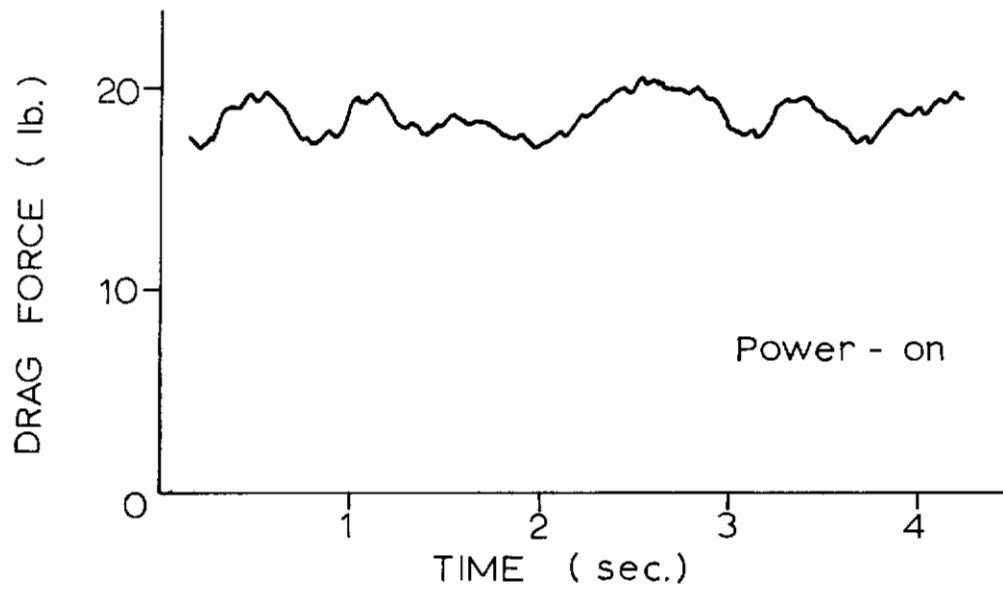


Fig 15. Steady State Drag on Cluster of 3 Ringslot Parachutes versus Time

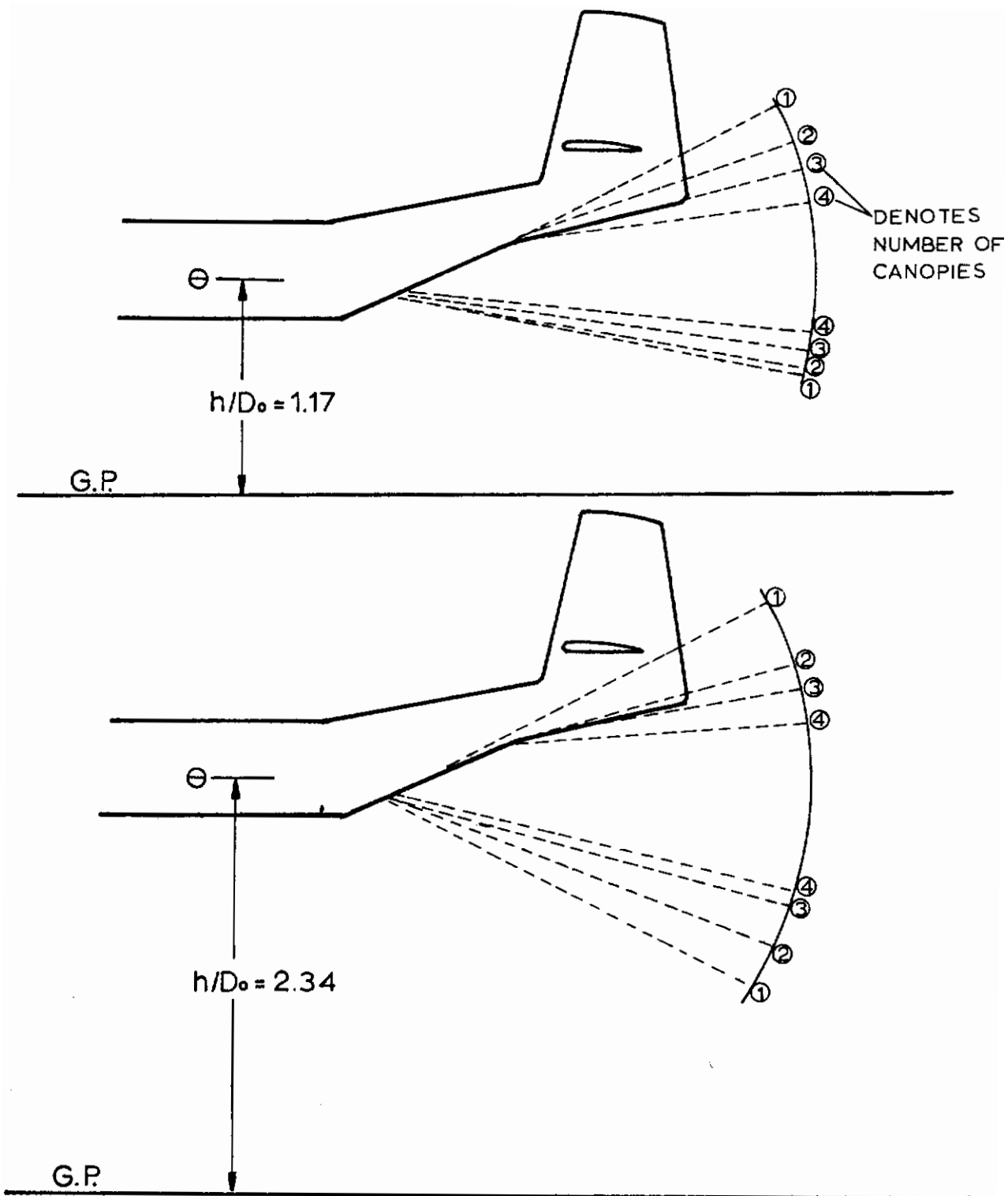


Fig 16. Schematic Illustration of Extreme Extraction Line Positions for Solid Flat Configurations with Power, No Flap Deflection

Contrails

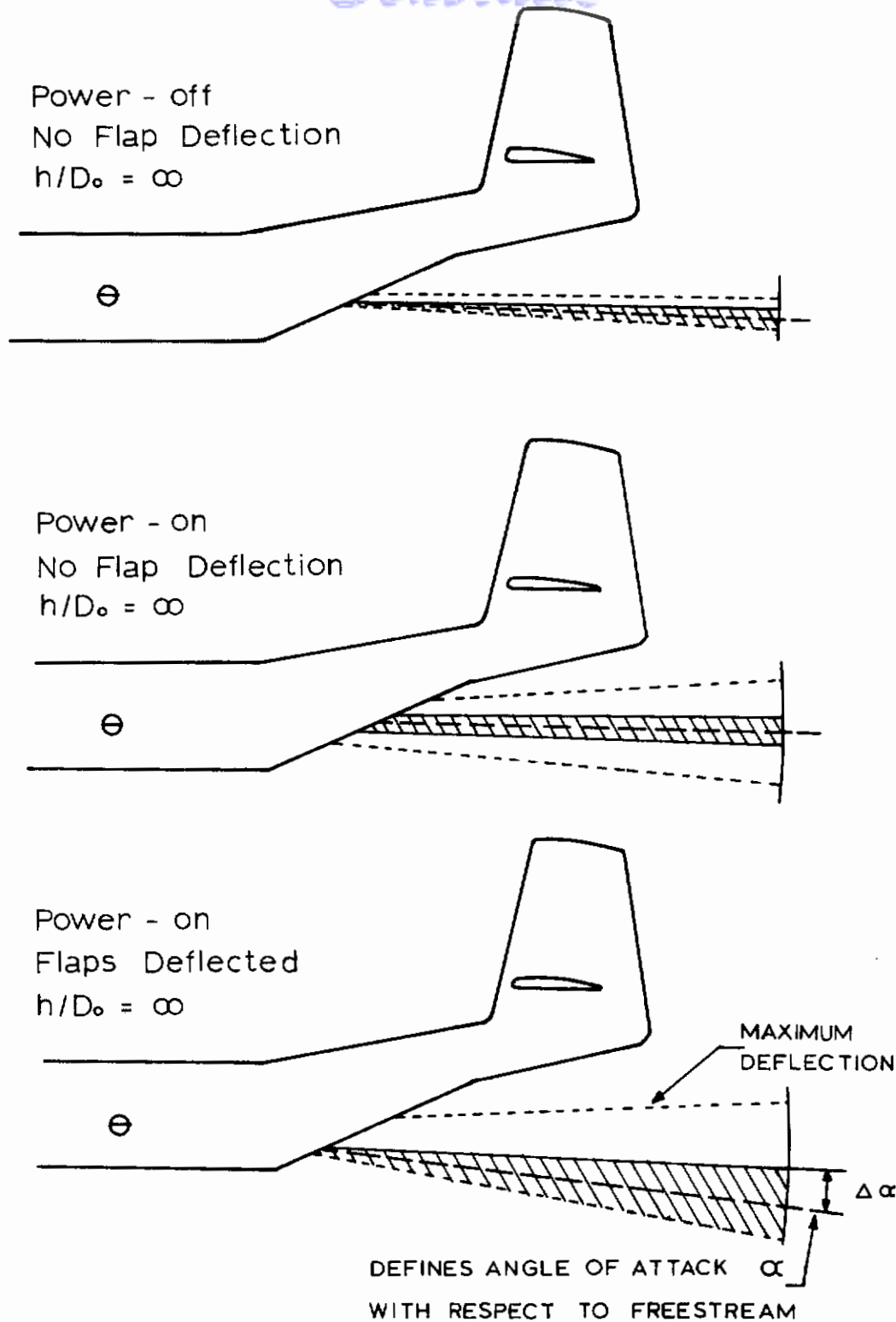


Fig 17. Extraction Line Range of Movement for Single Ringslot Parachute Configurations

4: 4 Solid Flat Parachute(s)
 3: 3 " " "
 2: 2 " " "
 1: 1 " " "

Scale
 D₀, 18.2 ft

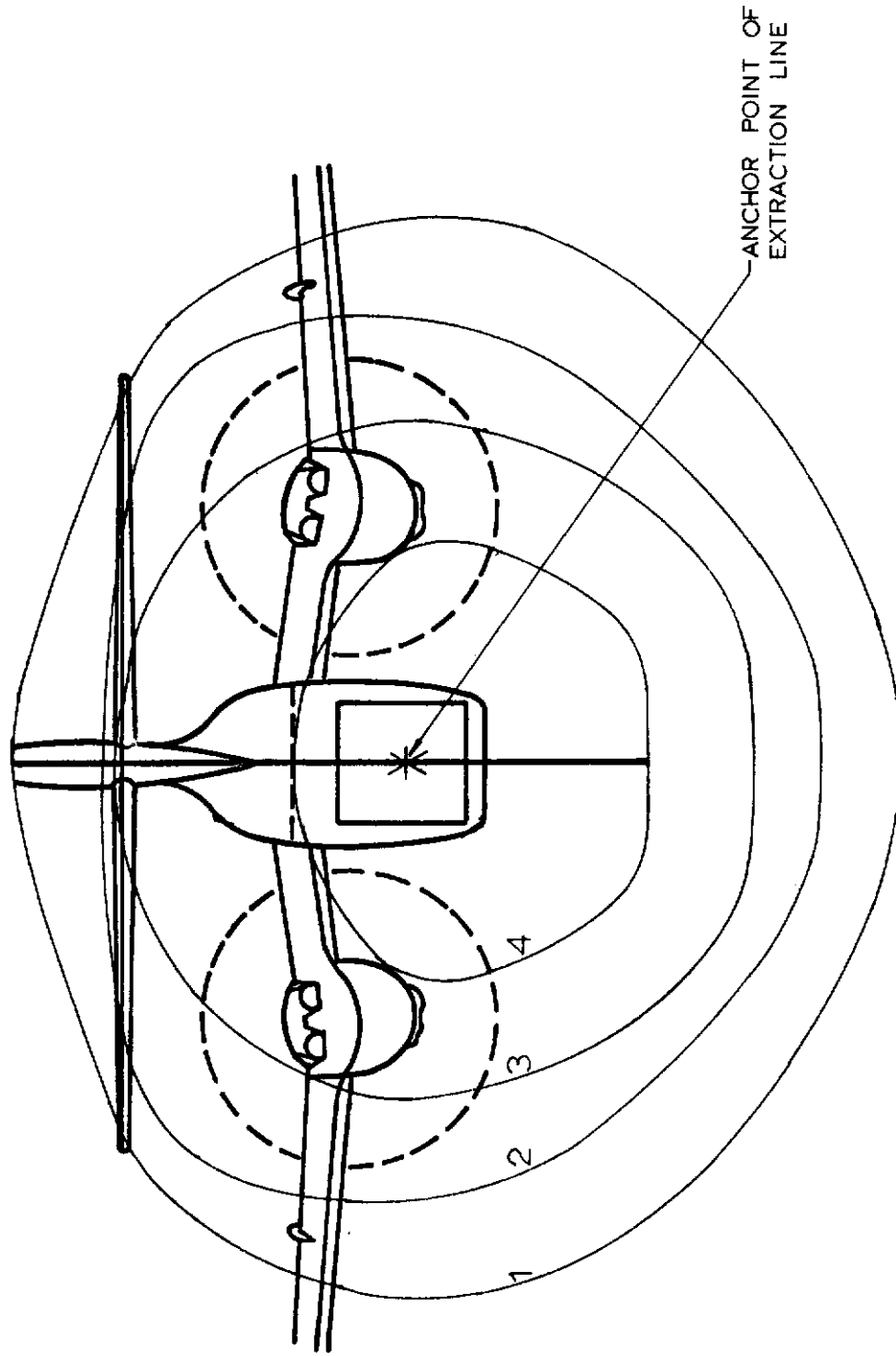


Fig 18. Envelopes of the Areas Swept by the Confluence Points of the Solid Flat Parachute Configurations, Power-Off, 0° Flap Setting and Freestream Condition

4: 4 Solid Flat Parachute(s)
 3: 3 " " "
 2: 2 " " "
 1: 1 " " "

Scale

D₀, 182 ft

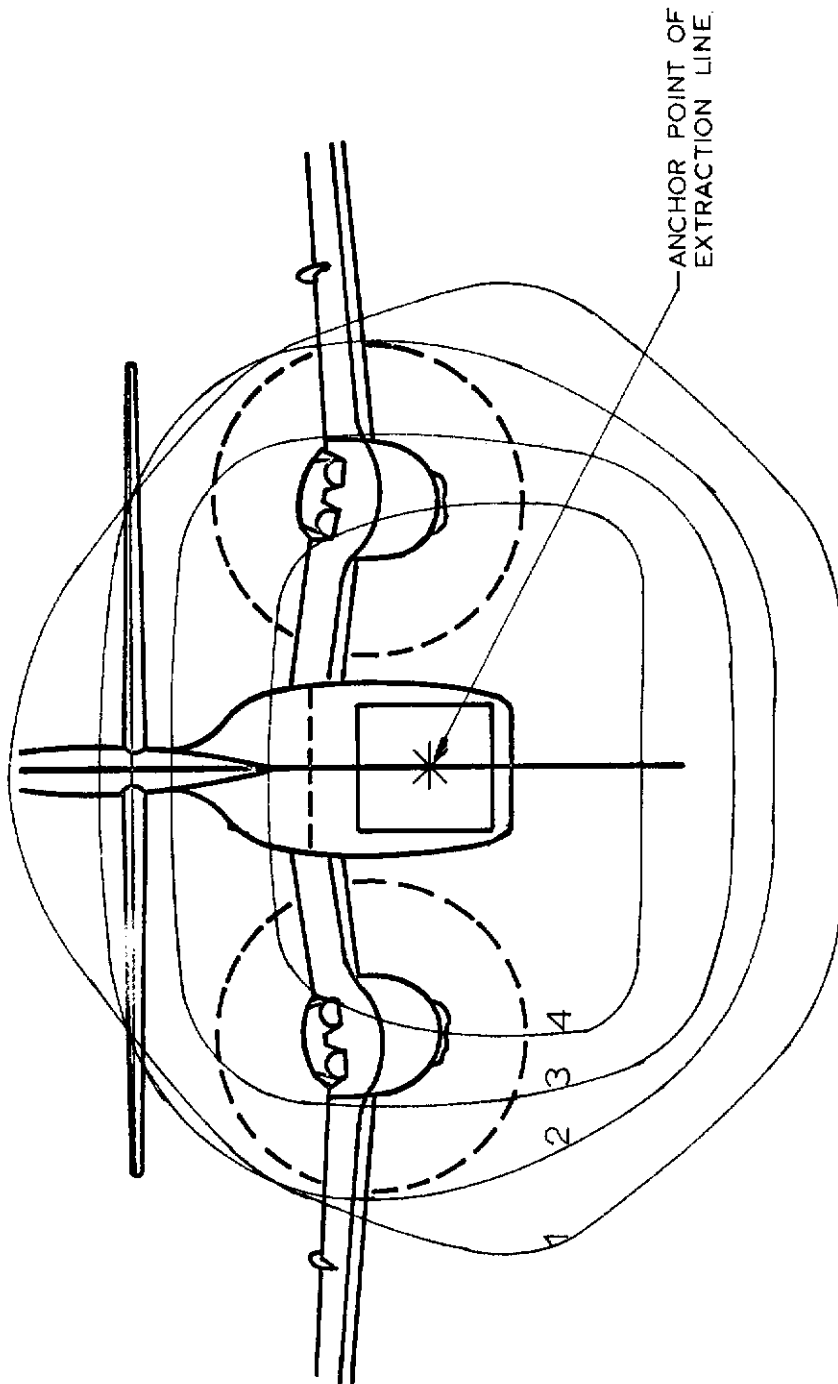


Fig 19. Envelopes of the Areas Swept by the Confluence Points of the Solid Flat Parachute Configurations, Power-Off, 0° Flap Setting and near the Ground Condition ($h/D_0 = 2.34$)

4: 4 Solid Flat Parachute(s)
 3: 3 " " "
 2: 2 " " "
 1: 1 " " "

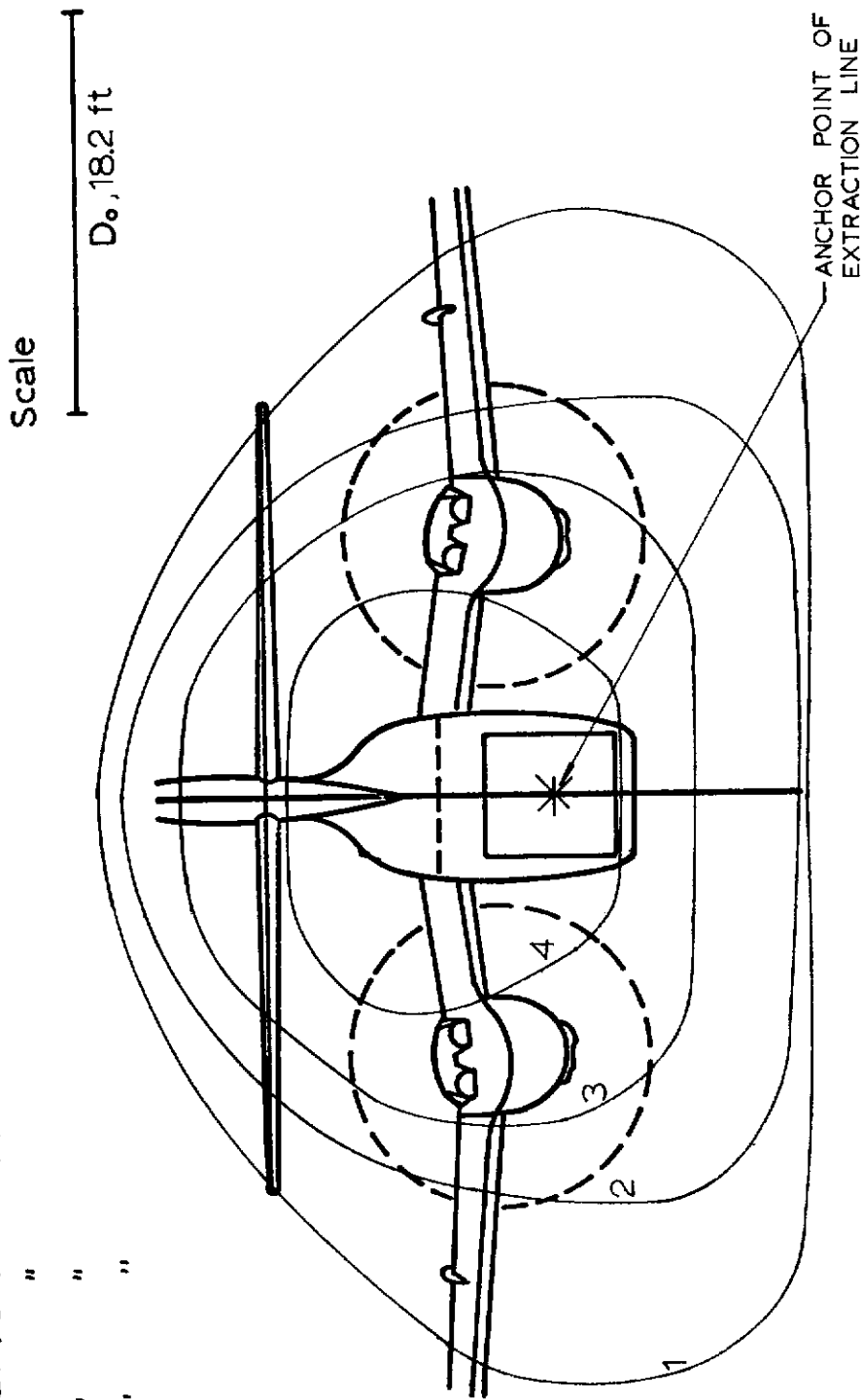


Fig 20. Envelopes of the Areas Swept by the Confluence Points of the Solid Flat Parachute Configurations, Power-Off, 0° Flap Setting and near the Ground Condition ($h/D_o = 1.17$)

4: 4 Solid Flat Parachute(s)
 3: 3 " " "
 2: 2 " " "
 1: 1 " " "

Scale

D_o, 18.2 ft

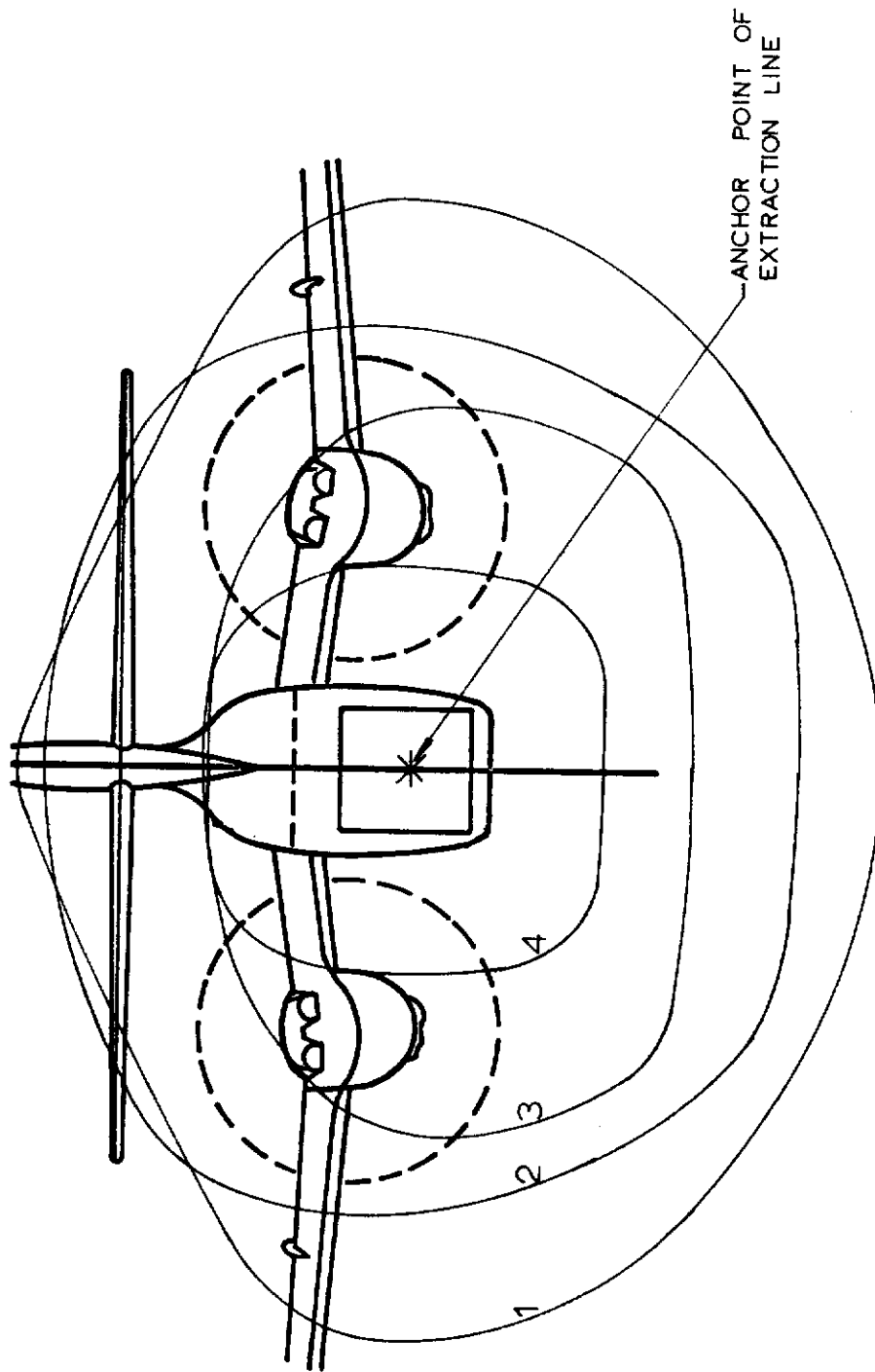


Fig 21. Envelopes of the Areas Swept by the Confluence Points of the Solid Flat Parachute Configurations, Power-On, 0° Flap Setting and Freestream Condition

4: 4 Solid Flat Parachute(s)

3: 3 " "

2: 2 " "

1: 1 " "

Scale

$D_o, 18.2 \text{ ft}$

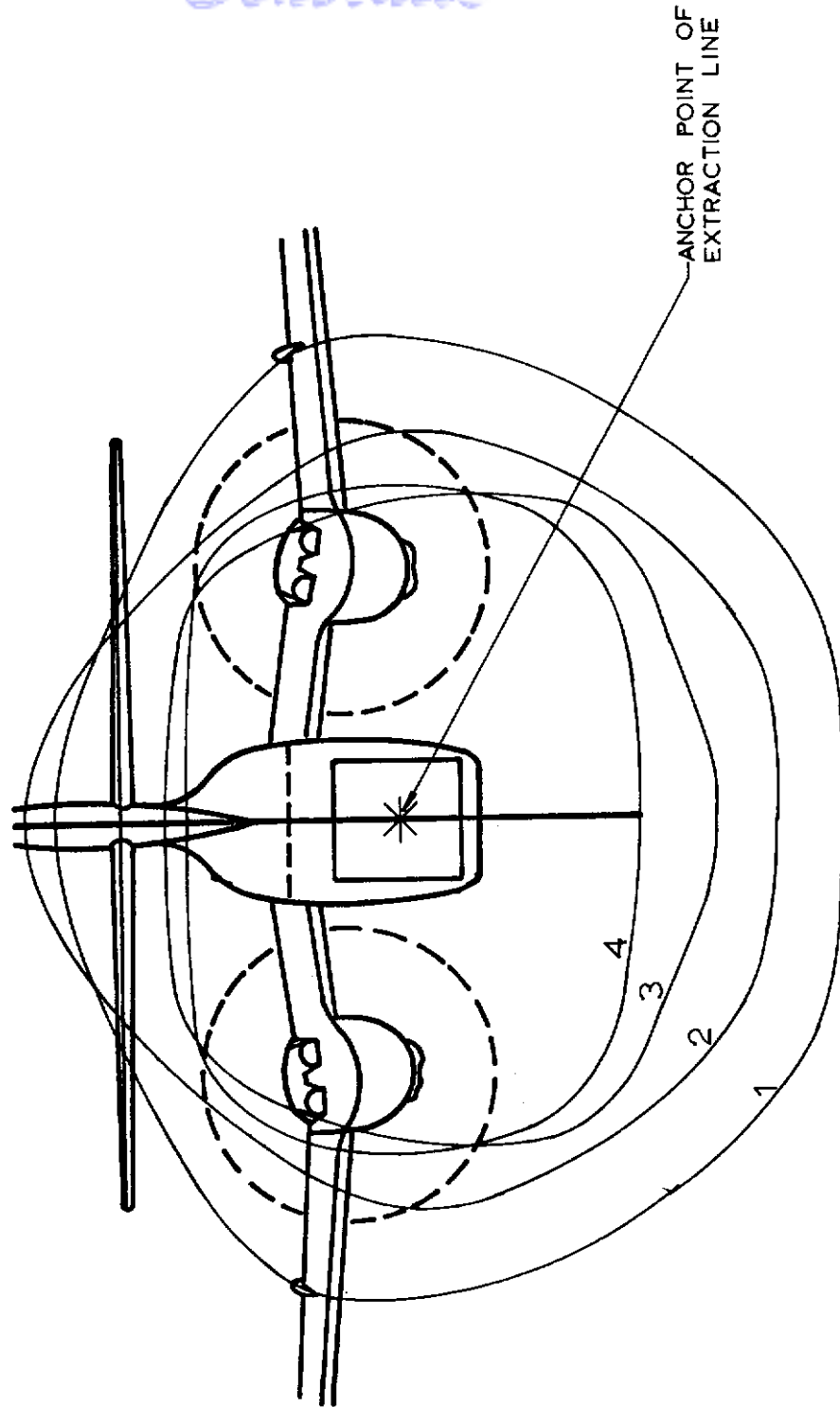


Fig 22. Envelopes of the Areas Swept by the Confluence Points of the Solid Flat Parachute Configurations, Power-On, 0° Flap Setting and near the Ground Condition ($h/D_o = 2.34$)

4:4 Solid Flat Parachute(s)
 3:3 " " "
 2:2 " " "
 1:1 " " "

Scale

D₀, 18.2 ft

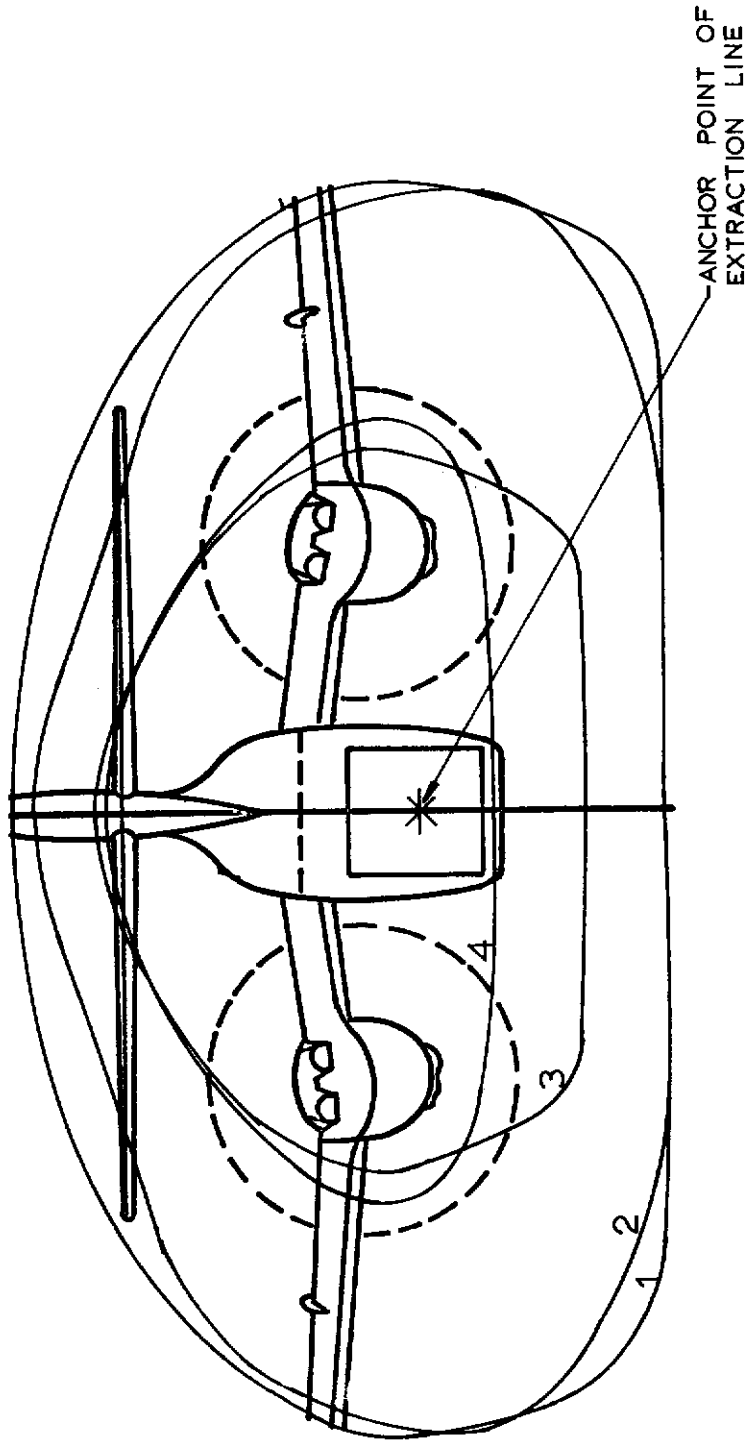


Fig 23. Envelopes of the Areas Swept by the Confluence Points of the Solid Flat Parachute Configurations, Power-On, 0° Flap Setting and near the Ground Condition ($h/D_0 = 1.17$)

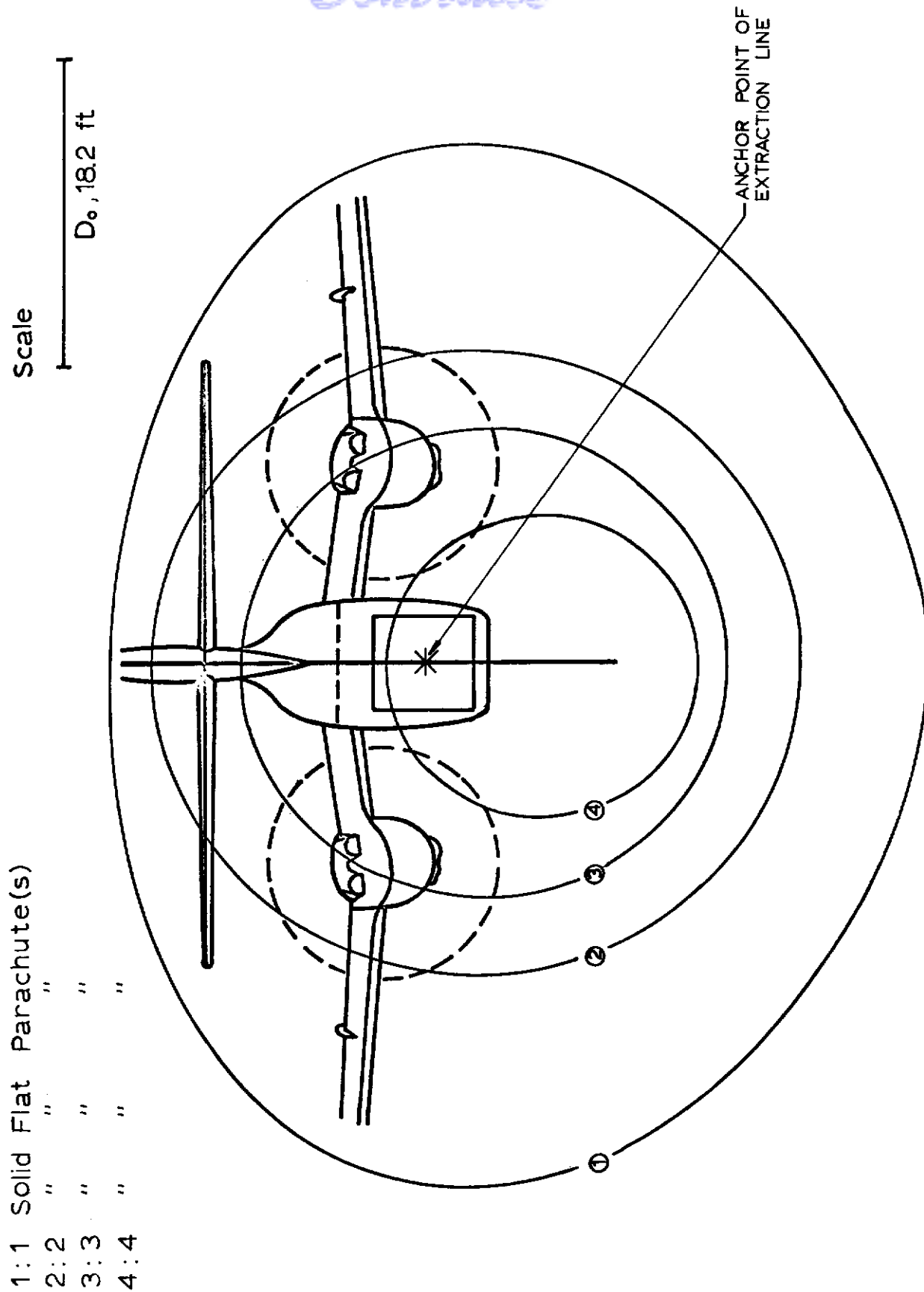


Fig 24. Envelopes of the Areas Swept by the Confluence Points of the Solid Flat Parachute Configurations, Power-Off, 15° Flap Setting and Freestream Condition

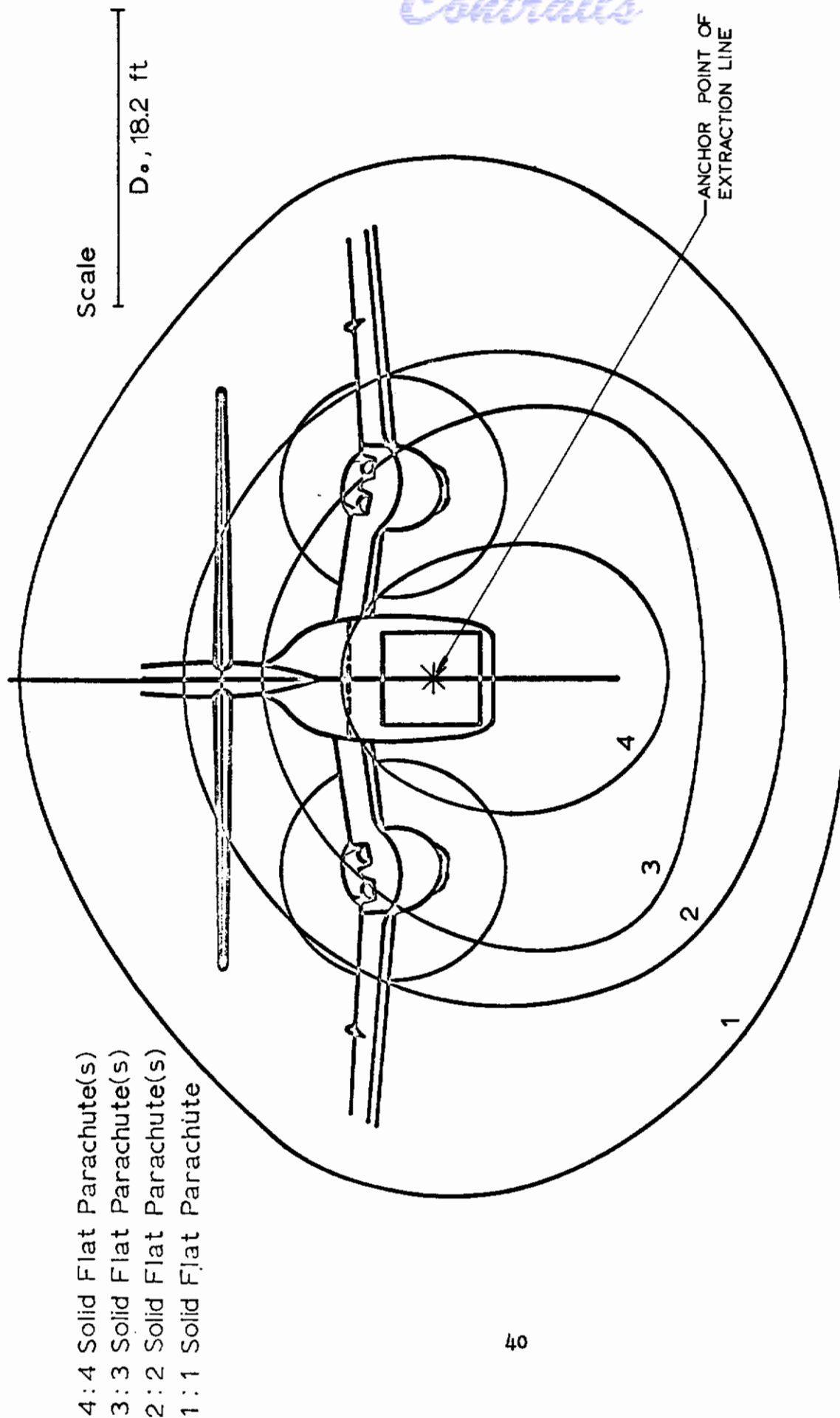


Fig 25. Envelopes of the Areas Swept by the Confluence Points of the Solid Flat Parachute Configurations, Power-Off, 15° Flap Setting and near the Ground Condition ($h/D_0 = 2.34$)

- 4:4 Solid Flat Parachute(s)
- 3:3 Solid Flat Parachute(s)
- 2:2 Solid Flat Parachute(s)
- 1:1 Solid Flat Parachute

Scale

$D_0, 18.2 \text{ ft}$

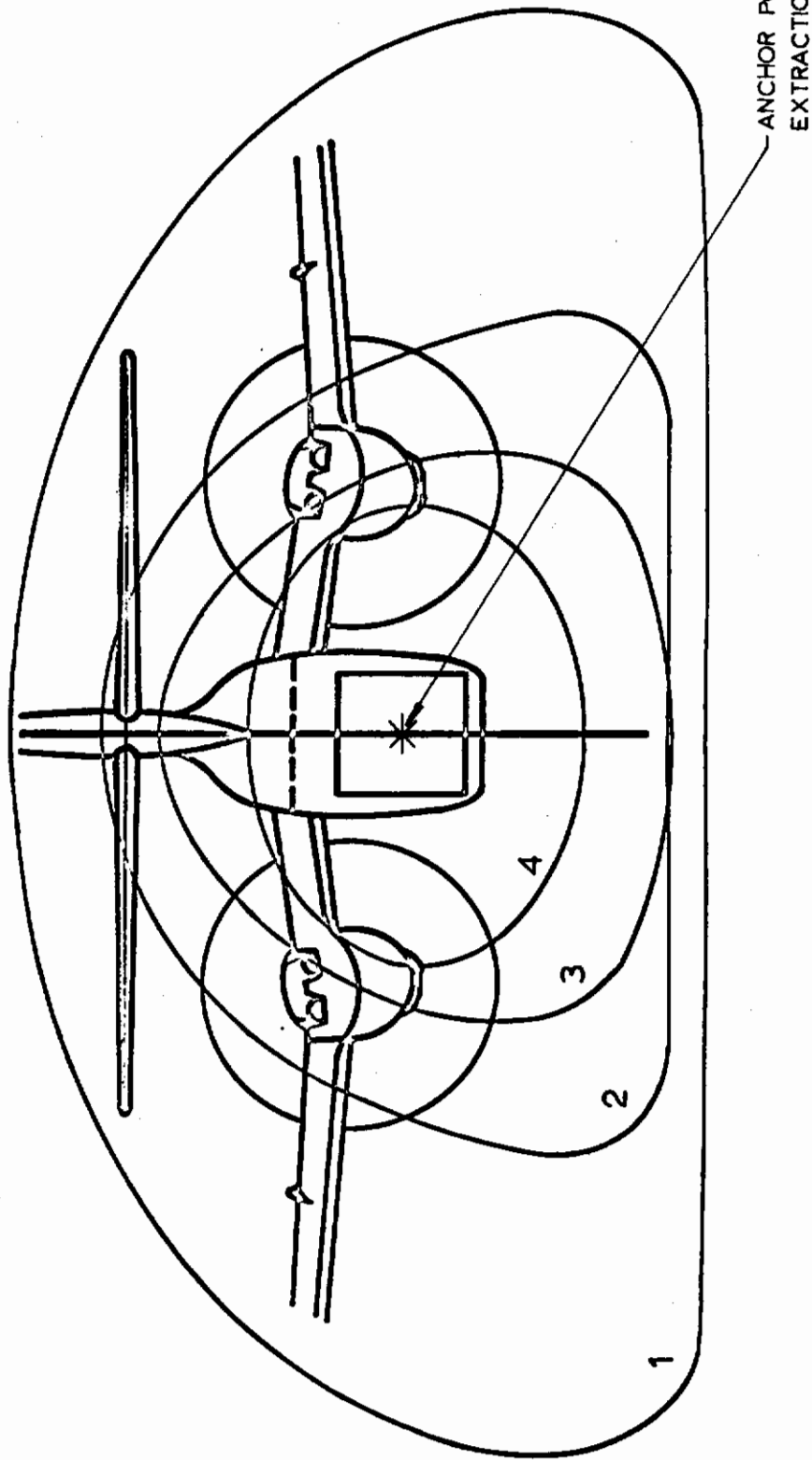


Fig 26. Envelopes of the Areas Swept by the Confluence Points of the Solid Flat Parachute Configurations, Power-Off, 15° Flap Setting and near the Ground Condition ($h/D_0 = 1.17$)

4: 4 Solid Flat Parachute(s)
 3: 3 " " "
 2: 2 " " "
 1: 1 " " "

Scale

D₀, 18.2 ft

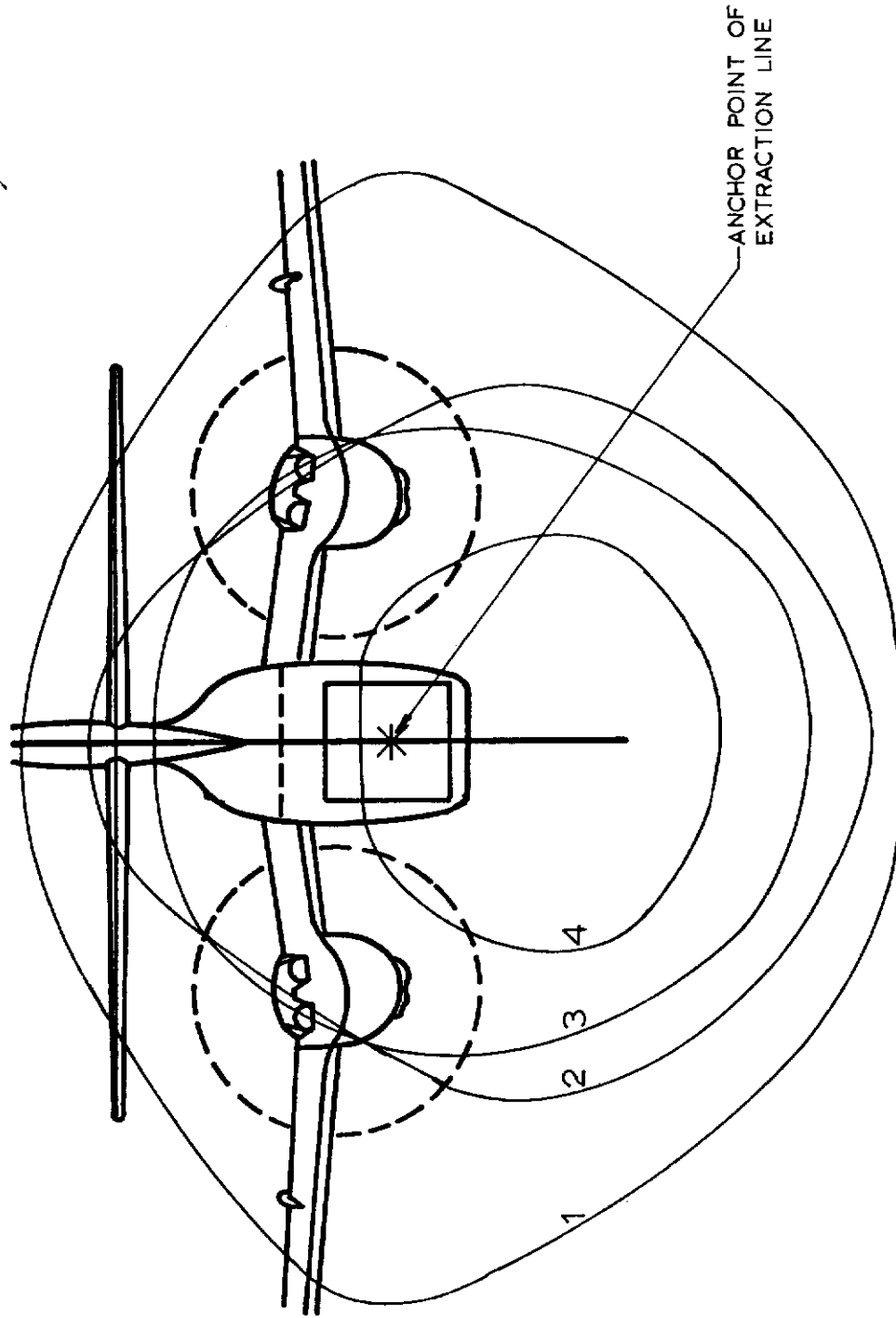


Fig 27. Envelopes of the Areas Swept by the Confluence Points of the Solid Flat Parachute Configurations, Power-On, 15° Flap Setting and in Freestream Condition

4: 4 Solid Flat Parachute(s)
 3: 3 " " "
 2: 2 " " "
 1: 1 " " "

Scale

$D_o, 18.2 \text{ ft}$

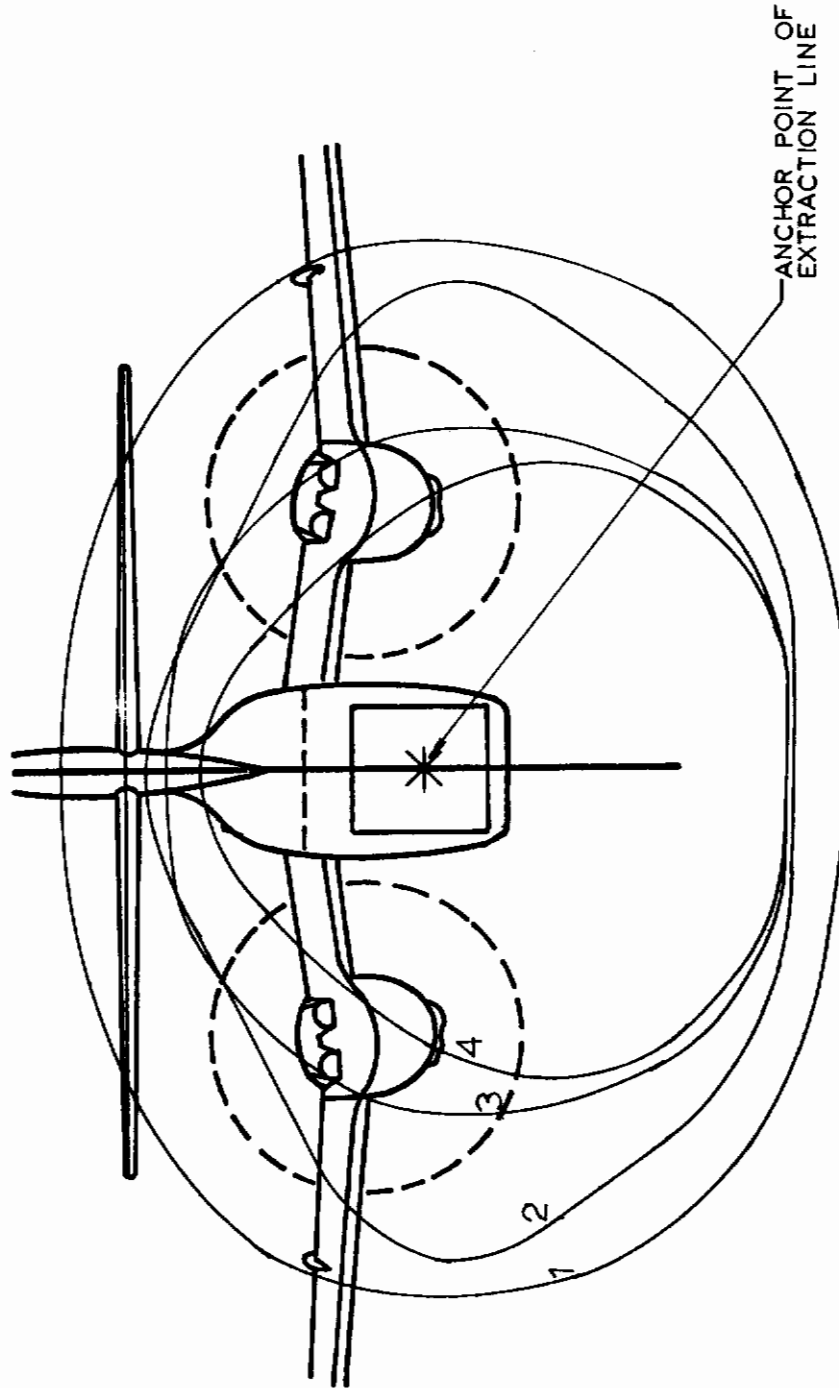


Fig 28. Envelopes of the Areas Swept by the Confluence Points of the Solid Flat Parachute Configurations, Power-On, 15° Flap Setting and near the Ground Condition ($h/D_o = 2.34$)

4: 4 Solid Flat Parachute(s)
 3: 3 " "
 2: 2 " "
 1: 1 " "

Scale

$D_o, 18.2 \text{ ft}$

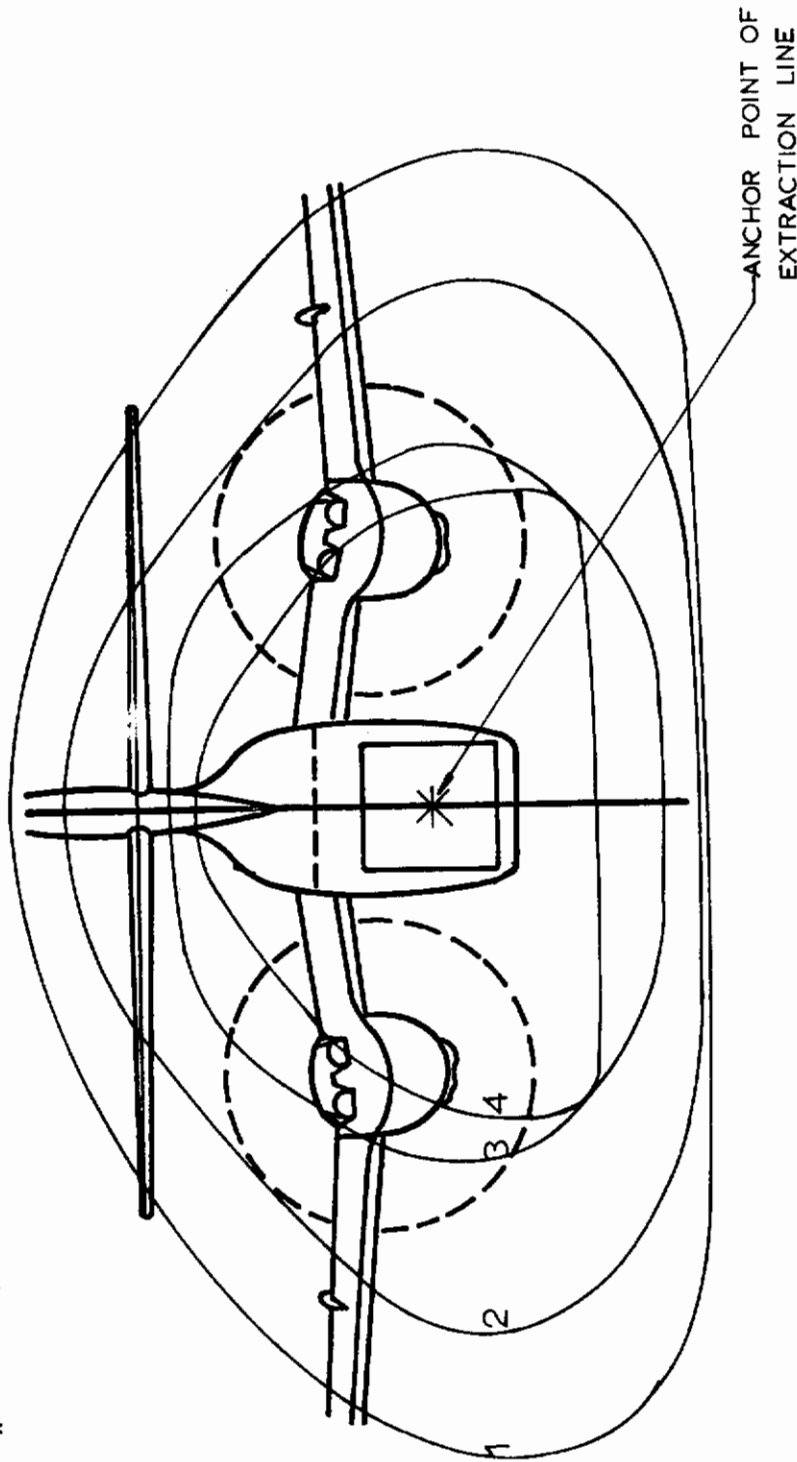


Fig 29. Envelopes of the Areas Swept by the Confluence Points of the Solid Flat Parachute Configurations, Power-On, 15° Flap Setting and near the Ground Condition ($h/D_o = 1.17$)

1:1 RINGSLLOT PARACHUTE(S)

2:2	"	"
3:3	"	"
4:4	"	"

Scale

D_0 , 22 ft

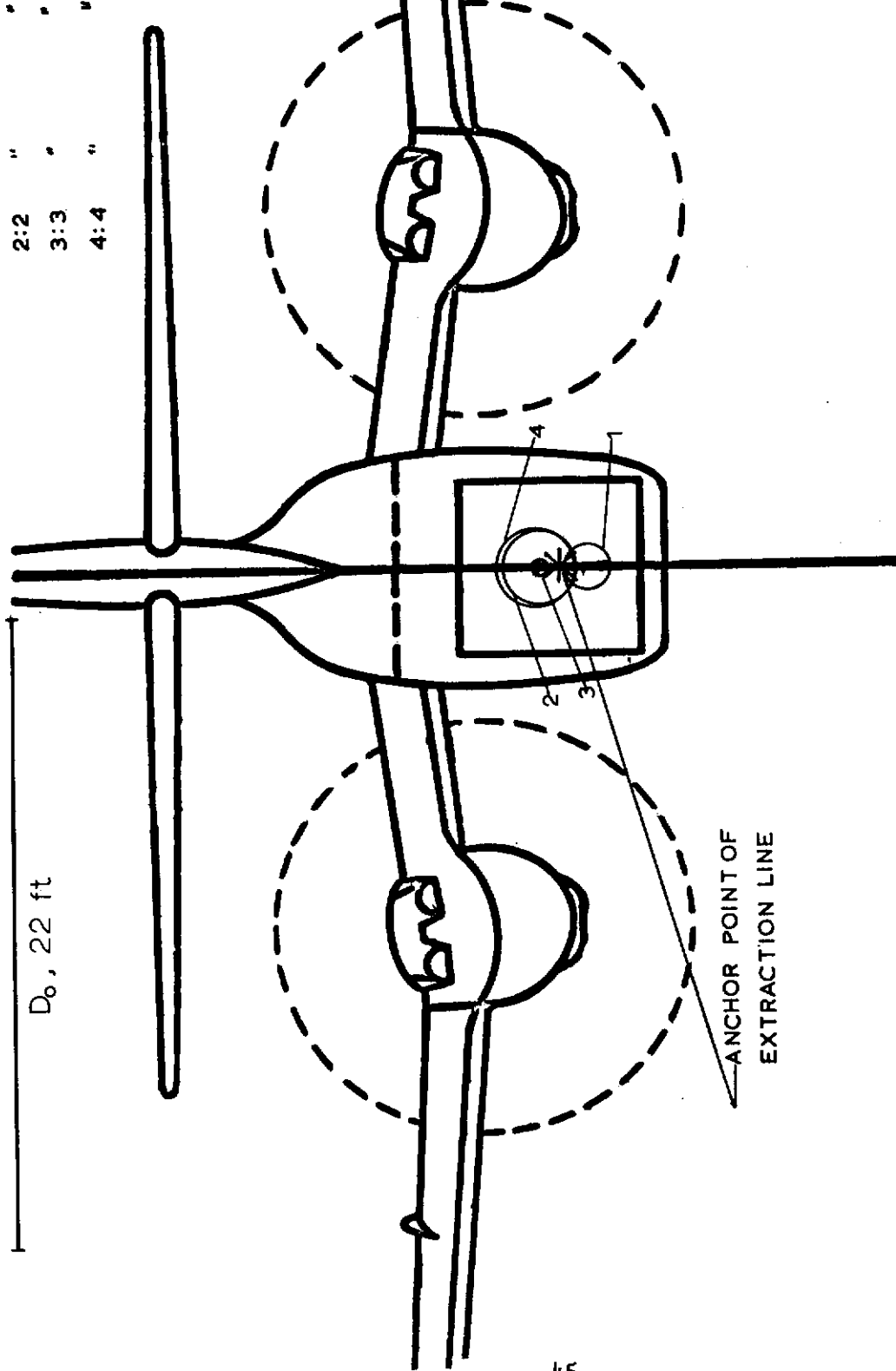


Fig 30. Envelopes of the Areas Swept by the Confluence Points of the Ringslot Parachute Configurations, Power-Off, 0° Flap Setting and in Freestream Condition

1:1 RINGSLOT PARACHUTE(S)

2:2	"	"
3:3	"	"
4:4	"	"

Scale

$D_0, 22 \text{ ft}$

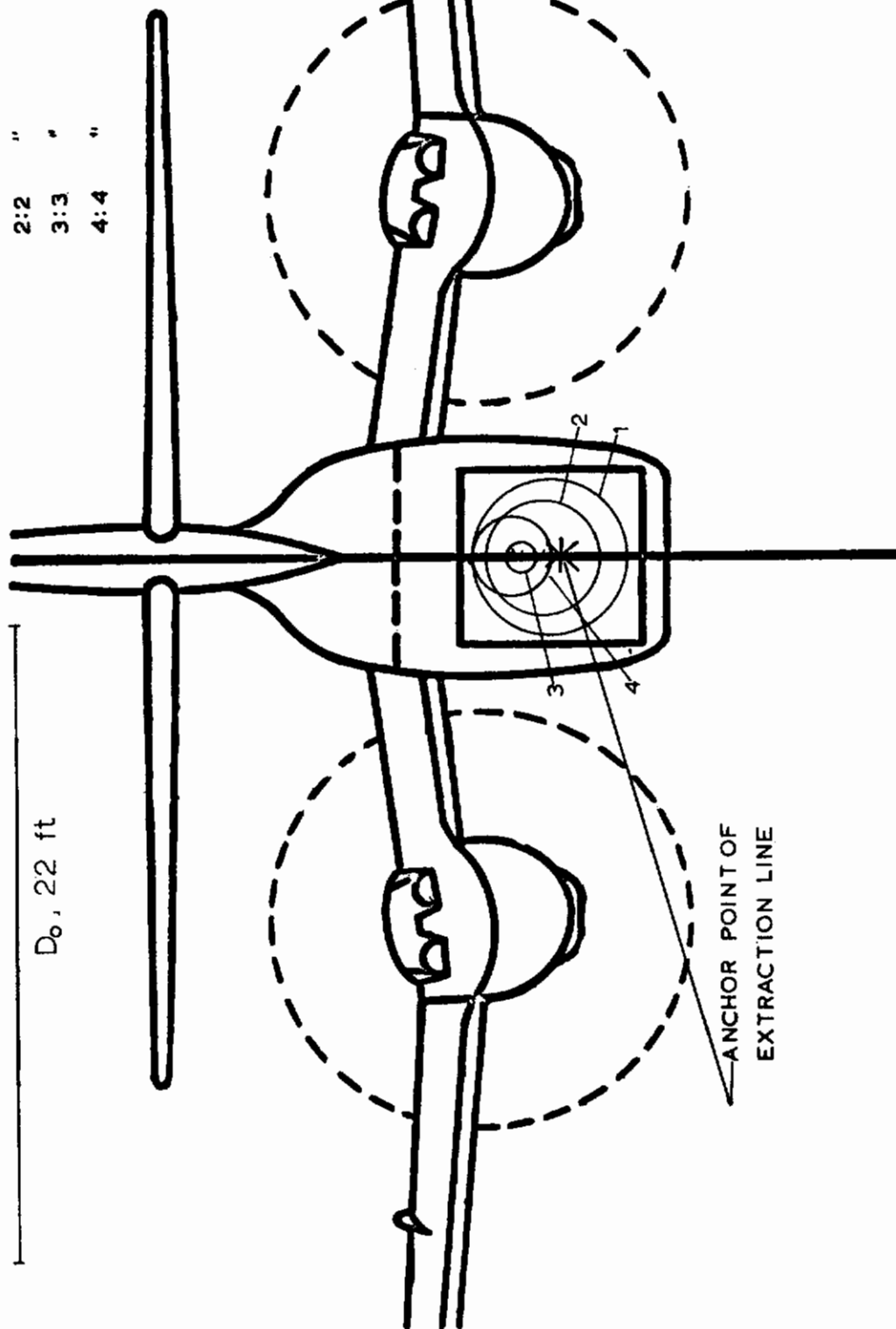


Fig 31. Envelopes of the Areas Swept by the Confluence Points of the Ringslot Parachute Configurations, Power-Off, 0° Flap Setting and near the Ground Condition ($h/D_0 = 2$)

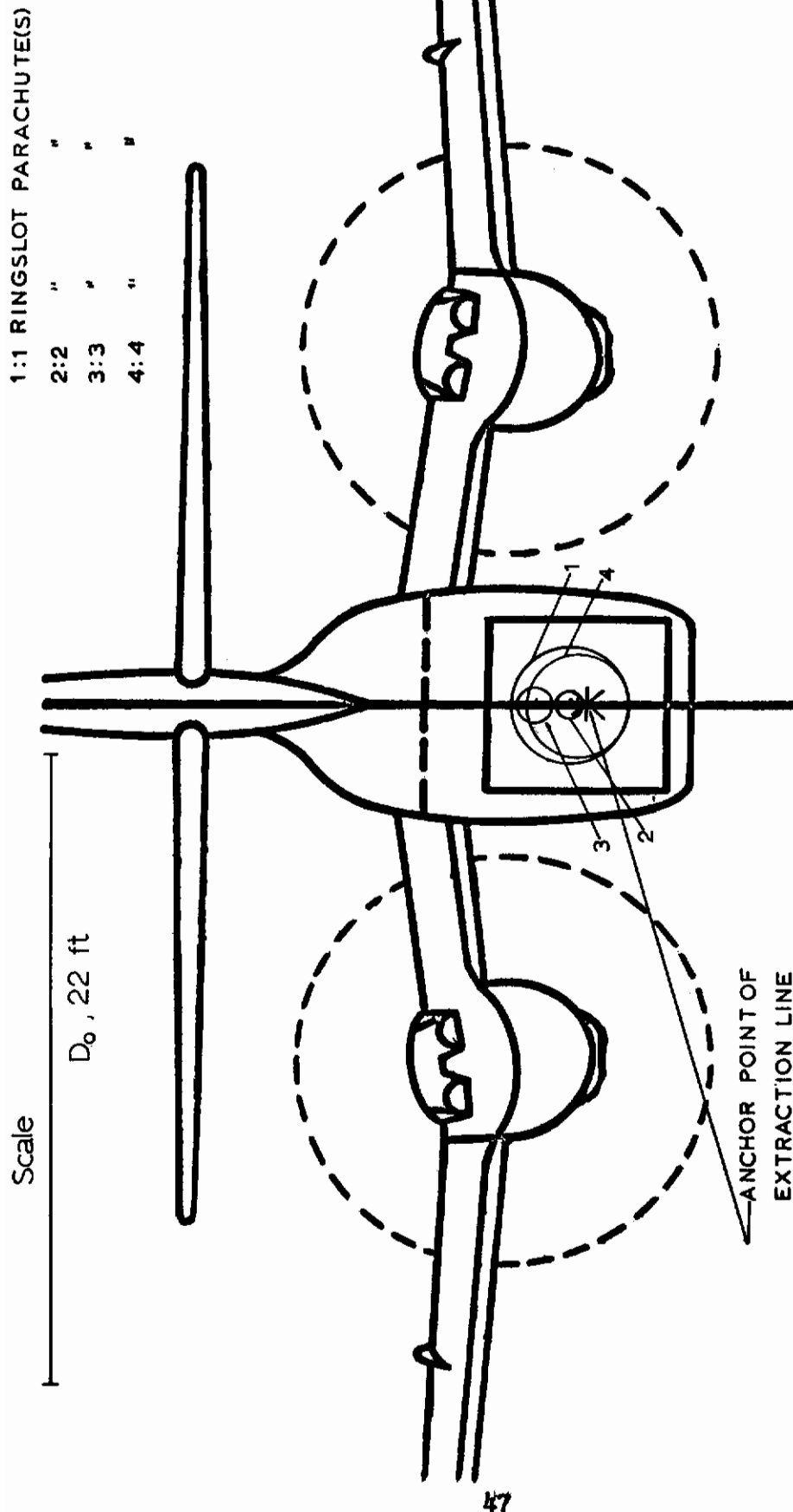


Fig 32. Envelopes of the Areas Swept by the Confluence Points of the Ringslot Parachute Configurations, Power-Off, 0° Flap Setting and near the Ground Condition ($h/D_0 = 1$)

1:1 RINGSLLOT PARACHUTE(S)

2:2 " "

3:3 " "

4:4 " "

Scale

$D_0, 22 \text{ ft}$

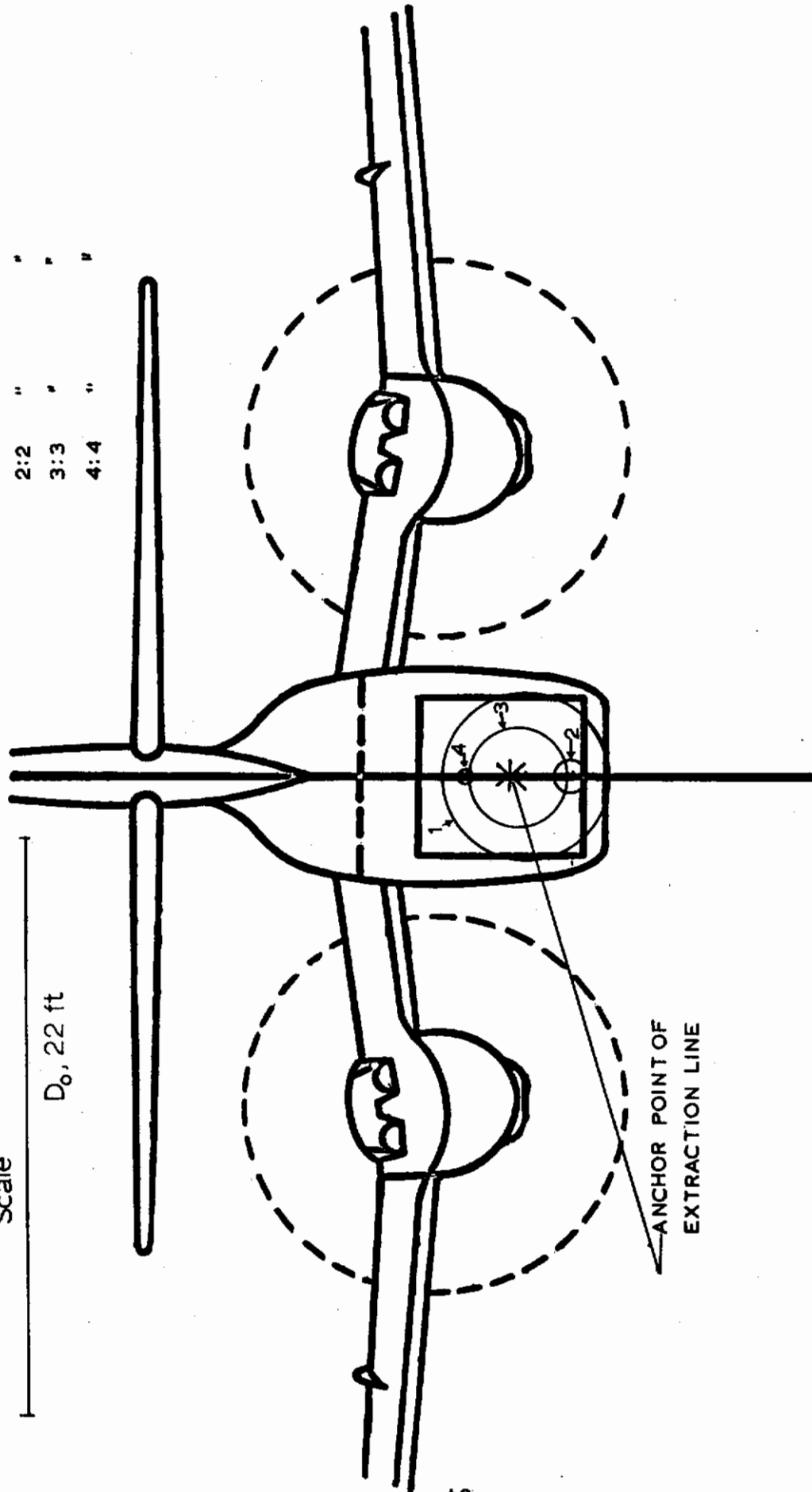


Fig 33. Envelopes of the Areas Swept by the Confluence Points of the Ringslot Parachute Configurations, Power-On, 0° Flap Setting and in Freestream Condition

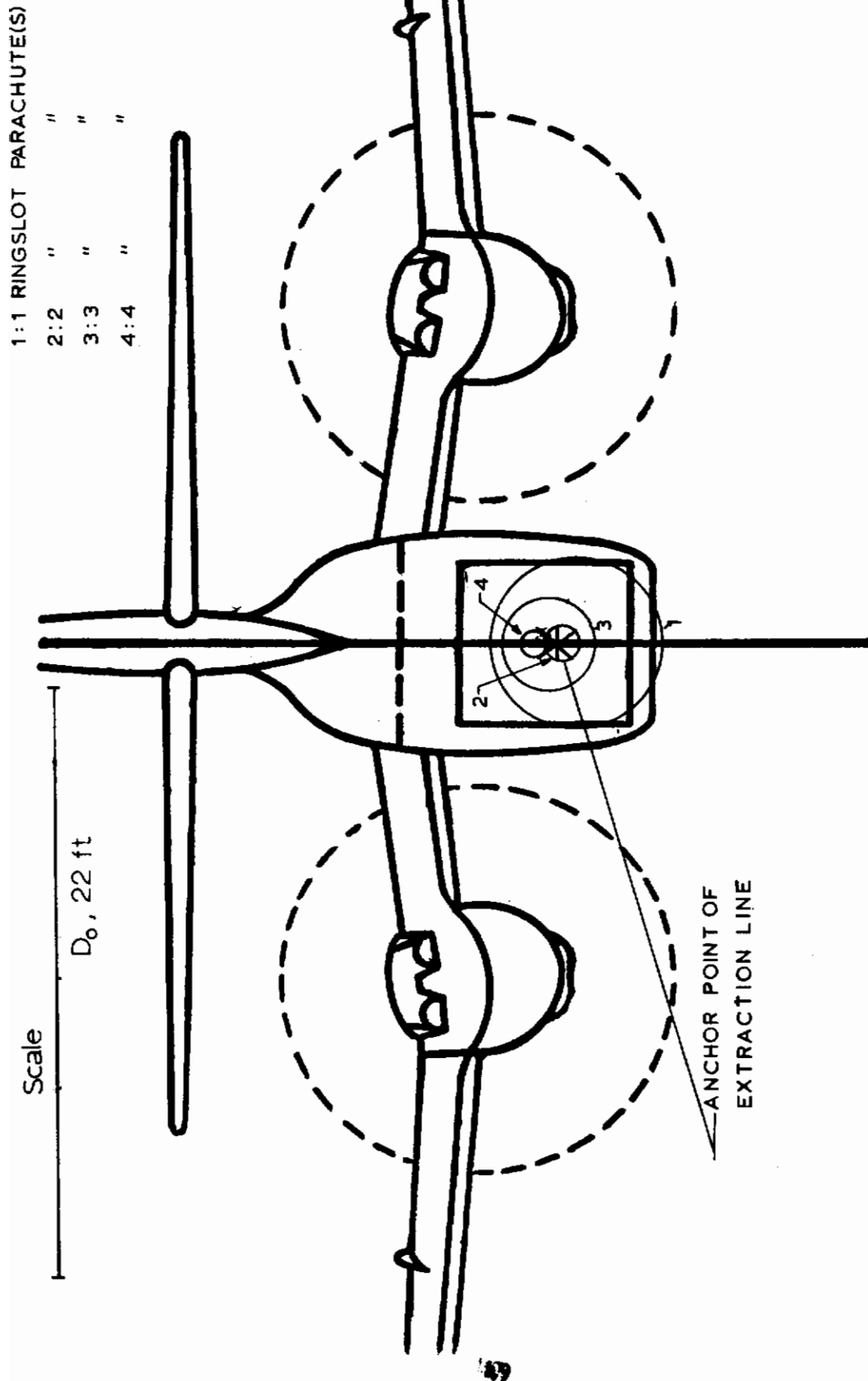
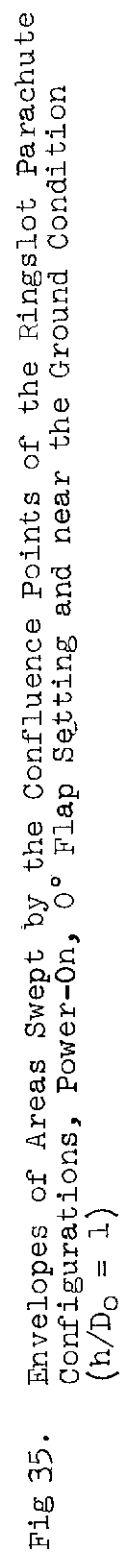


Fig 34. Envelopes of Areas Swept by the Confluence Points of the Ringslot Parachute Configurations, Power-On, 0° Flap Setting and near the Ground Condition ($h/D_0 = 2$)



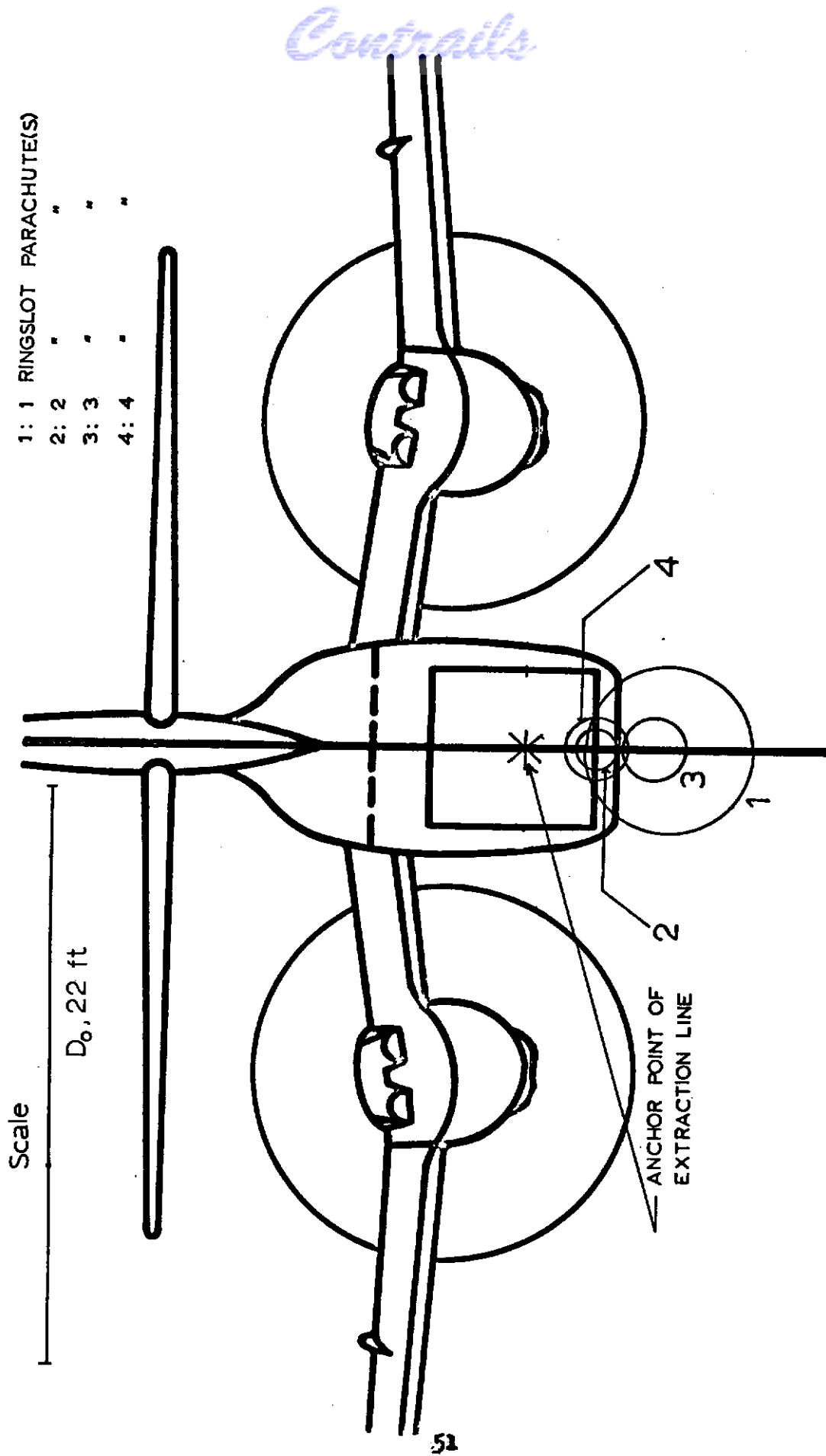


Fig 36. Envelopes of Areas Swept by the Confluence Points of the Ringslot Parachute Configurations, Power-Off, 15° Flap Setting and in Freestream Condition

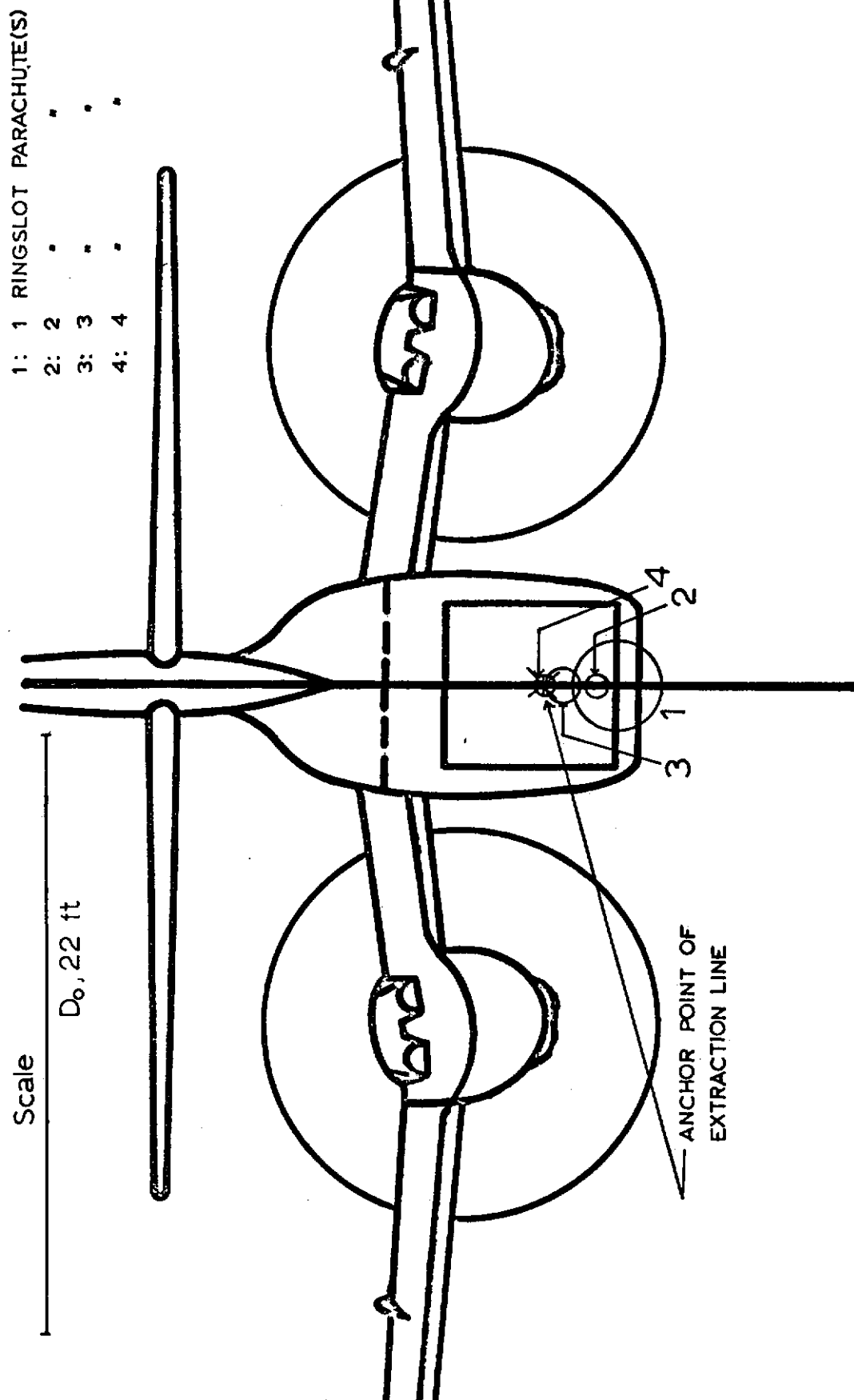


Fig 37. Envelopes of Areas Swept by the Confluence Points of the Ringslot Parachute Configurations, Power-Off, 15° Flap Setting and near the Ground Condition ($h/D_0 = 2$)

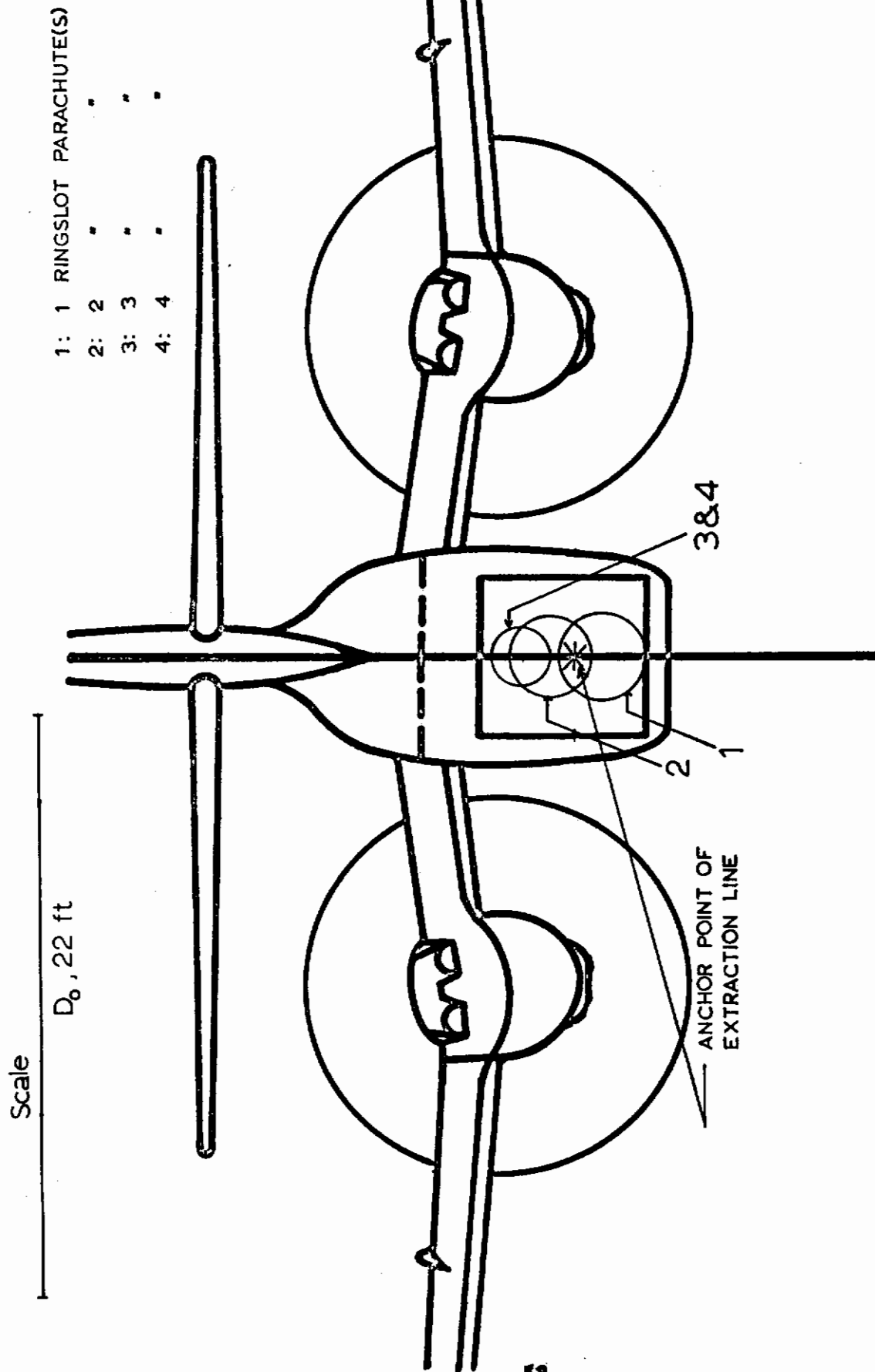


Fig 38. Envelopes of Areas Swept by the Confluence Points of the Ringslot Parachute Configurations, Power-Off, 15° Flap Setting and near the Ground Condition ($h/D_0 = 1$)

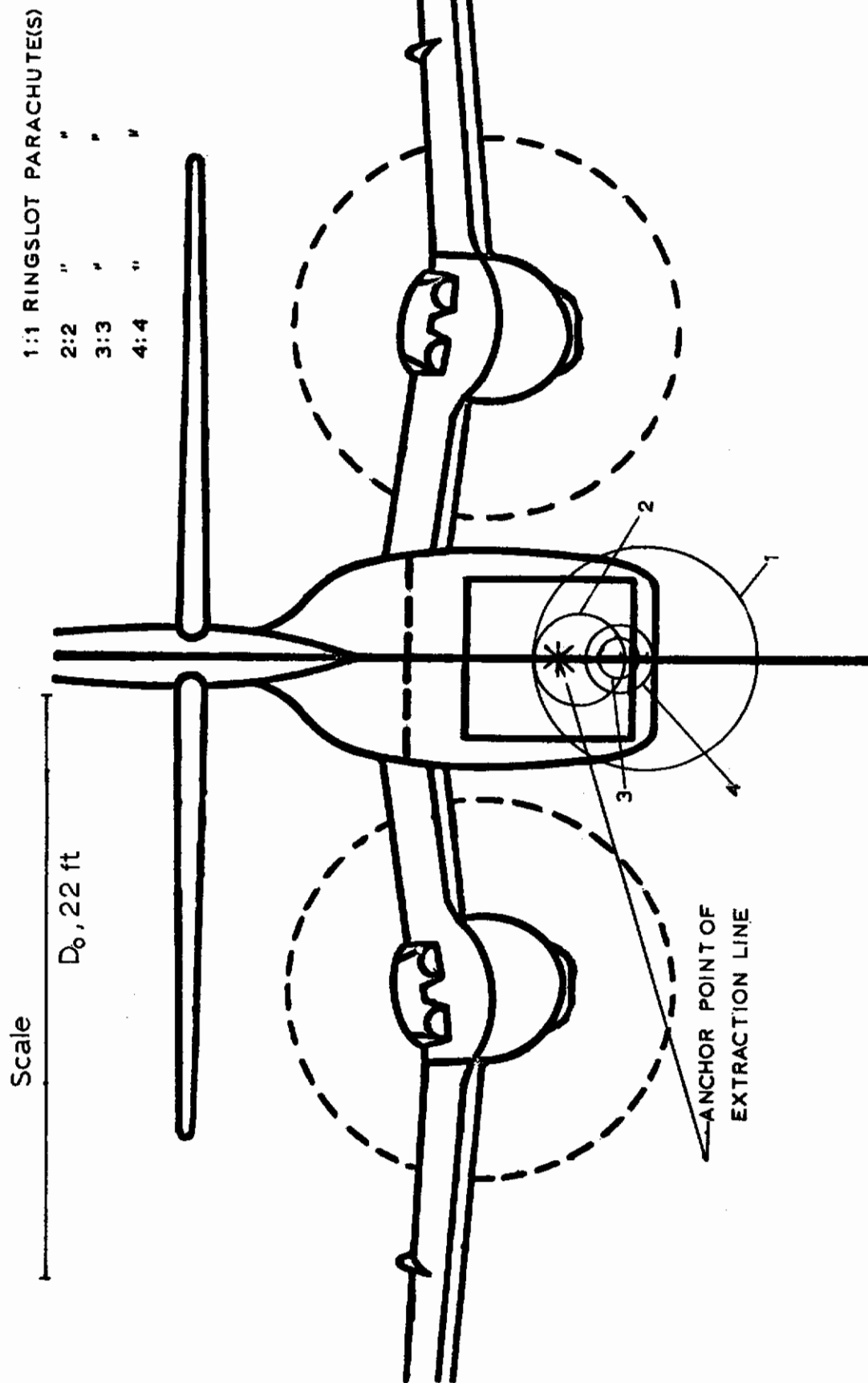


Fig 39. Envelopes of Areas Swept by the Confluence Points of the Ringslot Parachute Configurations, Power-On, 15° Flap Setting and in Freestream Condition

1:1 RINGSLLOT PARACHUTE(S)

2:2	"	"
3:3	"	"
4:4	"	"

Scale

D_0 , 22 ft

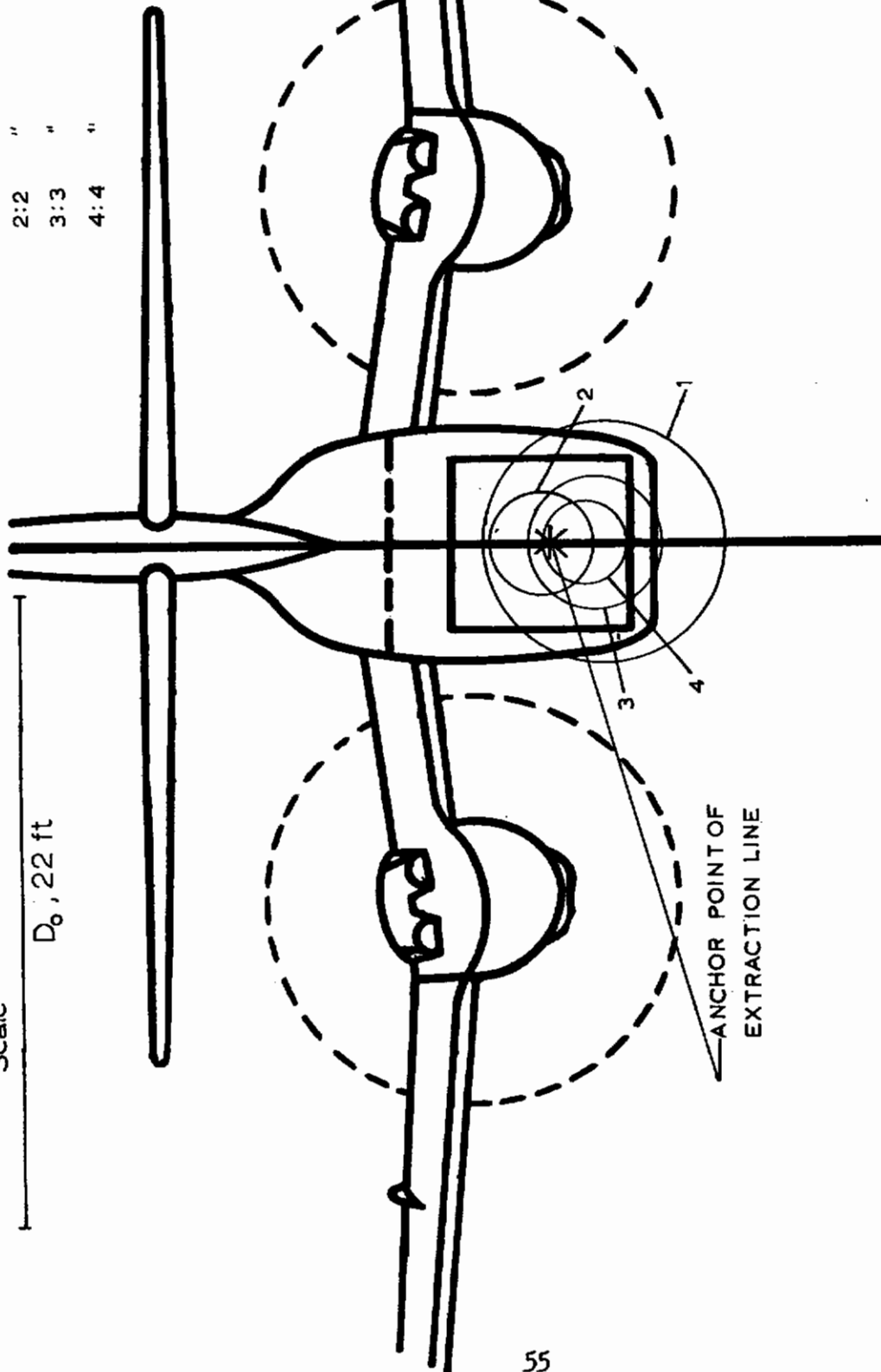


Fig 40. Envelopes of Areas Swept by the Confluence Points of the Ringslot Parachute Configurations, Power-On, 15° Flap Setting and near the Ground Condition ($h/D_0 = 2$)

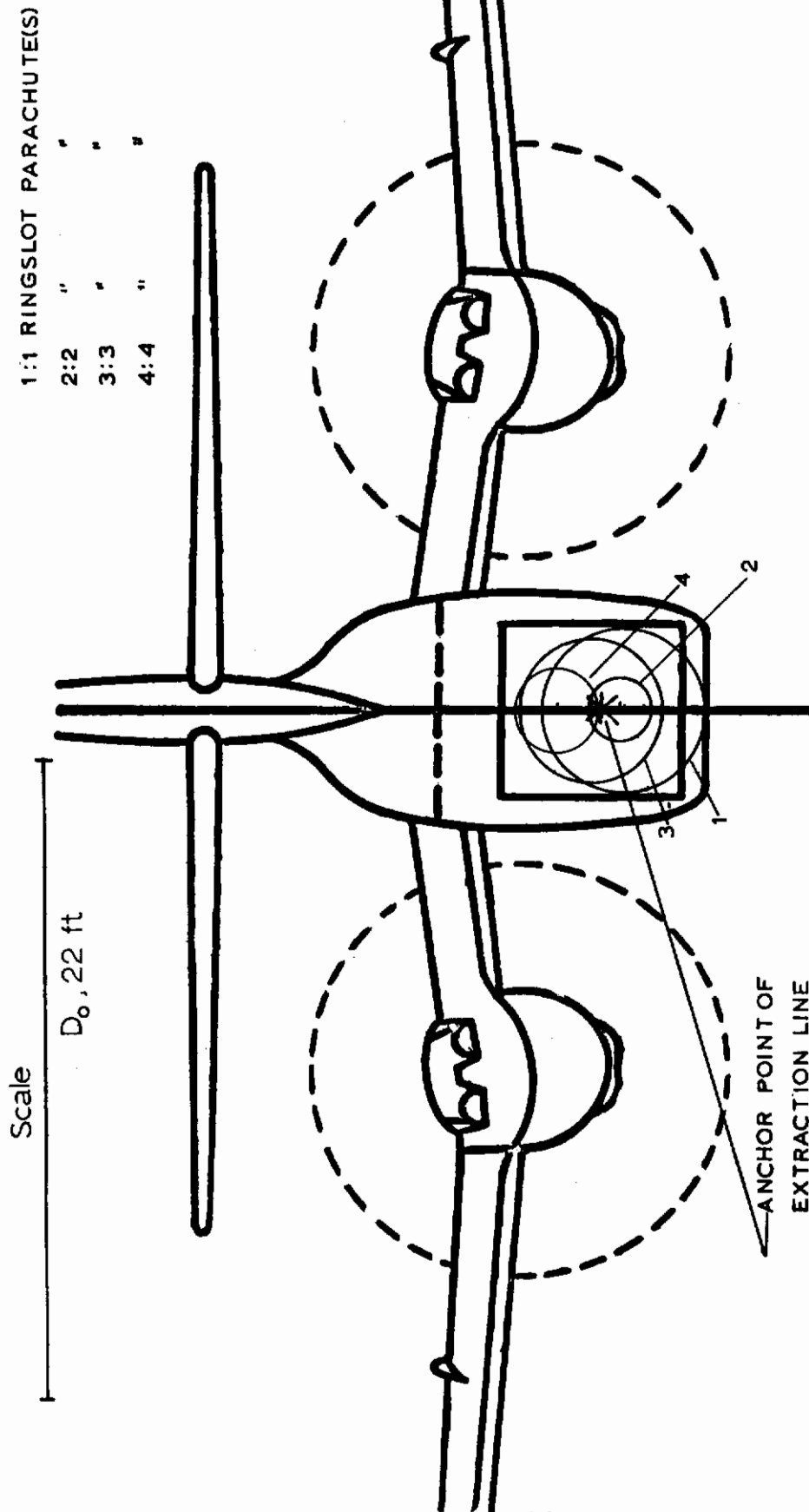
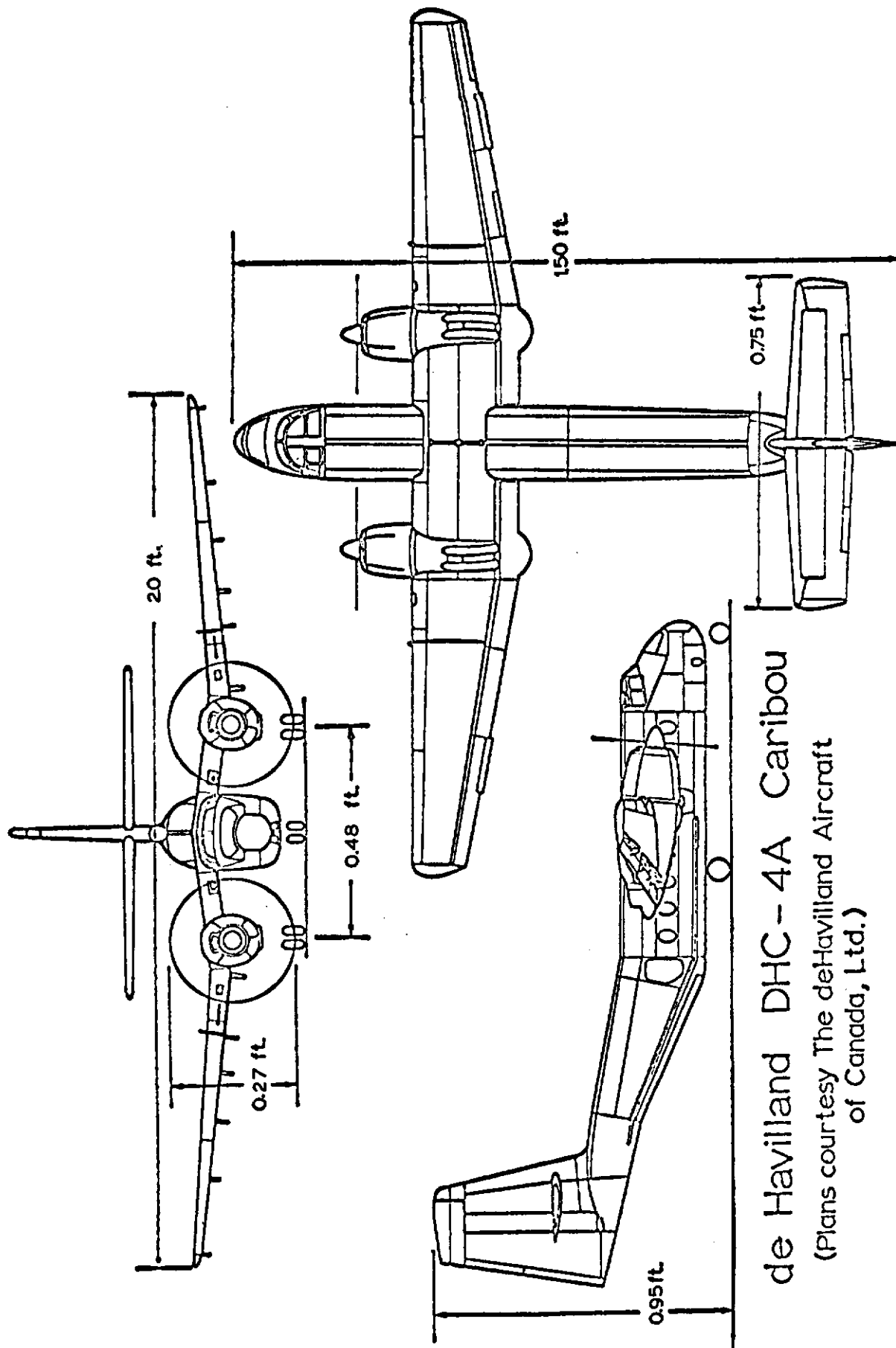


Fig 41. Envelopes of Areas Swept by the Confluence Points of the Ringslot Parachute Configurations, Power-On, 15° Flap Setting and near the Ground Condition ($h/D_o = 1$)



de Havilland DHC-4A Caribou
(Plans courtesy The deHavilland Aircraft
of Canada, Ltd.)

Fig 42. Three View of the 1/48 Scale Caribou Model Aircraft Used for Wake Surveys

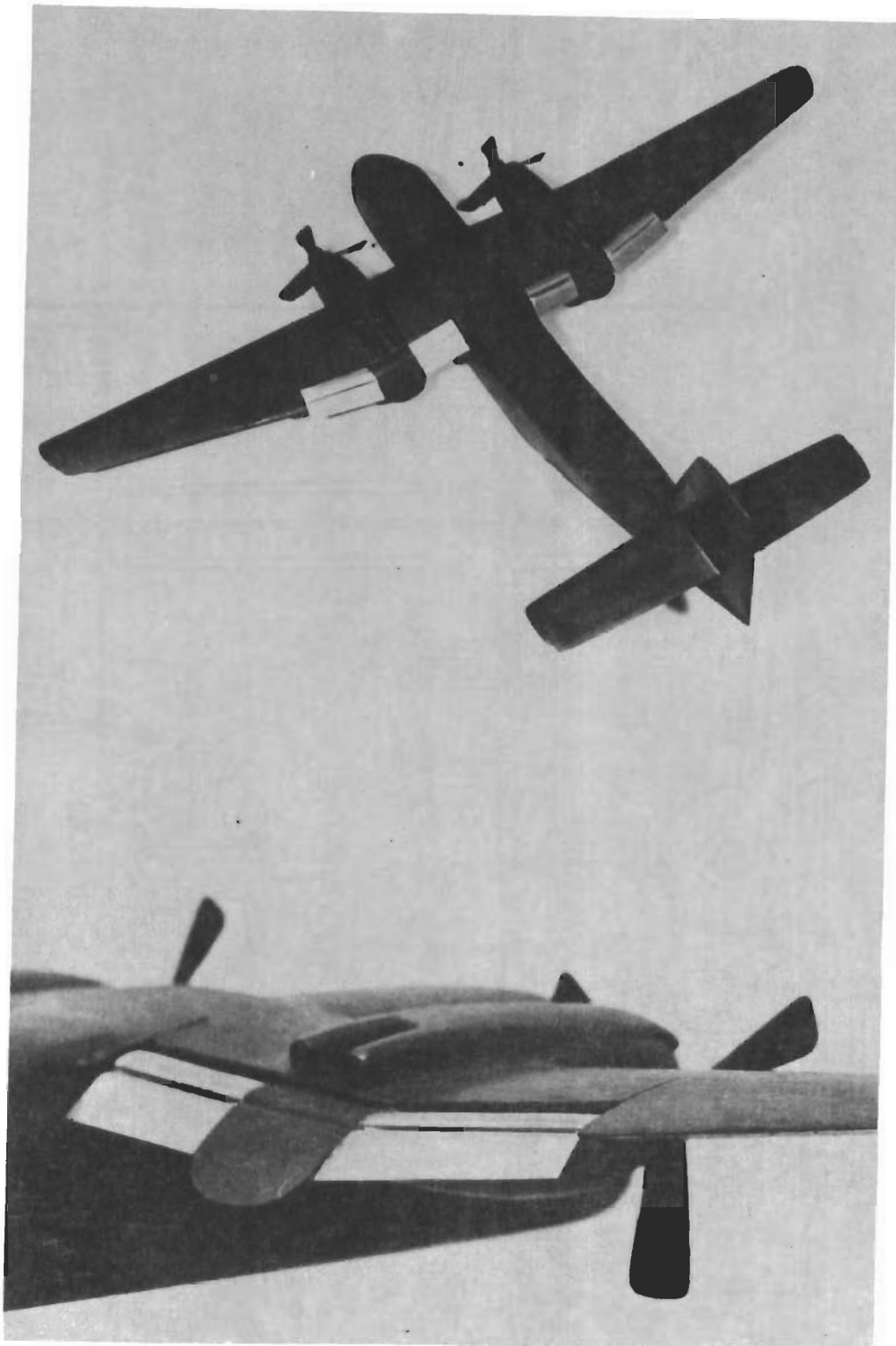
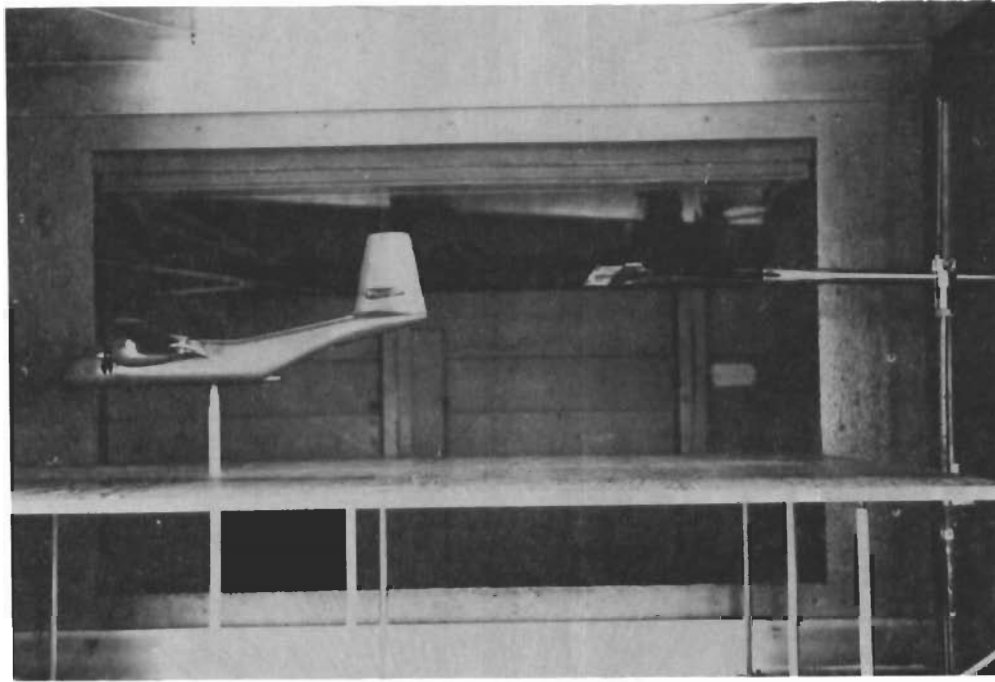
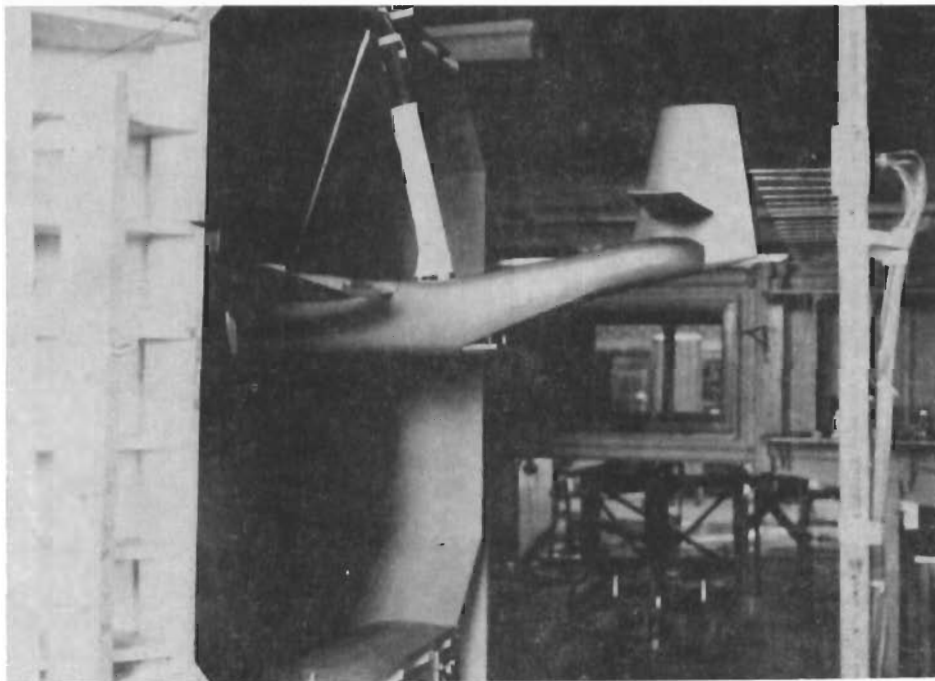


Fig 43. Caribou Airplane Model, 1/48 Scale, with Inboard Flaps



a. Caribou Airplane Model, 1/48 Scale, in Simulated Near Ground Flight in the Closed Section of the Wind Tunnel



b. Caribou Airplane Model, 1/16 Scale, in Open Section of the Wind Tunnel

Fig 44. Airplane Models Suspended in Wind Tunnel Test Sections

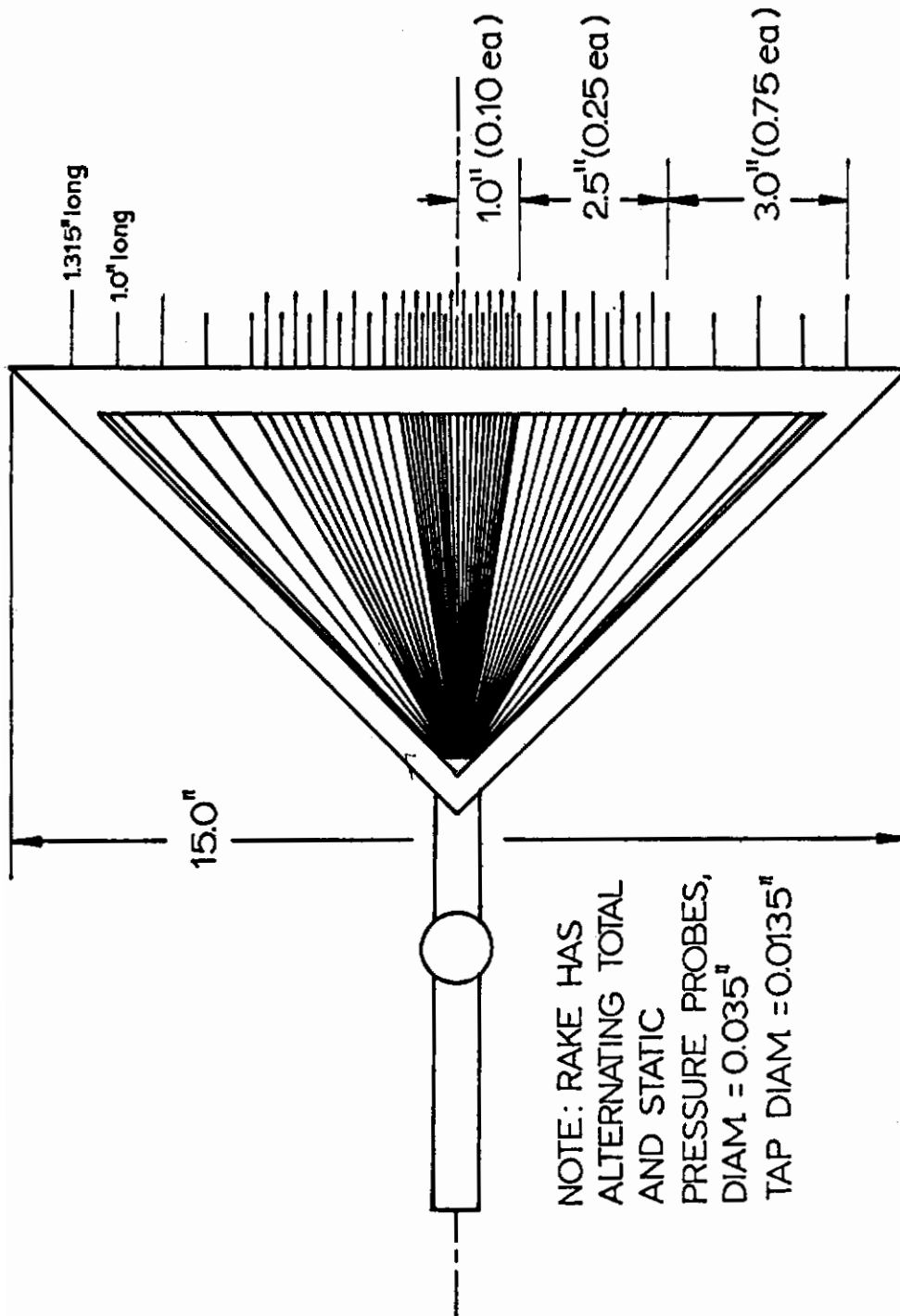
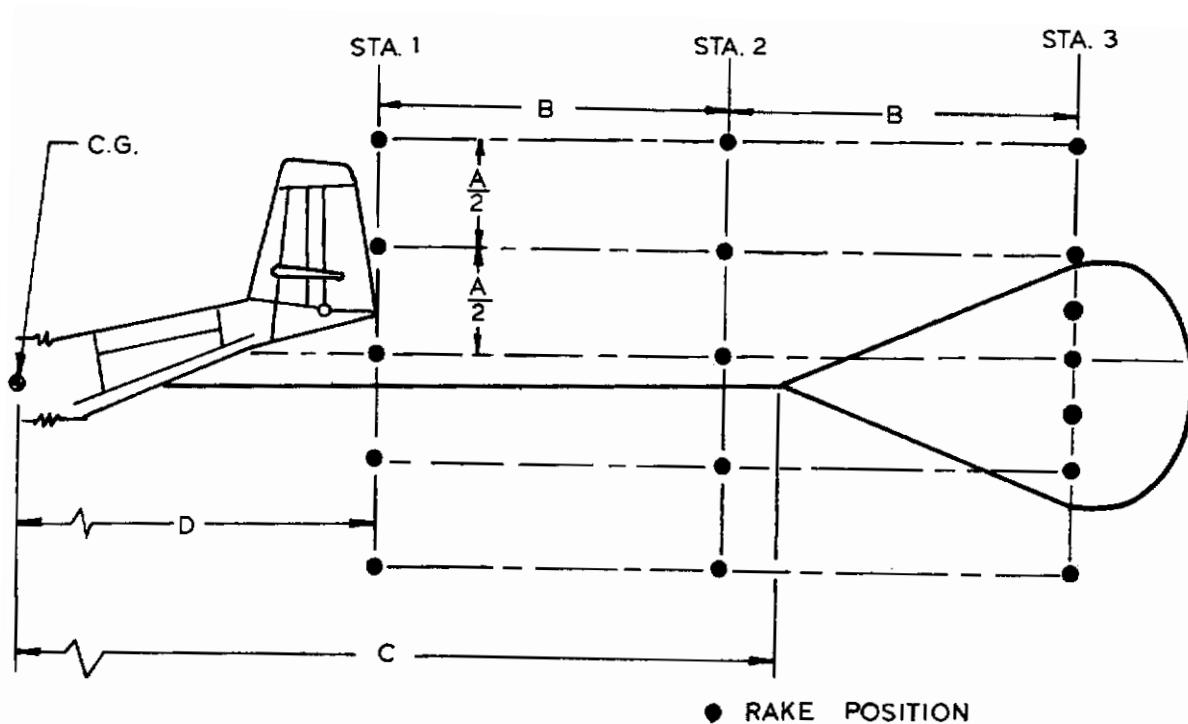


Fig 45. Pressure Survey Rake



	1/48 Model	1/16 Model	Full Size
A	3.68"	11.03"	14.7'
B	4.10"	12.30"	16.4'
C	15.00"	45.00"	60.0'
D	12.30"	36.90"	49.2'

Fig 46. Rake Positions for Wake Survey of Caribou Aircraft

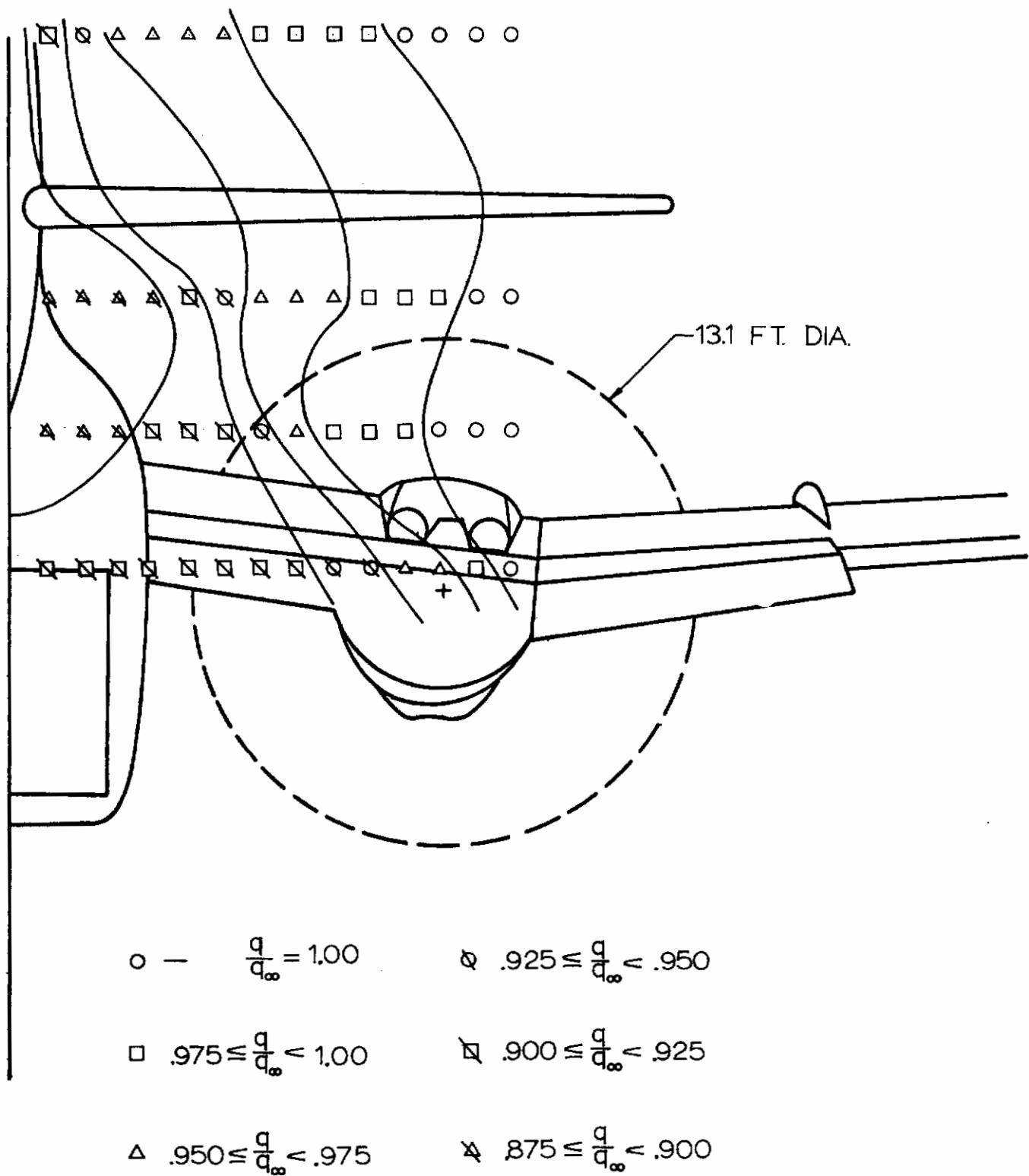


Fig 47. Pressure Field Indications and Constructed Isobars

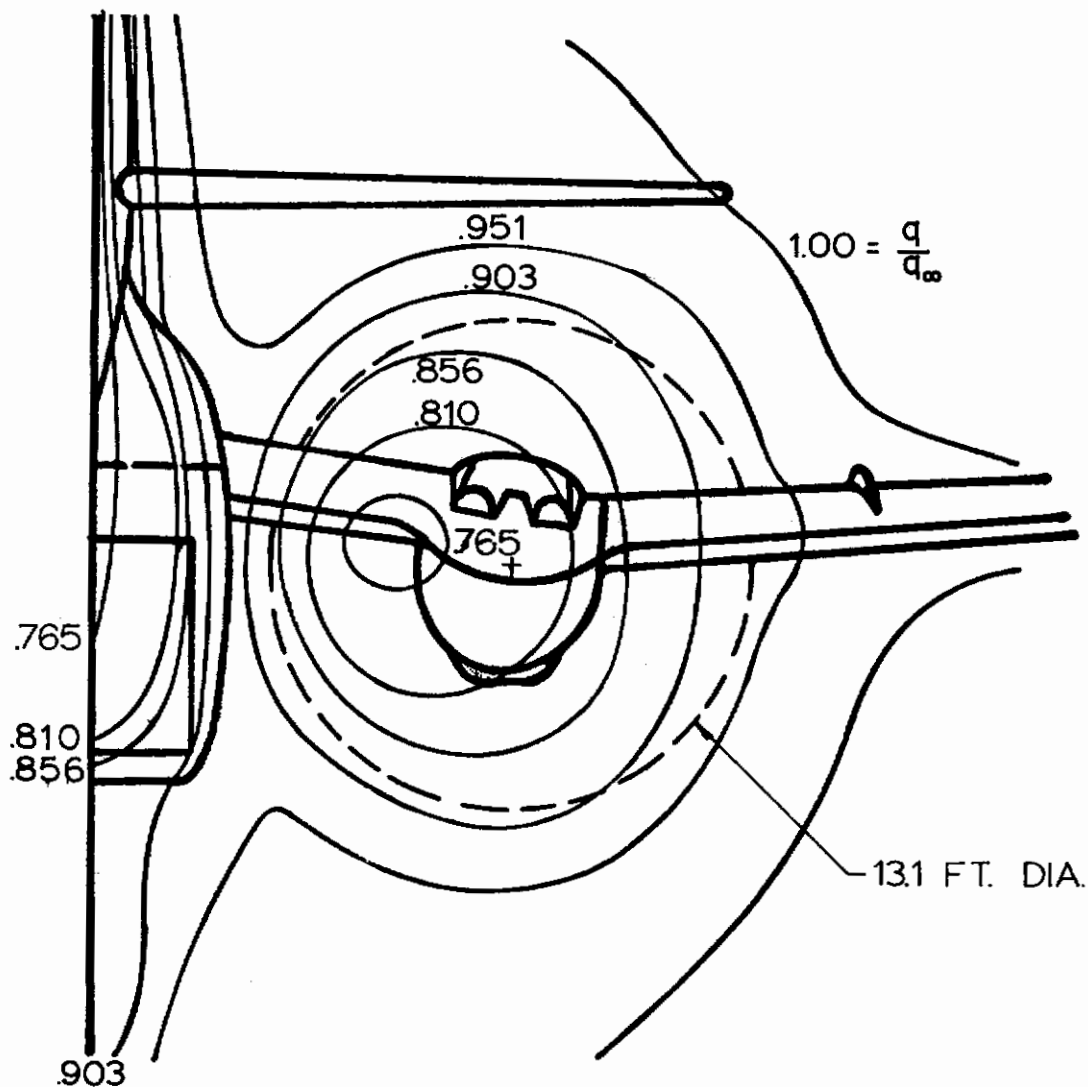


Fig 48. Dynamic Pressure Distribution of Caribou Airplane Model at Station 1 in Freestream, Unpowered and Flaps Normal Conditions (Taken from Ref 1)

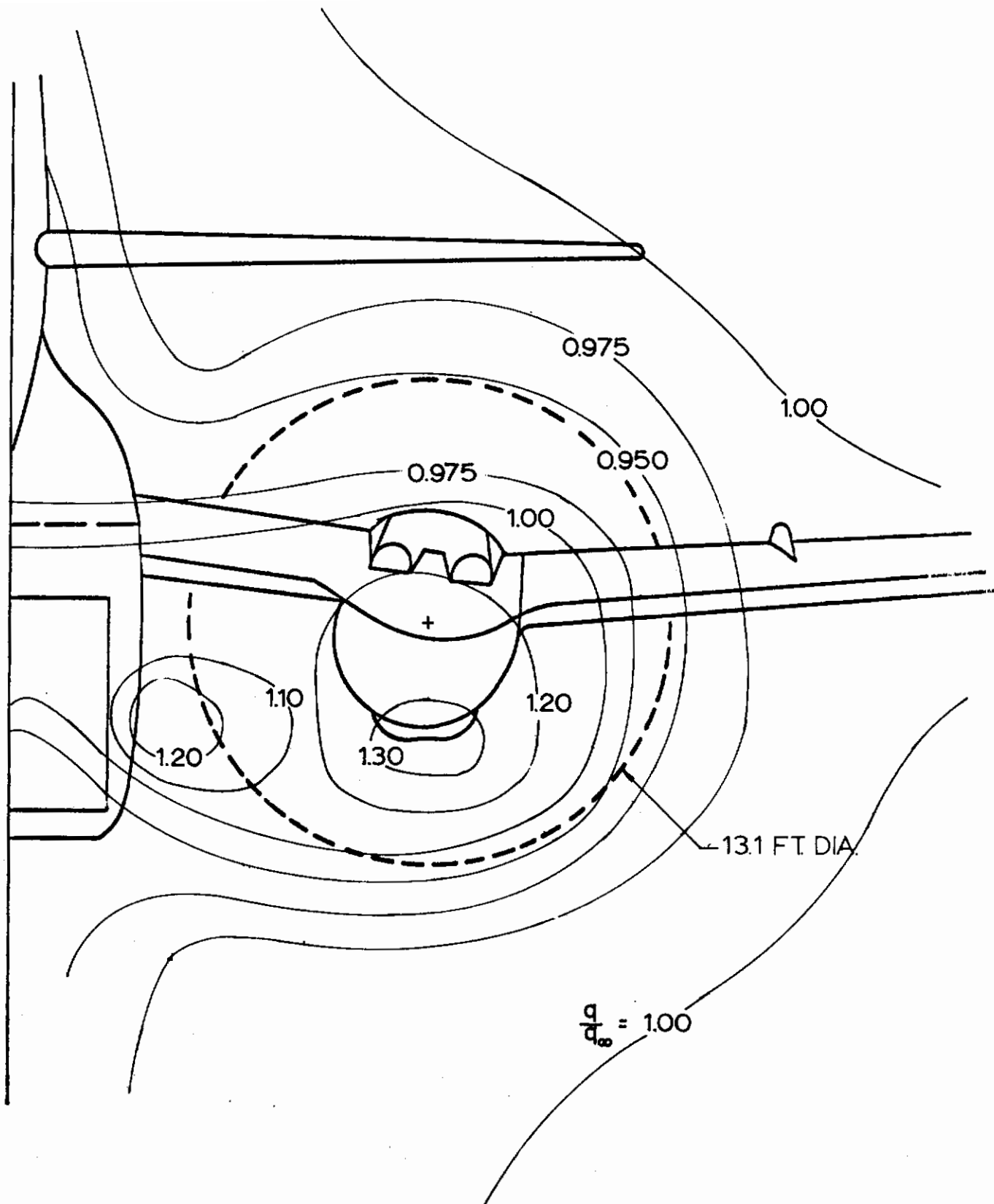


Fig 49. Dynamic Pressure Distribution of Caribou Airplane Model at Station 1 in Freestream, Powered and Flaps Normal Conditions

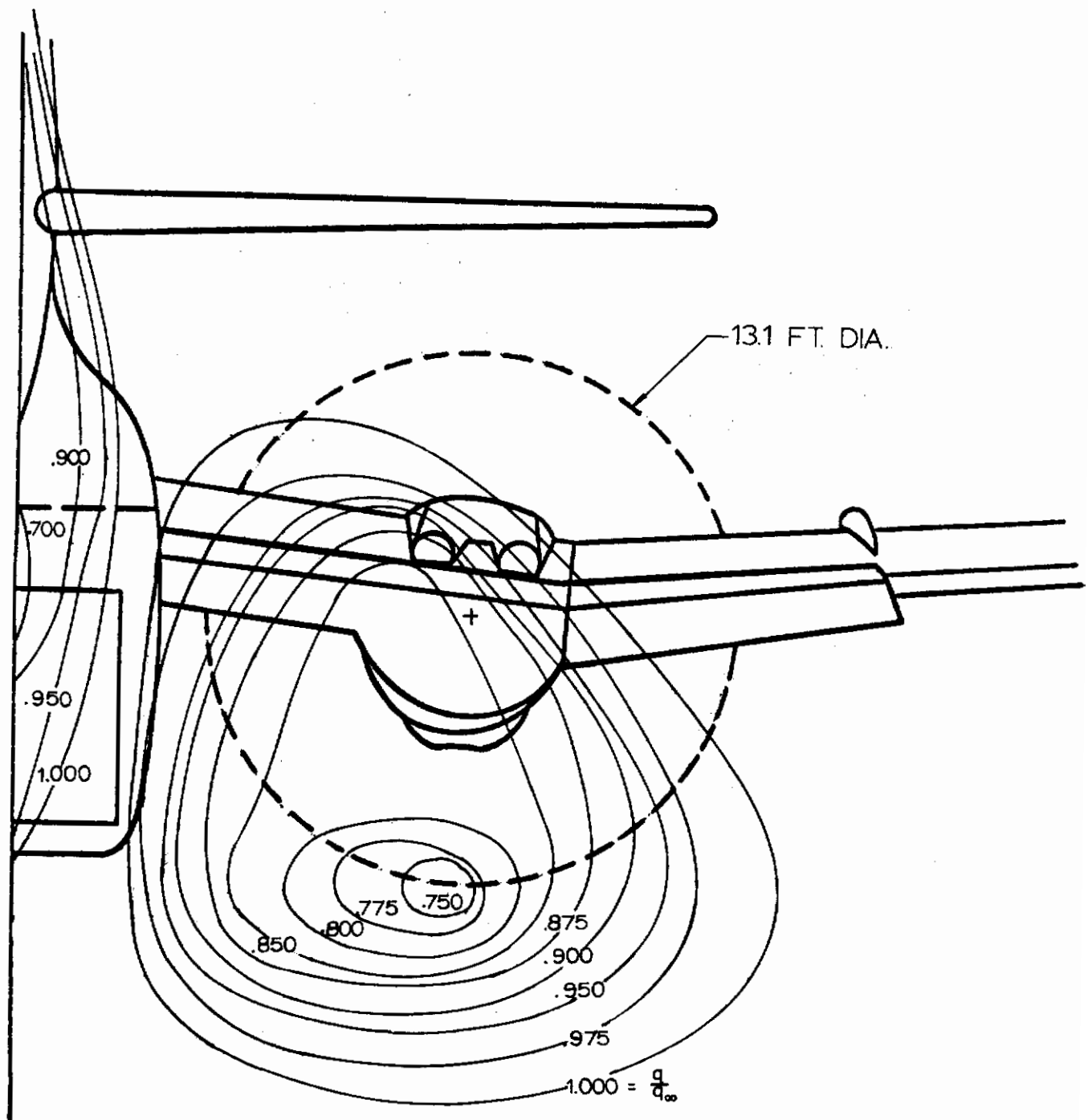


Fig 50. Dynamic Pressure Distribution of Caribou Airplane Model at Station 1 in Freestream, Unpowered and Flaps Down Conditions

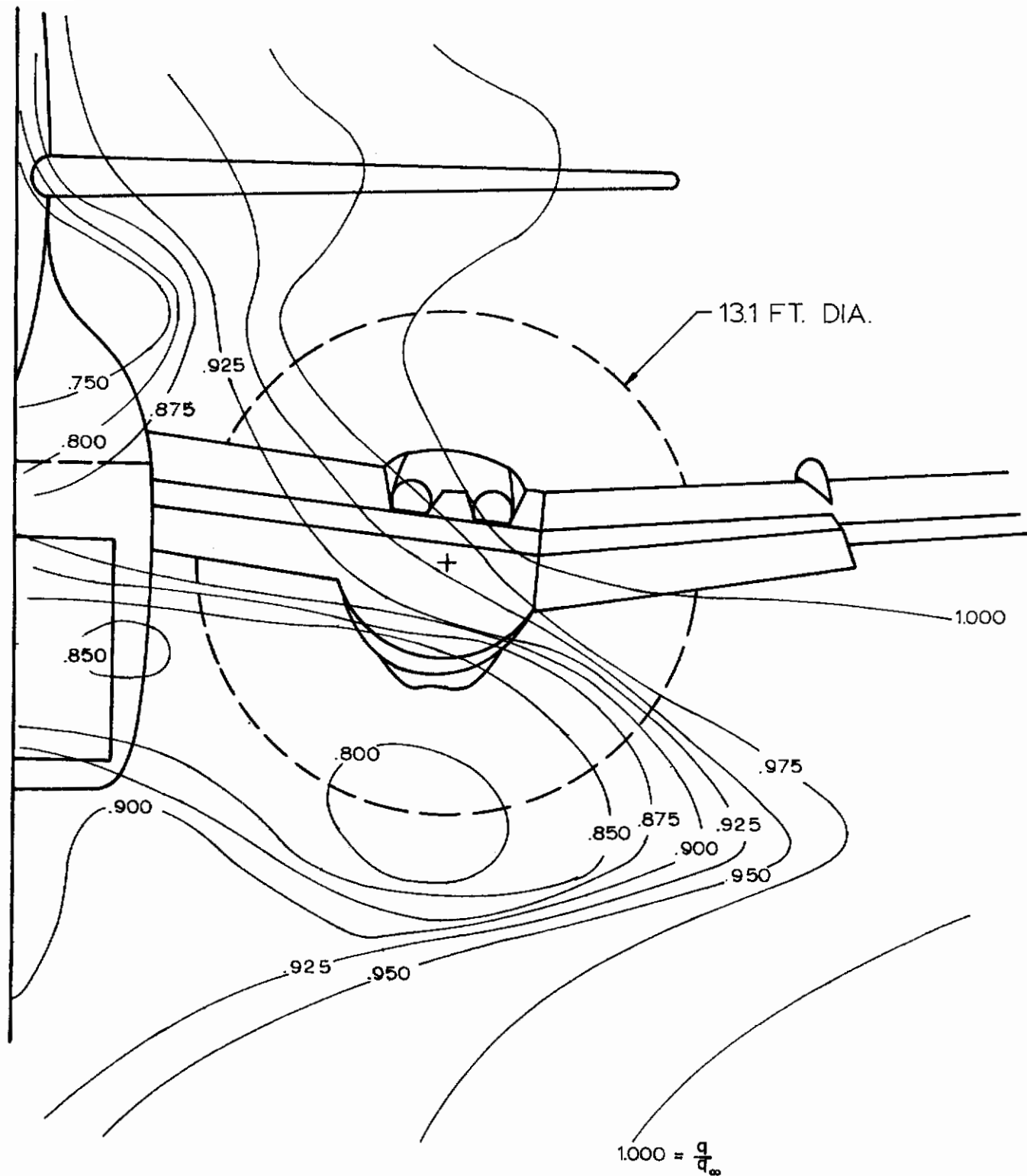


Fig 51. Dynamic Pressure Distribution of Caribou Airplane Model at Station 1 in Near Ground, Unpowered and Flaps Down Conditions

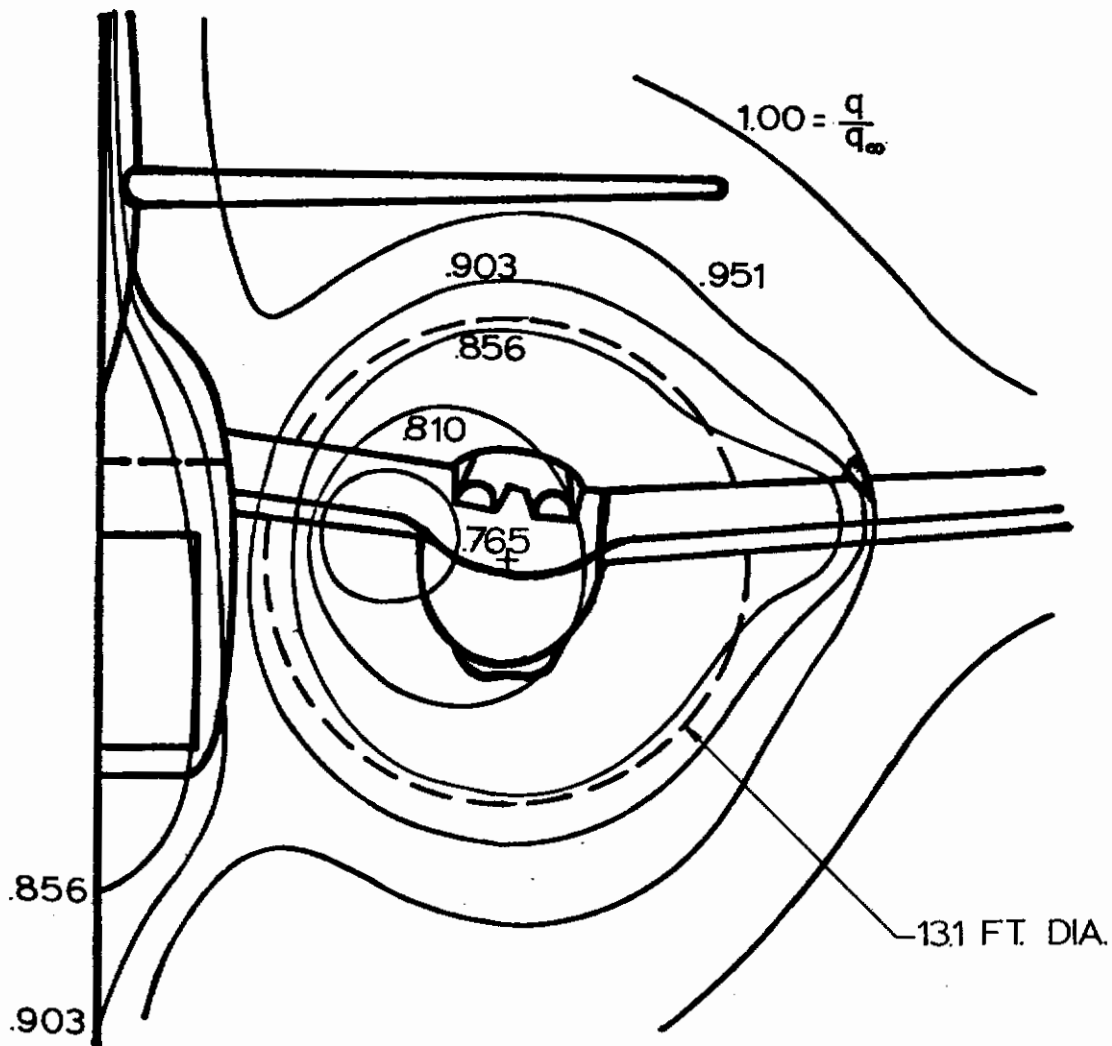


Fig 52. Dynamic Pressure Distribution of Caribou Airplane Model at Station 2 in Freestream, Unpowered and Flaps Normal Conditions (Taken from Ref 1)

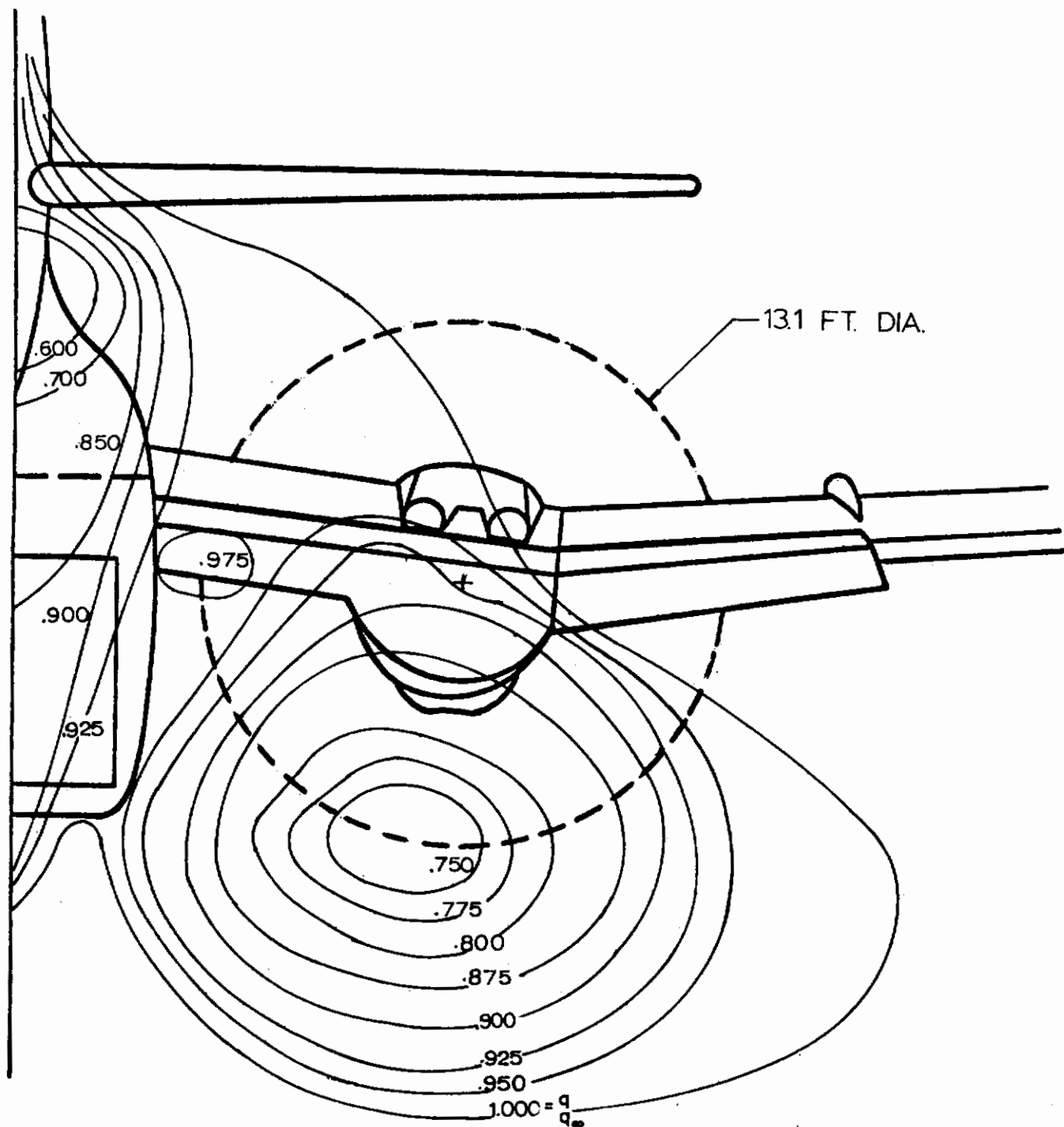


Fig 53. Dynamic Pressure Distribution of Caribou Airplane Model at Station 2 in Freestream, Unpowered and Flaps Down Conditions

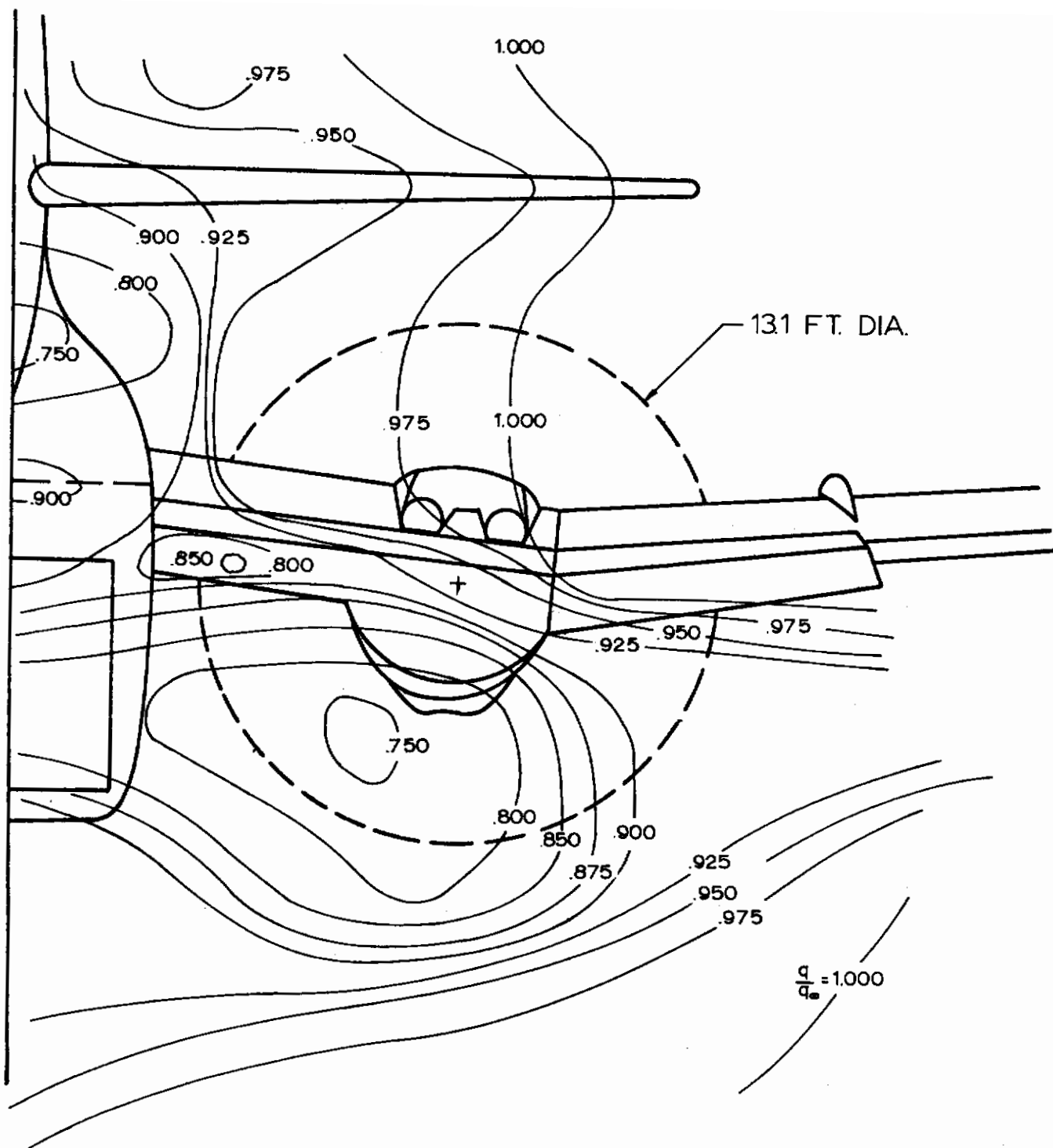


Fig 54. Dynamic Pressure Distribution of Caribou Airplane Model at Station 2 in Near Ground, Unpowered, Flaps Down Conditions

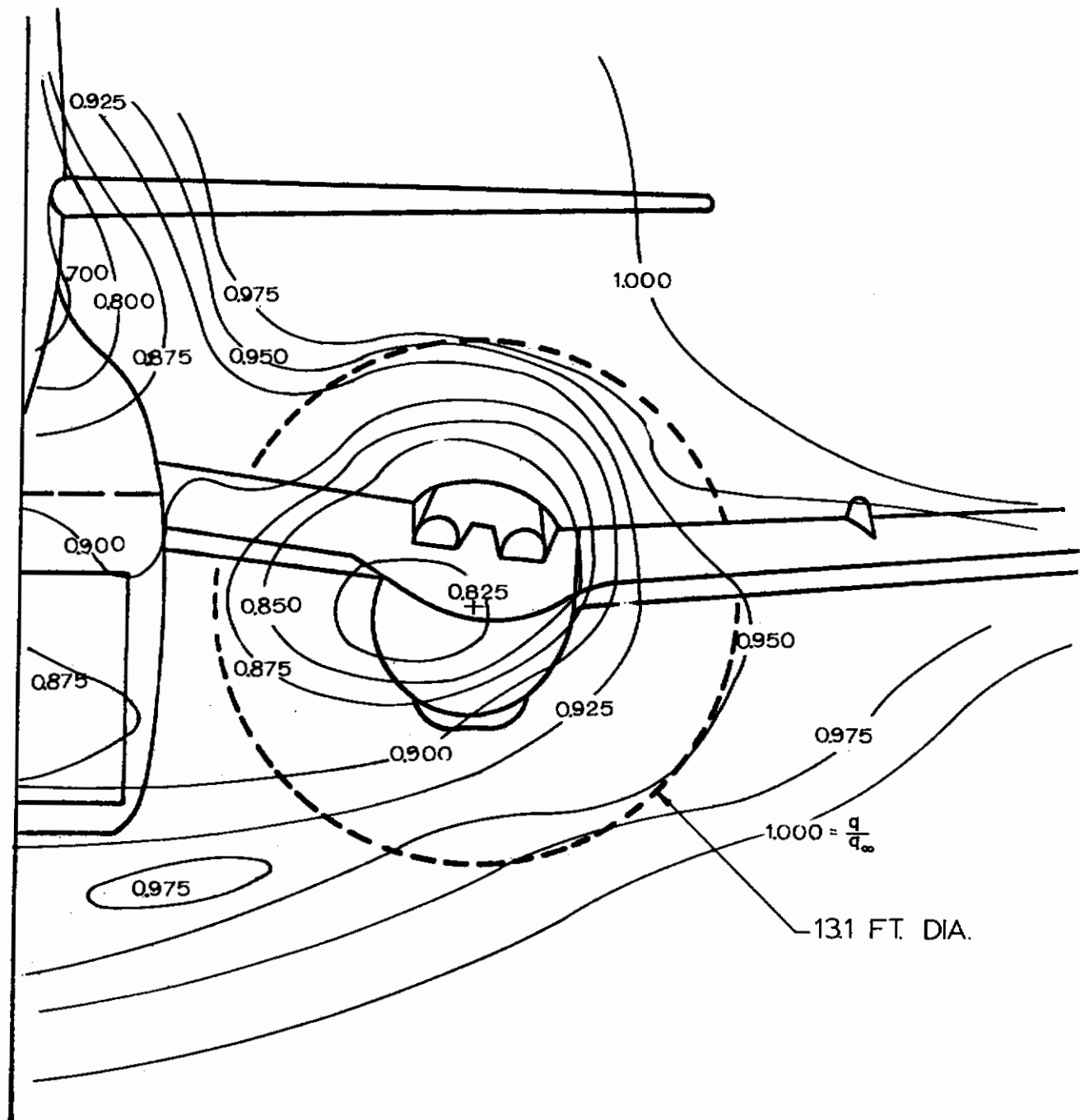


Fig 55. Dynamic Pressure Distribution of Caribou Airplane Model at Station 3 in Freestream, Unpowered and Flaps Normal Conditions

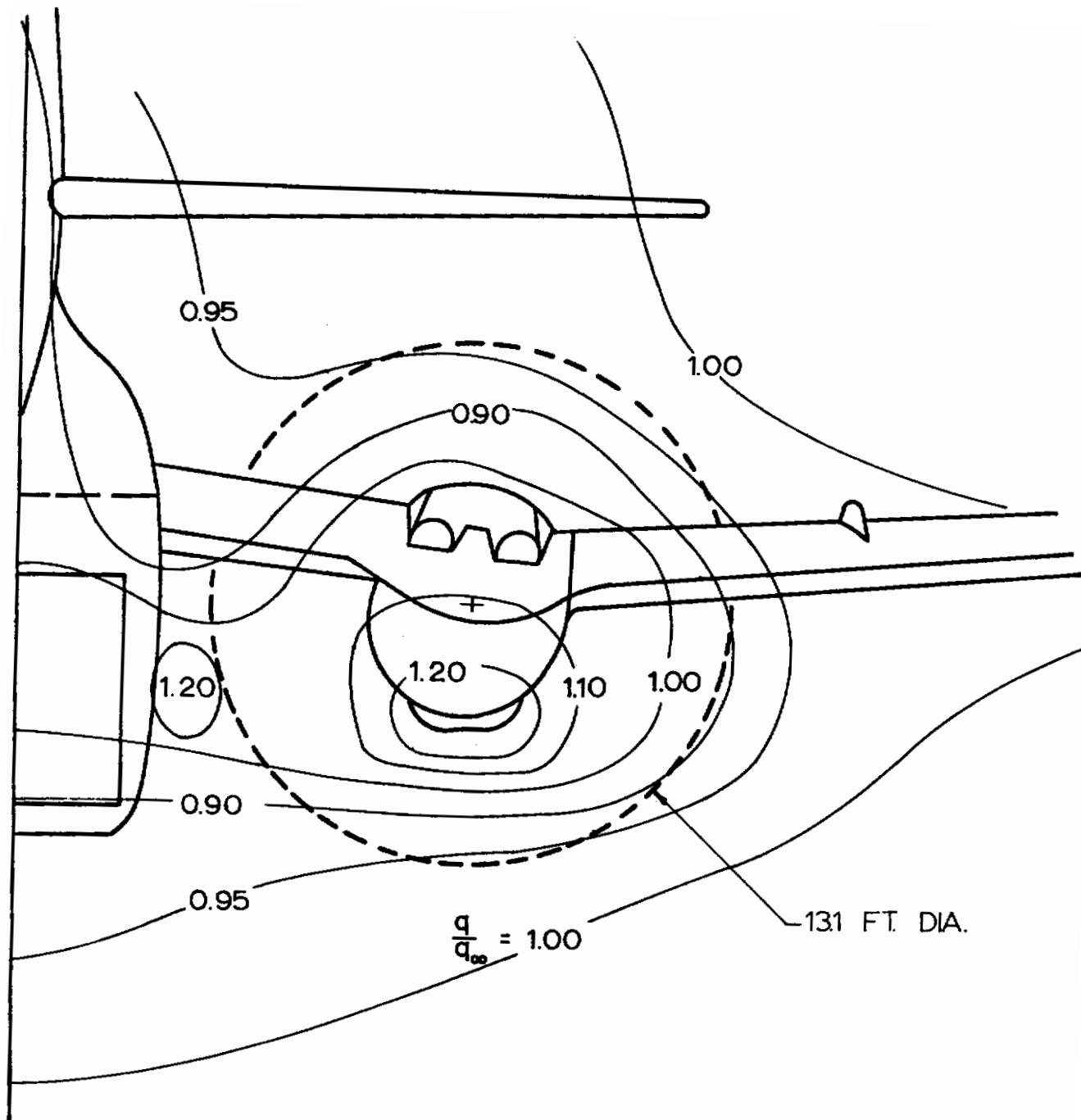


Fig 56. Dynamic Pressure Distribution of Caribou Airplane Model at Station 3 in Freestream, Powered and Flaps Normal Conditions

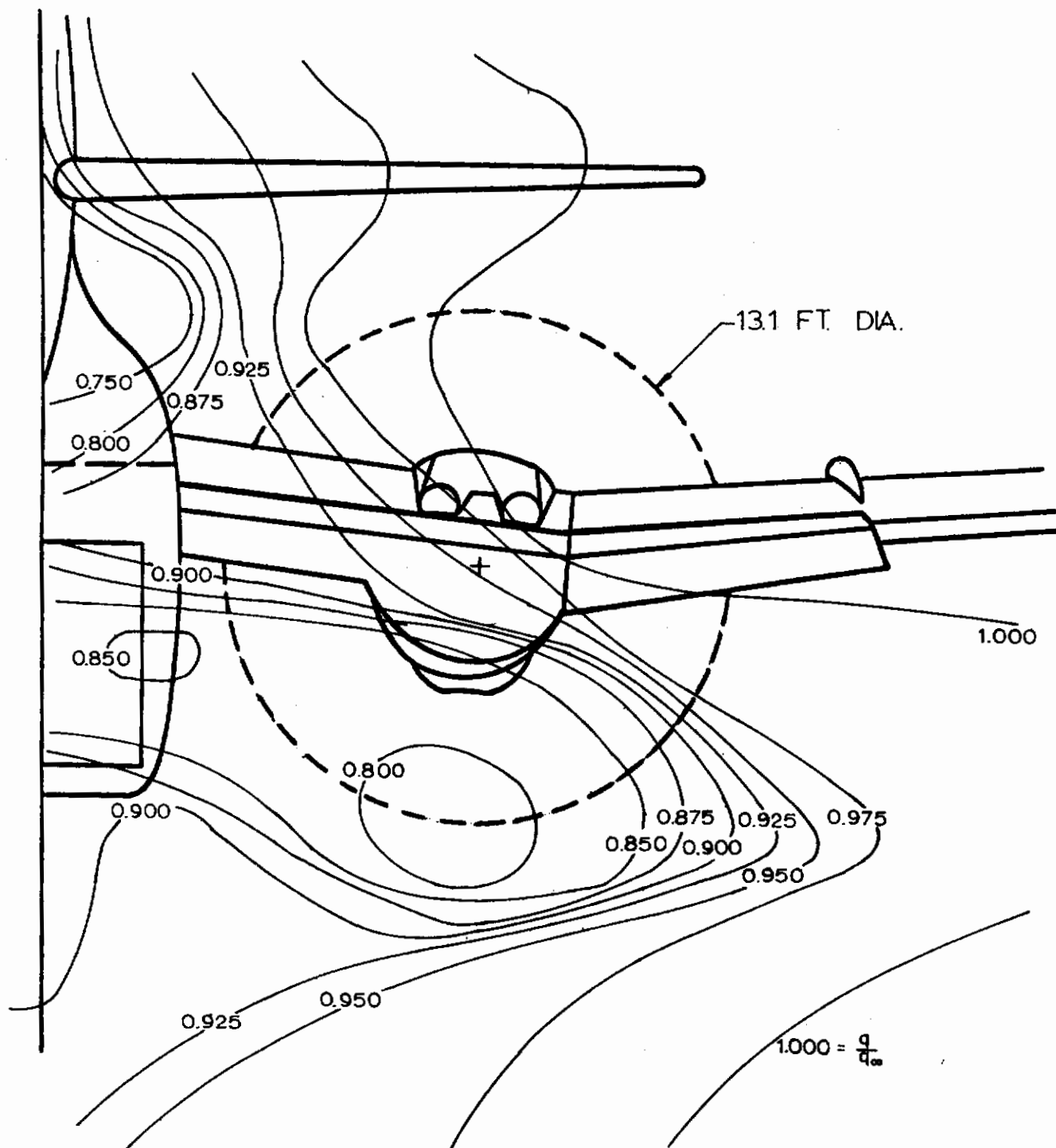


Fig 57. Dynamic Pressure Distribution of Caribou Airplane Model at Station 3 in Freestream, Unpowered and Flaps Down Conditions

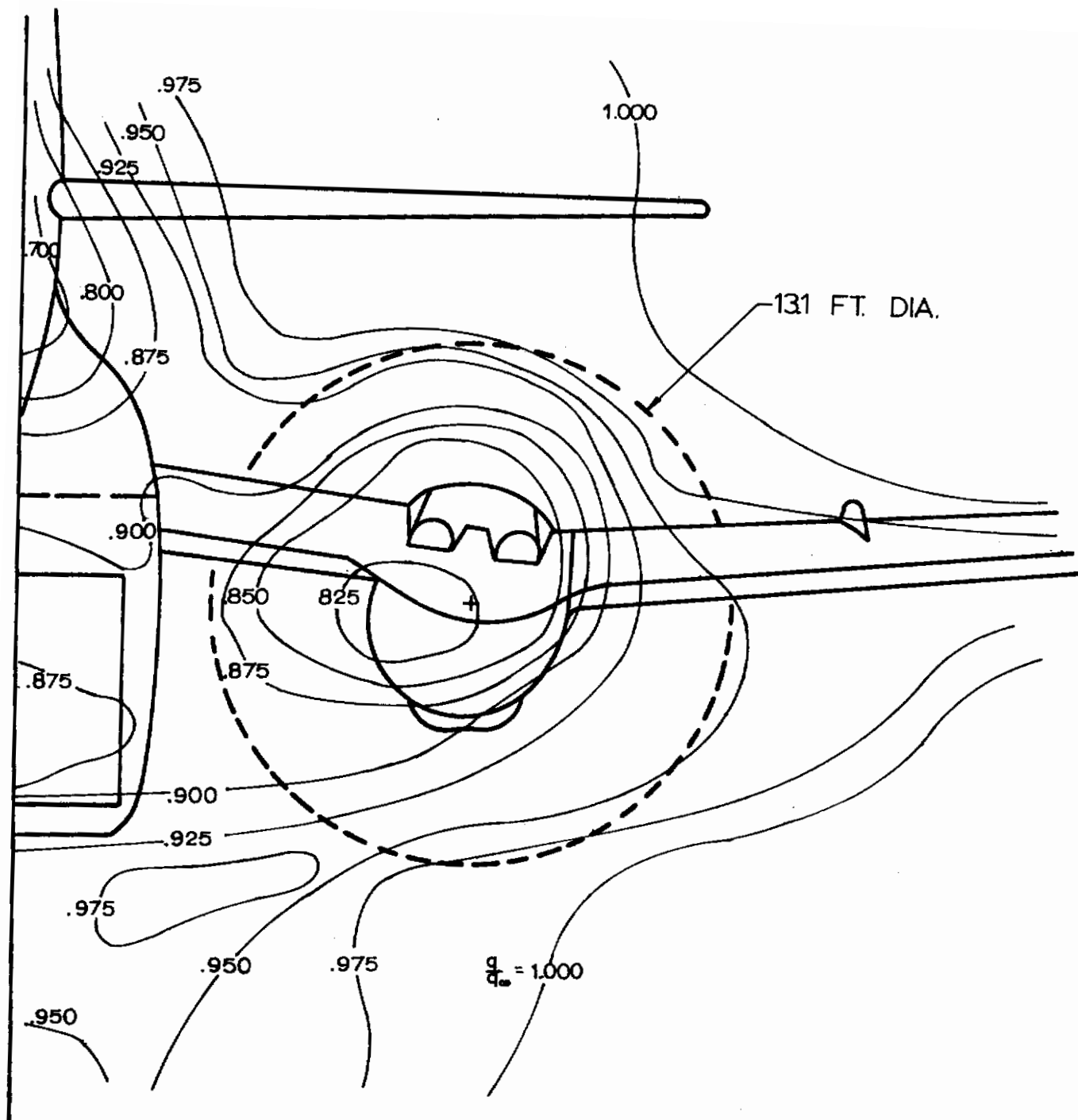


Fig 58. Dynamic Pressure Distribution of Caribou Airplane Model at Station 3 in Near Ground, Unpowered and Flaps Normal Conditions

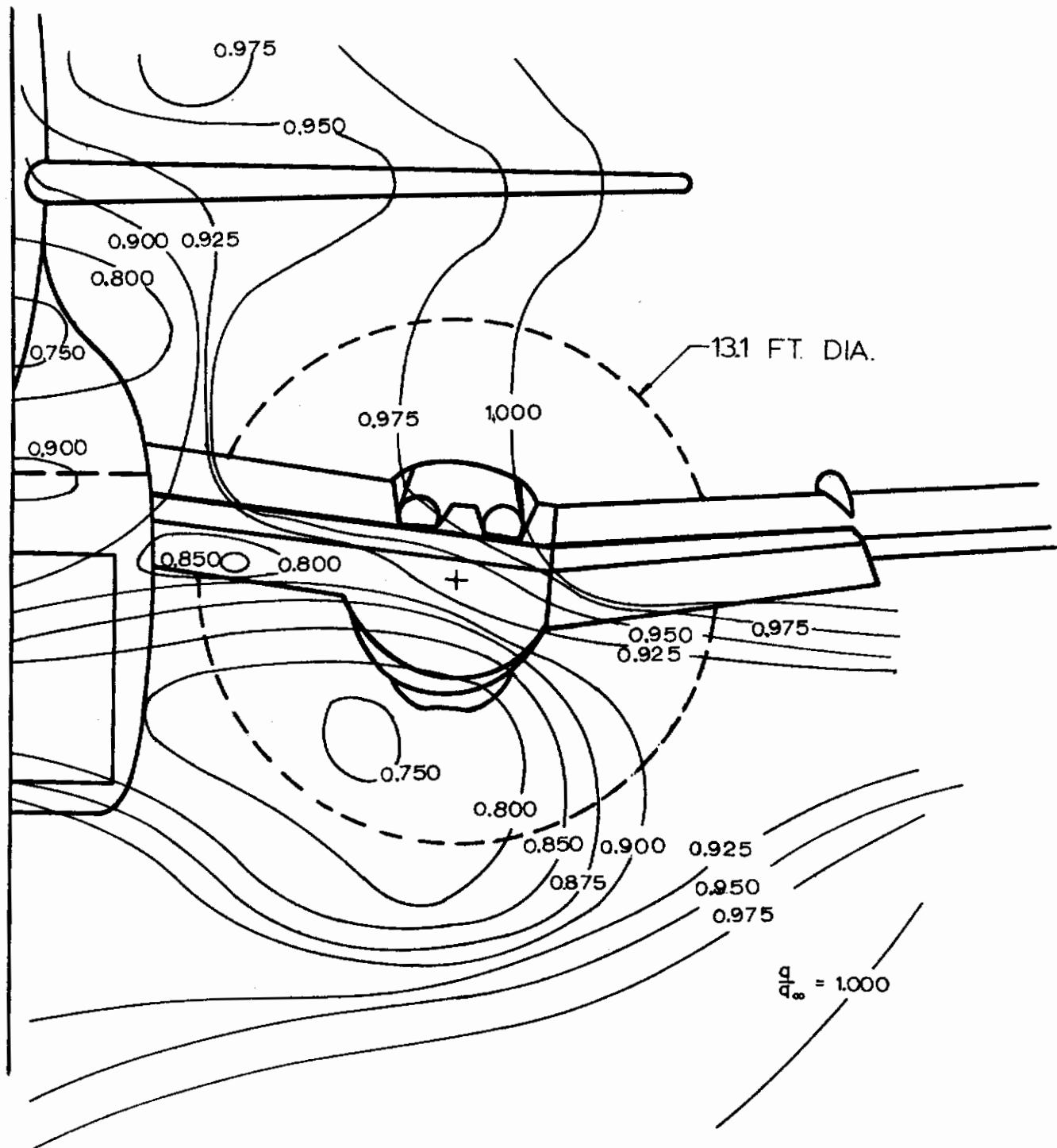


Fig 59. Dynamic Pressure Distribution of Caribou Airplane Model at Station 3 in Near Ground, Unpowered and Flaps Down Conditions

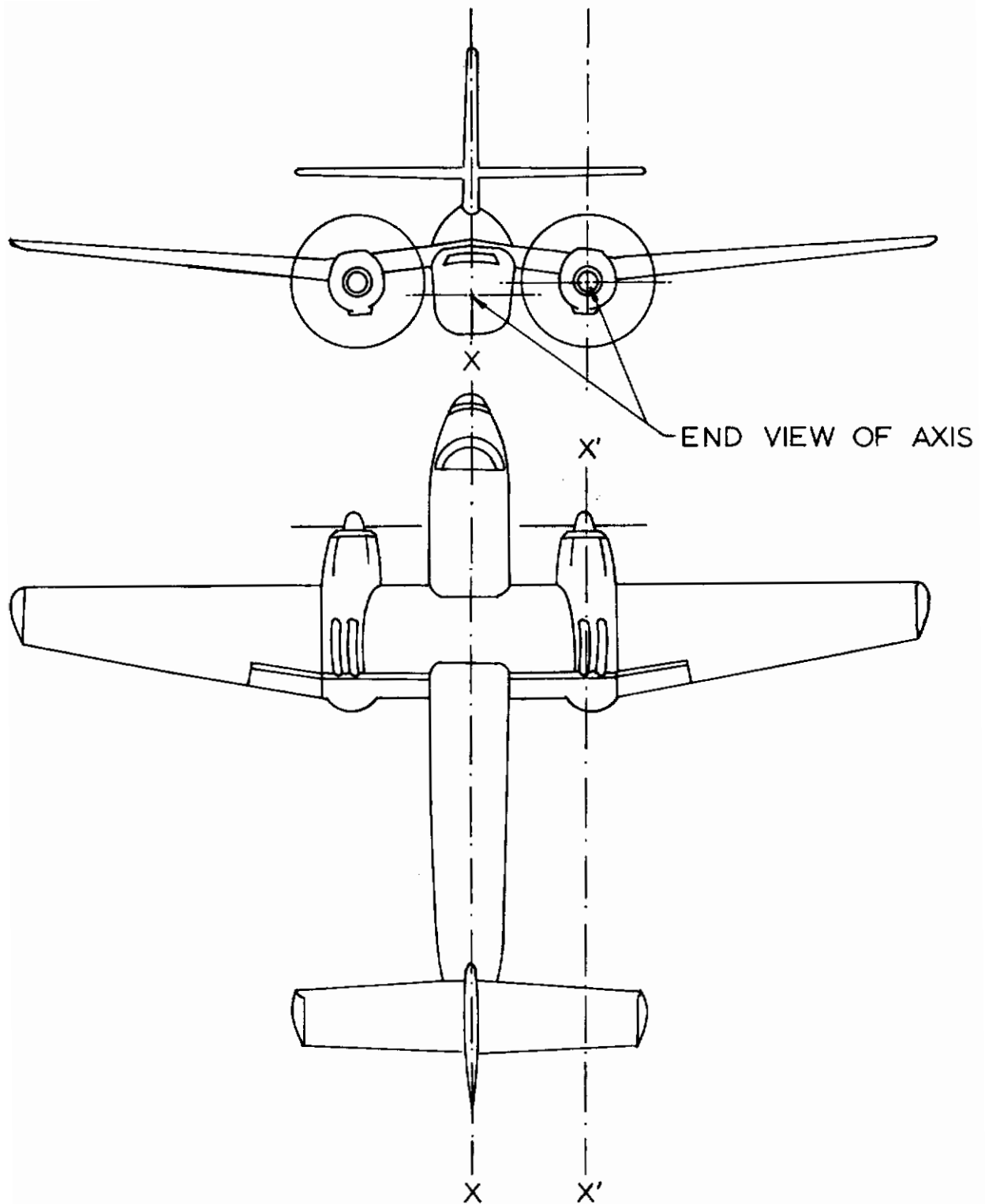


Fig 60. Airplane Axes X and X'

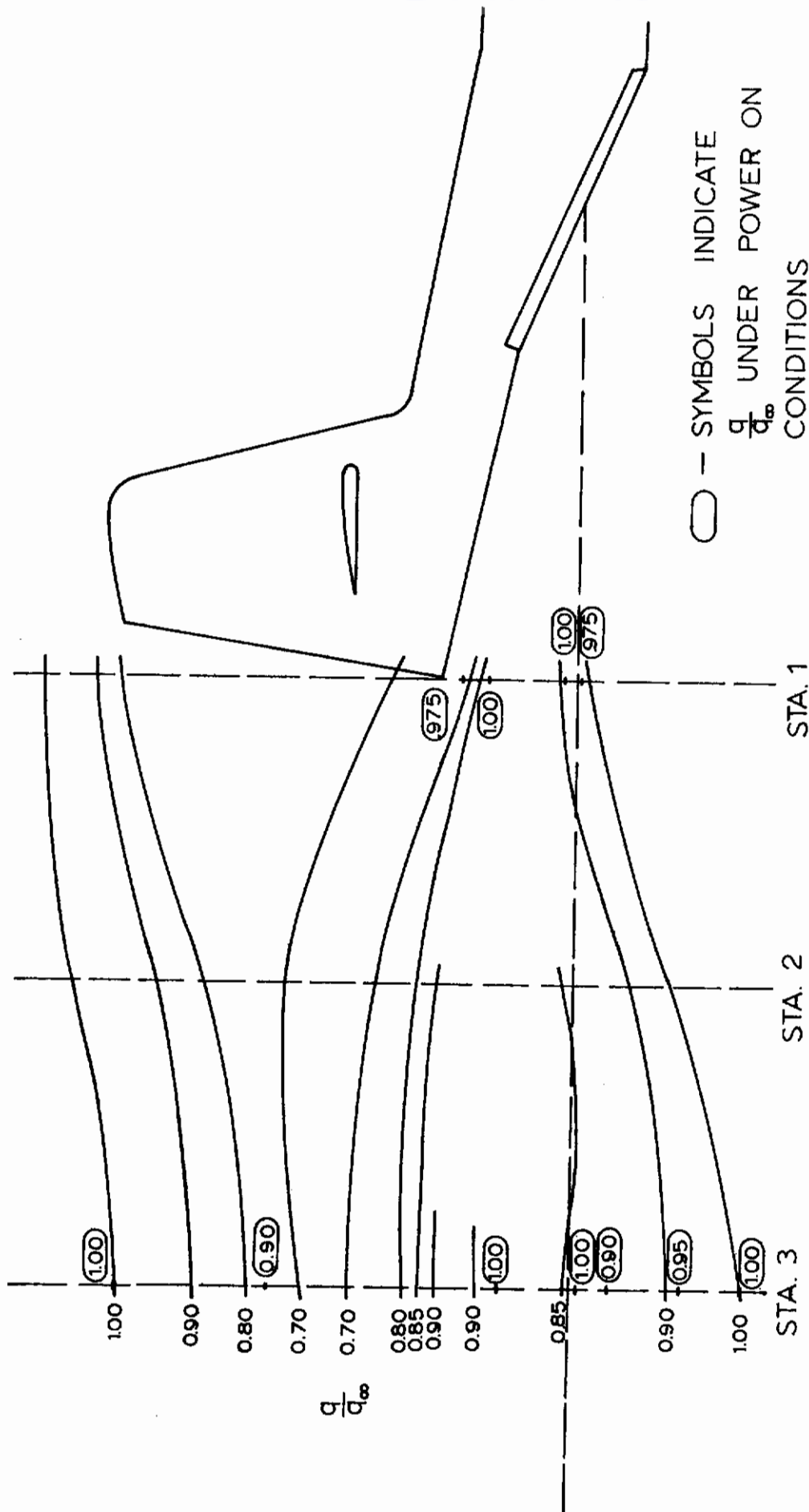


Fig 61. Dynamic Pressure Distribution of Caribou Airplane Model in Vertical Plane Containing Airplane Axis X in Freestream, Unpowered and Powered, Flaps Normal and Deflected Conditions

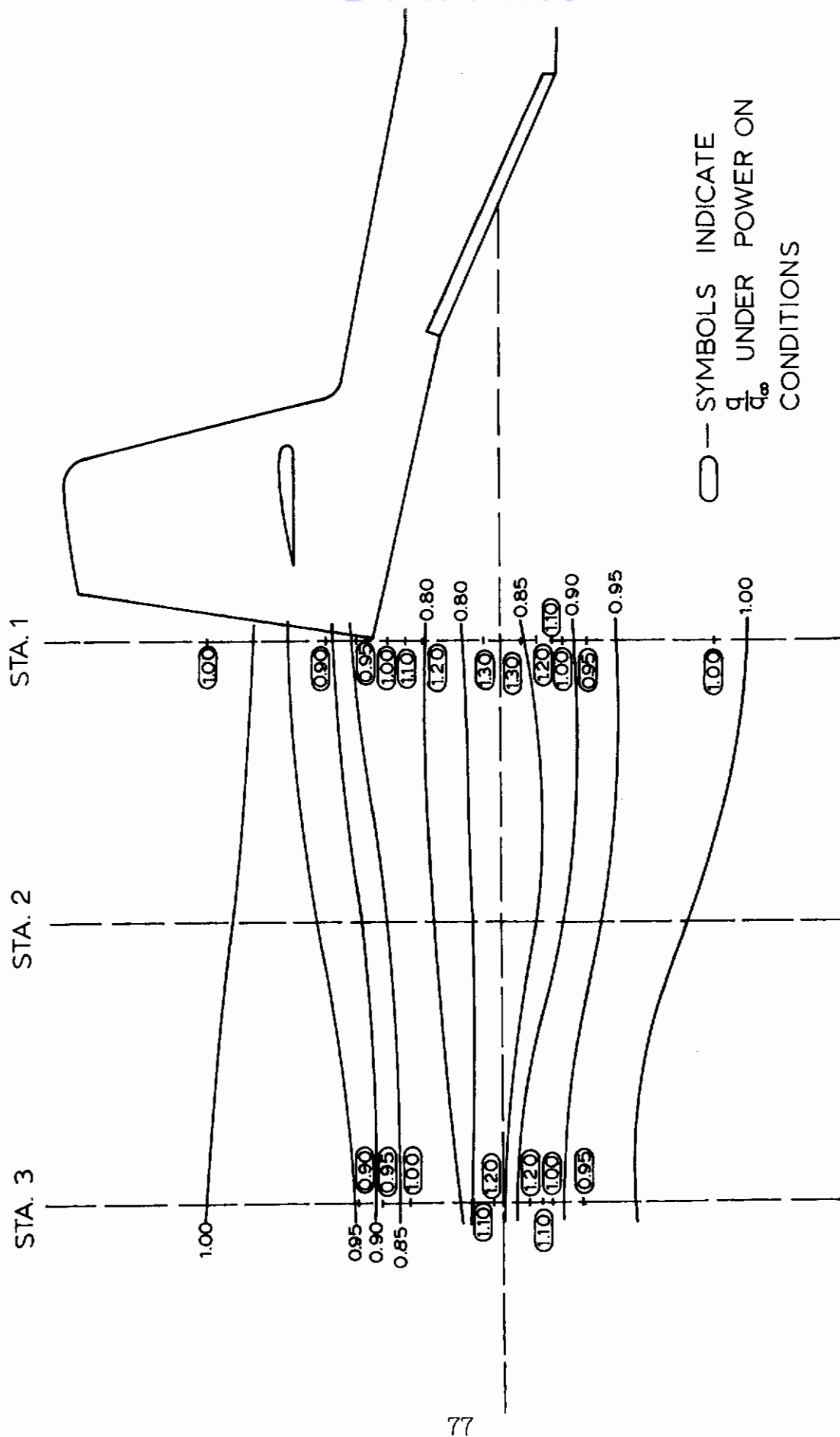


Fig 62. Dynamic Pressure Distribution of Caribou Airplane Model in Vertical Plane Containing Airplane Axis X' in Freestream, Unpowered and Powered, and Flaps Normal Conditions

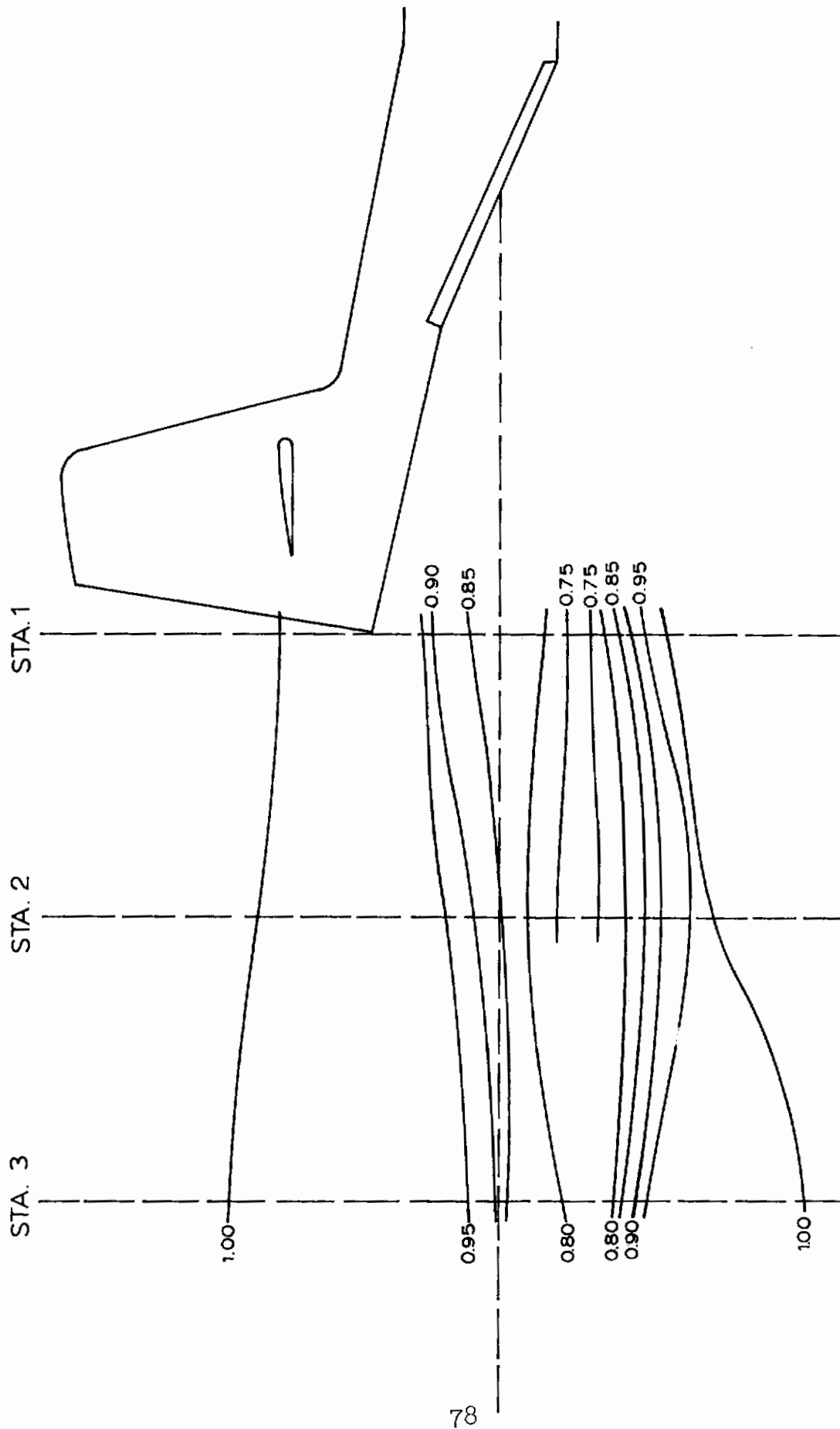


Fig 63. Dynamic Pressure Distribution of Caribou Airplane Model in Vertical Plane Containing Airplane Axis X' in Freestream, Unpowered and Flaps Deflected Conditions

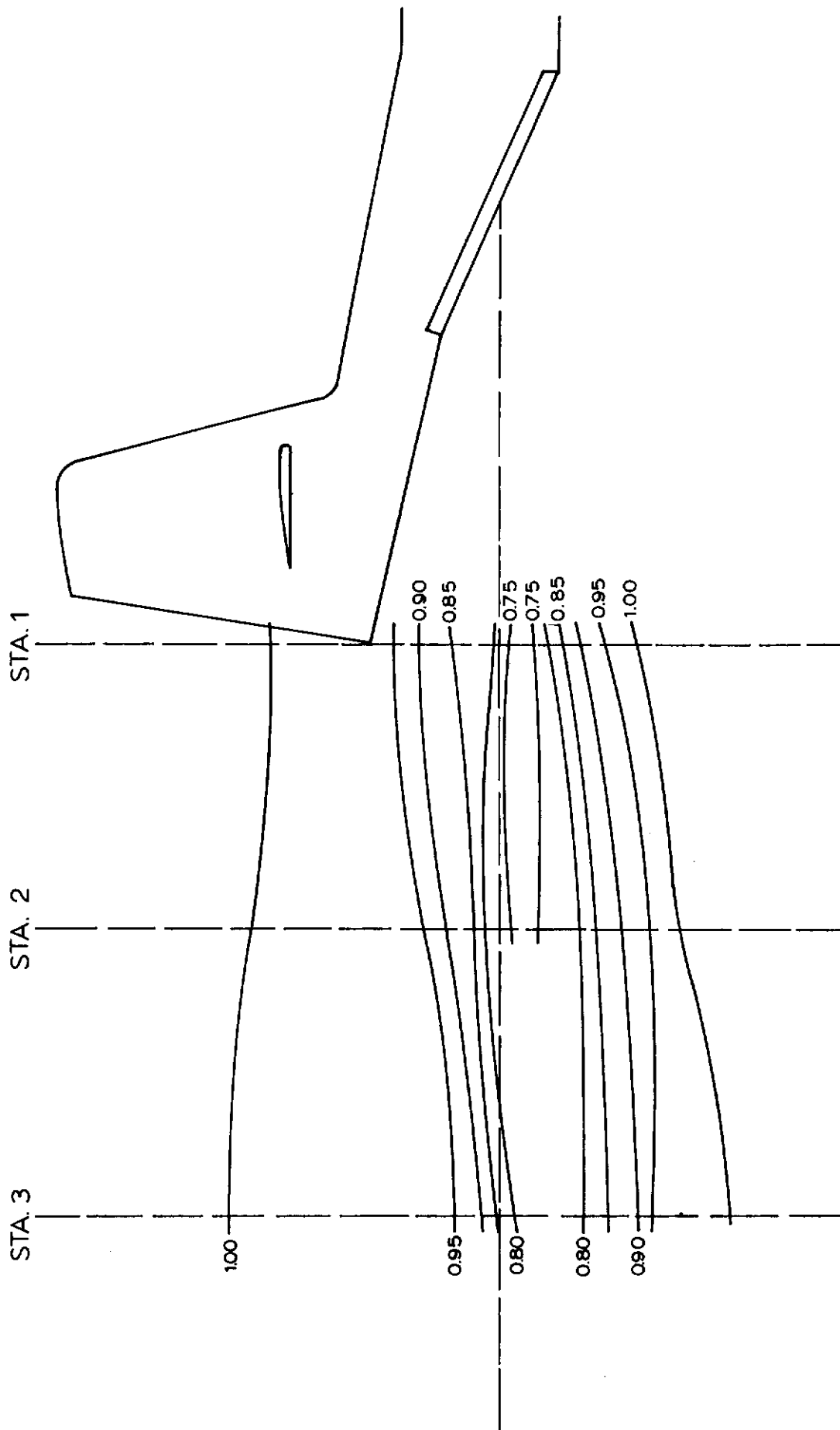


Fig 64. Dynamic Pressure Distribution of Caribou Airplane Model in Vertical Plane Containing Airplane Axis X' in Near Ground, Unpowered and Flaps Deflected Conditions

TABLE I

TEST PROGRAM FOR STUDY OF DRAG AND STABILITY
CHARACTERISTICS OF EXTRACTION PARACHUTE SYSTEMS
(Wind Tunnel Velocity $V_{\infty} = 91$ fps)

Flow Condition: Aircraft Wake	Altitude	Flap Deflection	Parachute Type	Number of Parachutes
Power ON, OFF	$h/D_0 = \infty$	0° 15°	Ringslot	1, 2, 3, & 4
		0° 15°	Solid Flat	1, 2, 3, & 4
Power ON, OFF	$h/D_0 = 1$ $h/D_0 = 2$	0° 15°	Ringslot	1, 2, 3, & 4
	$h/D_0 = 1.17$ $h/D_0 = 2.34$	0° 15°	Solid Flat	1, 2, 3, & 4

TABLE II

DRAG AND STABILITY CHARACTERISTICS OF THE
SOLID FLAT PARACHUTE CONFIGURATIONS

n = 1					
h/D ₀	Θ	Power	C _D	Ø ₁	Ø ₂
1.17	0°	On	0.605	23.5	11.3
		Off	0.679	23.5	12.5
	15°	On	0.619	24.5	11.7
		Off	0.665	27.0	11.0
2.34	0°	On	0.707	23.3	21.8
		Off	0.752	23.3	24.8
	15°	On	0.639	20.0	23.0
		Off	0.644	27.0	27.0
∞	0°	On	0.685	9.9	27.3
		Off	0.669	27.2	28.9
	15°	On	0.665	24.0	28.0
		Off	0.646	25.0	31.0

n = 2					
h/D ₀	Θ	Power	C _D	Ø ₁	Ø ₂
1.17	0°	On	0.673	21.8	12.5
		Off	0.670	23.5	8.2
	15°	On	0.650	18.1	9.9
		Off	0.670	18.0	0.1
2.34	0°	On	0.669	20.0	20.5
		Off	0.662	16.7	16.0
	15°	On	0.625	11.3	21.3
		Off	0.638	15.0	21.0
∞	0°	On	0.690	18.4	24.0
		Off	0.618	16.5	22.8
	15°	On	0.679	15.7	19.6
		Off	0.629	17.0	25.0

TABLE II (CONT.)

n = 3					
h/D ₀	Θ	Power	C _D	Ø ₁	Ø ₂
1.17	0°	On	0.650	15.3	7.1
		Off	0.632	16.6	7.0
	15°	On	0.606	9.8	9.7
		Off	0.625	14.0	8.0
2.34	0°	On	0.639	11.3	15.3
		Off	0.617	9.5	12.0
	15°	On	0.608	6.2	16.8
		Off	0.620	10.0	15.0
∞	0°	On	0.661	10.4	13.8
		Off	0.604	11.8	17.9
	15°	On	0.642	2.7	20.6
		Off	0.579	8.0	17.0

n = 4					
h/D ₀	Θ	Power	C _D	Ø ₁	Ø ₂
1.17	0°	On	0.604	8.9	3.2
		Off	0.568	9.9	3.5
	15°	On	0.587	9.5	7.1
		Off	0.575	7.0	6.0
2.34	0°	On	0.621	7.1	11.3
		Off	0.607	3.0	10.0
	15°	On	0.606	2.9	15.8
		Off	0.587	4.0	13.0
∞	0°	On	0.656	5.8	12.3
		Off	0.522	1.4	13.3
	15°	On	0.636	2.7	15.2
		Off	0.571	1.0	11.0

TABLE III

DRAG AND STABILITY CHARACTERISTICS OF THE
RINGSLOT PARACHUTE CONFIGURATIONS

n = 1						
h/D ₀	Θ	Power	C _D	Ø ₁	Ø ₂	α ± Δα
1	0°	On	0.494	+3.3	0.0	+1.6±1.6
		Off	0.469	+3.6	+2.0	+2.4±1.2
	15°	On	0.503	+2.7	+5.2	-3.8±1.0
		Off	0.473	+2.5	+4.5	+0.5±1.2
2	0°	On	0.501	+3.5	+5.4	-1.8±2.6
		Off	0.474	+4.3	+3.3	-2.0±1.3
	15°	On	0.522	+3.2	+8.8	-4.1±1.7
		Off	0.483	+1.0	+6.0	-2.5±3.6
∞	0°	On	0.534	+3.6	+5.4	-1.3±1.4
		Off	0.513	-0.9	+3.2	-2.5±0.7
	15°	On	0.492	+1.0	+10.6	-7.5±3.3
		Off	0.482	+2.0	+12.0	-6.0±2.3

n = 2						
h/D ₀	Θ	Power	C _D	Ø ₁	Ø ₂	α ± Δα
1	0°	On	0.500	+0.6	0.0	+0.4±0.2
		Off	0.473	+1.3	-0.1	+0.7±0.6
	15°	On	0.430	+3.9	+2.9	-2.0±0.9
		Off	0.437	+4.0	+2.5	+0.5±1.3
2	0°	On	0.479	+1.1	+0.7	-0.4±0.3
		Off	0.438	+3.6	+1.8	+0.2±1.1
	15°	On	0.401	+2.8	+1.6	+1.3±1.5
		Off	0.452	-1.0	+2.5	-1.5±0.5
∞	0°	On	0.494	-2.7	+4.4	-3.6±0.8
		Off	0.448	+2.9	+0.9	+1.0±1.9
	15°	On	0.429	+1.2	+3.6	-0.1±1.1
		Off	0.452	-1.0	+4.0	-2.0±0.3

TABLE III (CONT.)

n = 3						
h/D ₀	θ	Power	C _D	ϕ ₁	ϕ ₂	α ± Δα
1	0°	On	0.432	+3.6	-1.2	+2.4±1.2
		Off	0.429	+2.5	-0.9	+1.7±0.8
	15°	On	0.418	+3.3	+1.4	+2.3±1.0
		Off	0.419	+4.0	+0.5	+1.5±1.0
2	0°	On	0.448	+2.9	+2.0	+0.1±1.8
		Off	0.433	+2.6	-1.2	+1.9±0.7
	15°	On	0.433	+1.0	+5.7	-0.4±1.0
		Off	0.441	+0.5	+2.0	-1.0±0.5
∞	0°	On	0.462	+2.2	+3.1	+1.1±1.1
		Off	0.416	+1.3	-0.6	+1.0±0.4
	15°	On	0.463	-2.4	+4.5	-3.7±1.2
		Off	0.432	-2.0	+7.0	-5.0±0.6

n = 4						
h/D ₀	θ	Power	C _D	ϕ ₁	ϕ ₂	α ± Δα
1	0°	On	0.427	+5.7	-3.3	+4.0±0.9
		Off	0.440	+3.0	+2.0	+2.5±0.4
	15°	On	0.366	+4.1	-0.2	+1.1±0.9
		Off	0.390	+4.0	+0.5	+1.5±1.0
2	0°	On	0.421	+3.2	-1.0	+2.1±1.1
		Off	0.433	+3.8	-0.9	+2.6±1.2
	15°	On	0.420	+0.8	+4.3	-1.5±2.2
		Off	0.394	+0.5	+0.5	0.0±0.5
∞	0°	On	0.415	+2.7	-2.0	+2.3±0.4
		Off	0.404	+3.1	+0.8	+0.1±0.9
	15°	On	0.441	-1.5	+5.2	-2.9±1.6
		Off	0.424	0.0	+5.0	-2.0±0.8

Table IV
Wake Survey Test Configurations

Configurations				Sta.	Model Scale
No.	Power	Flaps	Stream		
1/1a	off/on	normal	free	1	1:48/1:16
2	off	deflect	free	1	1:48
3	off	deflect	ground	1	1:48
4	off	normal	free	2	1:48
5	off	deflect	free	2	1:48
6	off	deflect	ground	2	1:48
7/7a	off/on	normal	free	3	1:48/1:16
8	off	deflect	free	3	1:48
9	off	normal	ground	3	1:48
10	off	deflect	ground	3	1:48

Contrails

Security Classification

DOCUMENT CONTROL DATA - R & D

(Security classification of title, body of abstract and indexing annotation must be entered when the overall report is classified)

1. ORIGINATING ACTIVITY (Corporate author) University of Minnesota Minneapolis, Minnesota 55455		2a. REPORT SECURITY CLASSIFICATION Unclassified	
		2b. GROUP N/A	
3. REPORT TITLE Behavior of Extraction Parachutes in the Wake of a Powered Airplane Model.			
4. DESCRIPTIVE NOTES (Type of report and inclusive dates) Final Report December 1966 - October 1967			
5. AUTHOR(S) (First name, middle initial, last name) Heinrich, Helmut G. Hulcher, G. D.			
6. REPORT DATE August 1968	7a. TOTAL NO. OF PAGES 85	7b. NO. OF REFS 2	
8a. CONTRACT OR GRANT NO. F33615-67-C-1010 b. PROJECT NO. 6065 c. Task No. 606503 d.	9a. ORIGINATOR'S REPORT NUMBER(S) None 9b. OTHER REPORT NO(S) (Any other numbers that may be assigned this report) AFFDL-TR-68-15		
10. DISTRIBUTION STATEMENT This document is subject to special export controls and each transmittal to foreign governments or foreign nationals may be made only with prior approval of the AF Flight Dynamics Laboratory.			
11. SUPPLEMENTARY NOTES		12. SPONSORING MILITARY ACTIVITY Air Force Flight Dynamics Laboratory AFFDL (FDFR) Wright-Patterson AFB, Ohio 45433	
13. ABSTRACT <p style="margin-top: 10px;"> The drag and stability characteristics of single and clustered solid flat and ringslot parachutes as cargo extraction systems in the wake of a model of the Caribou airplane with windmilling and powered propellers are reported. The investigation also includes the effect of actuated wing trailing flaps, and the variation of the parachute performance parameters in midair and near the ground. It was found that in all cases the drag coefficient of the cluster decreases with the increased number of canopies in the cluster, and a single ringslot parachute is more stable than the most stable cluster of solid flat canopies. The effects of the powered propeller slipstream and flap actuation are noticeable but not dominating. Also, wake surveys of the airplane showed characteristic dynamic pressure defects or increases for power off or on flight conditions. The location of these pressure fields was noticeably influenced by flap actuation and ground effects. </p> <p style="margin-top: 10px;"> (The distribution of this Abstract is unlimited). </p>			

DD FORM 1473
1 NOV 65

UNCLASSIFIED

Security Classification

UNCLASSIFIED

Security Classification

14. KEY WORDS	LINK A		LINK B		LINK C	
	ROLE	WT	ROLE	WT	ROLE	WT
Extraction Parachute Clustered Canopies Solid Flat Canopy Ring Slot Canopy Wind Tunnel Tests Model Caribou Aircraft						

UNCLASSIFIED

Security Classification